INDEX

UNCLASSIFIED

Distribution

Prepared under

Contract NASW-1221
National Aeronautics and
Space Administration
Washington, D.C.

ANALYZATION, DESIGN, FABRICATION,
AND TESTING OF A FOIL BEARING
ROTOR SUPPORT SYSTEM
Final Technical Report

RR 66-21 June 1966

A. Kushner & F. Stahl
Prepared by

M. Wildi
Approved by

V. E. Ragosine
Approved by

AMPEX CORPORATION

RESEARCH AND ENGINEERING PUBLICATION

ACKNOWLEDGMENT

This effort was conducted in the Research Department of Ampex Corporation under the direction of Dr. W. A. Gross. The help of the following members of the Research Department is gratefully acknowledged.

Alan Huckabay aided in the mechanical design of the test equipment, conducted the calibration and test program, reduced the data, and helped in the writing of the reports.

Dr. A. Eshel's doctoral thesis formed the basis of the analytic comparisons contained in this report. Dr. Eshel also provided the analysis of the attitude angle of foil bearings.

Stephen Lammé helped with the mechanical design, made all the detail drawings, and assembled the test rigs.

Edward Barlow contributed significantly to the understanding of the attitude angle of foil bearings.

Richard Hepperle helped with the design, de-bugging, and operation of the electronic instrumentation.

Charles Steele created the computer program which automatically plotted whirl orbits.

Fred Schneider and Kenneth Severs did an excellent job of machining the many complex parts.

Manfred Wildmann gave direction, support, and innumerable helpful suggestions.

32962

ABSTRACT

For this study a self-acting, gas lubricated foil journal bearing rotor support system was designed and fabricated. The system was designed for a maximum rotational speed of 570,000 rpm and was instrumented to continuously measure shaft speed, shaft motion in two planes, foil tension, wrap angle, and the torque exerted by the rotating shaft on the foil journal bearing. The highest speed recorded while testing was 381,000 rpm, and at no time was half-frequency whirl observed.

A study of the stress and vibration characteristics of high-speed rotors showed that rotor designs are often limited by the first free-free bending critical speed because conventional gas lubricated bearings cannot support a shaft during acceleration through this critical speed.

Three rotors supported on self-acting gas lubricated journal bearings were accelerated up to a rotational speed corresponding to their free-free critical speed. The speed and shaft orbital motion data were recorded on magnetic tape. It was not possible to rotate these shafts at speeds in excess of their free-free critical speeds. There was no damage either to the shaft or to the foil journal bearings after operation at this critical speed.

No signs of half-frequency whirl instability were observed during the operation of a shaft (1 in. in diameter by 4.5 in. long) supported by helium lubricated, self-acting foil journal bearings at rotational speeds from zero to 381,000 rpm. However, at certain speeds the shaft acquired a low frequency motion which corresponded to the natural frequency of the shaft supported on the Havar* foil.

*Trade Mark, Hamilton Watch Company

CONTENTS

LIST OF FIGURES

LIST OF FIGURES (Continued)

LIST OF FIGURES (Continued)

LIST OF FIGURES (Continued

LIST OF FIGURES (Continued)

APPENDIX II

NOMENCLATURE

C	Radial clearance (in.)
E	Young's modulus of elasticity (lb/in.^{2})
F	Centering force (lb/in.)
K	Positional stiffness (lb/in./in.)
K_B	Lubricating film stiffness (lb/in./in.)
K_F	Foil positional stiffness (lb/in.)
P	Pressure (psi)
P_a	Ambient pressure (psi)
R	Radius (in.)
T	Foil tension (lb/in.)
U	Velocity (in/sec)
Z	Rectangular coordinate
e	Eccentricity (in.)
f	Frictional force (lb/in.)
h	Lubricating film thickness (in.)

ℓ	Foil length (in.)
t	Foil thickness (in.)
Λ	Compressibility number
α	Whirl angular speed ($d\alpha/dt$)
θ	Wrap angle (radians)
μ	Viscosity (lb-sec/in.^{2})
ξ	Z/R
ω	Angular velocity (radians/sec)

ANALYZATION, DESIGN, FABRICATION AND TESTING OF A FOIL BEARING ROTOR SUPPORT SYSTEM

1.0 INTRODUCTION

A foil bearing is a fluid film bearing in which one member is flexible. The flexible wall allows an almost constant pressure over the bearing arc[1]. The resulting displacement vector was therefore assumed to be very closely aligned with the load vector and, consequently, the attitude angle would be quite small for a foil bearing.

As a result of further analytical work, it has been found that the attitude angle is not necessarily zero. In a single-foil system of 180° wrap and fixed foil bearing centerline, the attitude angle is -48°. However, in a three-foil system with initial foil tension, the attitude angle is zero. The derivation and a detailed explanation are given in Appendix II.

From Fig. 1 it can be seen that for the bearing with rigid surfaces, the resultant of the fluid film forces has a component which is tangential to the surface of the bearing. It is this tangential component which causes the nonsynchronous whirl of the rotor. All fluid film bearings in which the tangential component is present have a tendency to whirl. Since the lubricant between the rotating shaft and the stationary boundaries moves at approximately one-half the rotational speed of the shaft and the shaft must displace the fluid if it is to whirl, self-excited whirl usually takes place at approximately one-half the rotational speed of the shaft. This whirl tendency is aggravated when there is little damping; i.e., when the lubricant is a low viscosity fluid such as gas or a liquid metal.

If it is assumed that the frequency and amplitude of any whirling motion are constant, the load capacity of a cylindrical journal bearing can be obtained from the Reynolds equation[2]. (See Fig. 2.)

$$\frac{\partial}{\partial\theta}\left[\left(\frac{h}{c}\right)^3 P \frac{\partial P}{\partial\theta}\right] + \frac{\partial}{\partial\xi}\left[\left(\frac{h}{c}\right)^3 P \frac{\partial P}{\partial\xi}\right] = \Lambda\left(1 - \frac{2\dot{\alpha}}{\omega}\right) P_a \frac{1}{c}\left(\frac{\partial(hP)}{\partial\theta}\right)$$

$$\xi = z/R$$

$$h = c + e\cos\theta \qquad (1)$$

$$\Lambda = \frac{6\mu U R}{P_a c^2}$$

The right-hand side of Eq. (1) describes the driving function and, together with the diffusion terms on the left-hand side, determines the load capacity of the bearing. This equation assumes isothermal flow of a Newtonian gas between perfectly smooth rigid surfaces.

From the equation it can be seen that whenever $\dot{\alpha}$, the whirl velocity, is one-half the spin velocity ω, the load capacity goes to zero because $(1 - 2\dot{\alpha}/\omega)$ goes to zero. When this occurs, failure usually results. Occurrence of the half-frequency whirl instability determines the maximum speed and/or operating conditions of most conventional self-acting, gas lubricated journal bearings.

However, in a system of at least three equally spaced, perfectly flexible, self-acting foils, the attitude angle is zero, and there will be no self-excited instabilities due to a tangential component of the load. It is this characteristic of the self-acting foil bearing that makes it particularly attractive for high-speed rotor support applications.

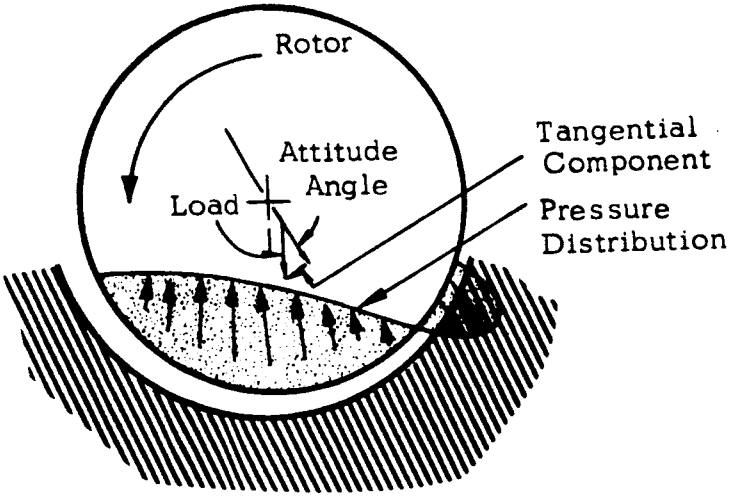

Fig. 1 Load, Attitude Angle, and Pressure Distribution in Self-Acting, Rigid Surface Bearing

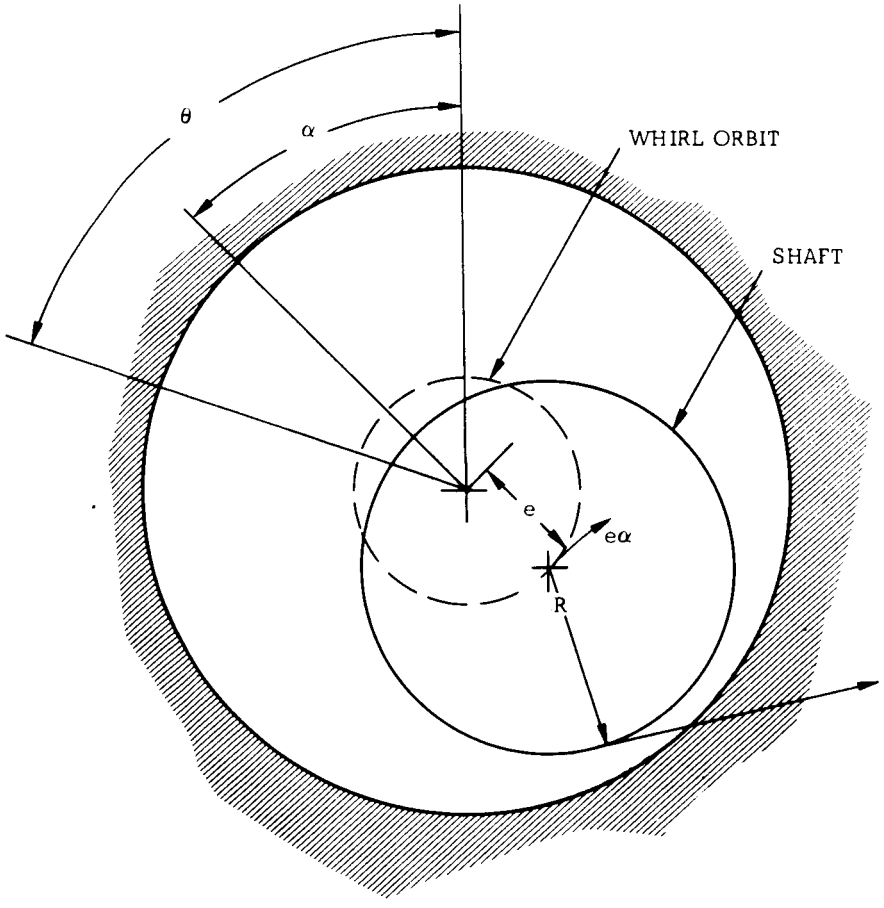

Fig. 2 Schematic Diagram of a Journal Bearing in Circular Whirl

2.0 OBJECTIVES

The objectives of this study are to determine by analytical and experimental means the characteristics and limits of applicability of high-speed rotor supports using self-acting, gas lubricated foil journal bearings. This work is organized into three major categories:

a. The analysis of a self-acting gas lubricated foil bearing rotor support system consisting of three symmetrical steel foils operated in an inert gas atmosphere;

b. The design and fabrication of a self-acting, gas lubricated foil journal bearing rotor support system;

c. The test of this rotor support system with the primary emphasis on the determination of the maximum speed at which the rotor can be operated without encountering self-excited "whirl" instability.

3.0 PROGRAM DESCRIPTION

The self-acting, gas lubricated foil journal bearing has been used to support rotors at speeds in excess of one-quarter million rpm. The apparent absence of half-frequency whirl instability in this type of journal bearing has made it attractive for use in high-speed applications, or under the conditions of light load, particularly in a space environment. There are, however, some undesirable characteristics associated with foil journal bearings. These bearings obtain their freedom from self-excited half-frequency whirl from the flexibility of the foil; it is this flexibility which creates many of the problems that have prevented their use in practical applications.

There are four major problem areas associated with the support of high-speed rotors on gas lubricated, self-acting foil journal bearings:

a. The possibility of a limited rotational speed due to the occurence of self-excited, half-frequency whirl instability;

b. The high starting torque resulting from the "capstan effect";

c. The low frequency critical speeds associated with the mass of the rotor and the small positional stiffness of the foil journal bearings;

d. Structural limitations which, thus far, have prevented the operation of rotors supported on gas lubricated journal bearings beyond their first free-free bending critical speed.

These four problem areas were separated into two categories: (1) high speed investigations, and (2) flexural critical speed investigations.

It was felt that the objectives of this program would be best satisfied if the test equipment for each of the areas of investigation were designed specifically for testing in that area rather than using a single piece of test equipment for all studies.

3.1 High Speed Test Rig

The high-speed test rig is designed for a maximum shaft speed of 570,000 rpm. The speed of the shaft is limited by two factors: radial and tangential stresses which would cause the shaft to burst and the first free-free flexural critical speed. The effects of shaft length and diameter on these two criteria are shown in Fig. 3. It can be seen that very high rotational speeds are limited to short, small-diameter rotors. The design point shown in this illustration represents a compromise between high speed and adequate length to allow for instrumentation; i.e., the shaft must be designed to place its free-free and burst speeds close together and above 500,000 rpm.

During operation, continuous measurements can be made of the shaft motion and/or growth by capacitance probes located in two planes: one near each end of the shaft. Four capacitance probes are installed in each of these planes. The journal bearings used to support the shaft consist of three separate foils spaced at 120°, each having individually controlled foil tensions and wrap angles. The foil material is 1/2 in. Havar* of thicknesses varying from 0.0005 to 0.001 in.

*Trade Mark, Hamilton Watch Company

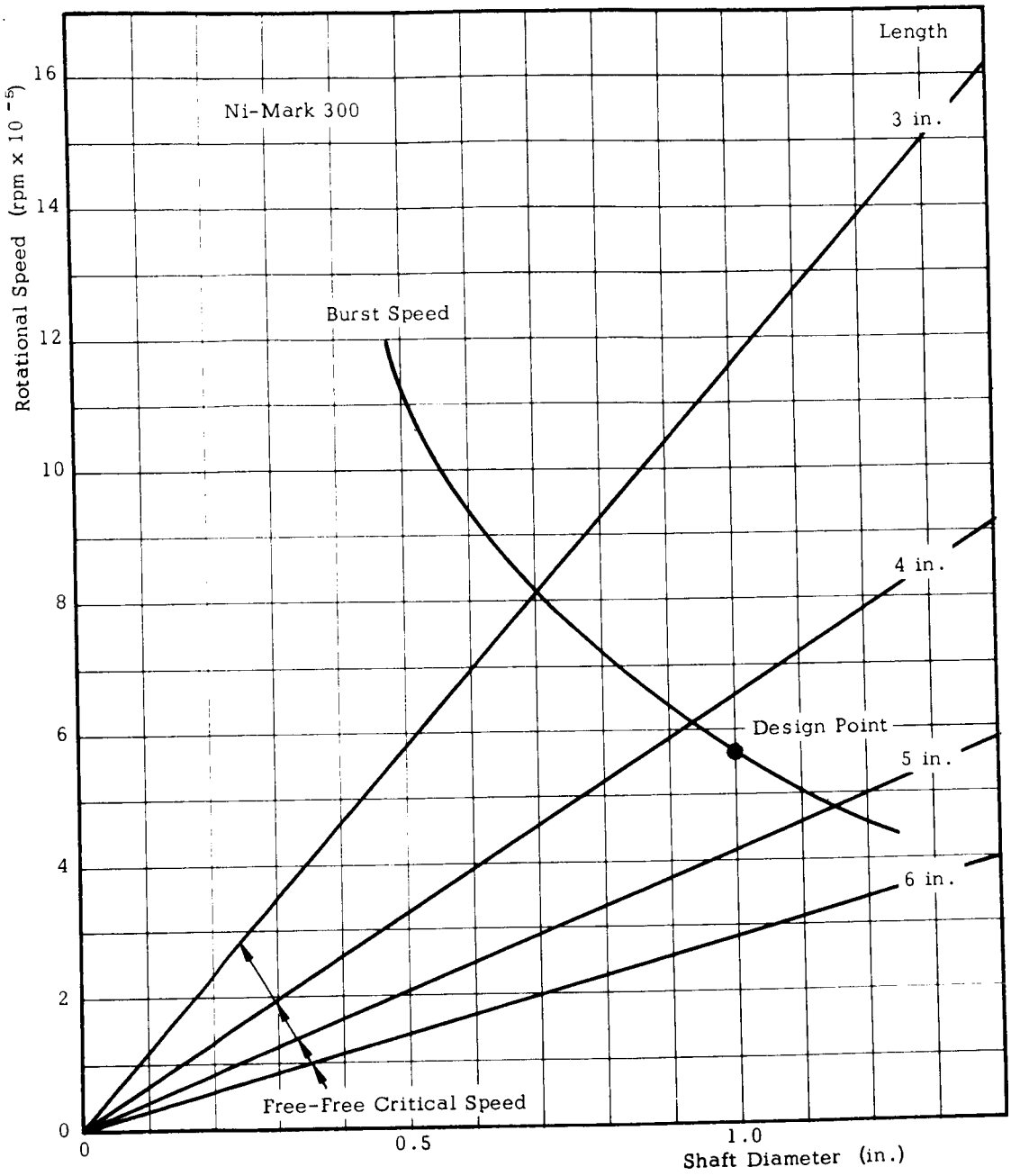

Fig. 3 Burst Speed and Flexural Vibration Characteristics of a High Speed Rotor

Figures 4 through 7 show the step-by-step buildup and instrumentation of the high-speed test rig. The entire unit may be enclosed within a 17 in. diameter cylinder of a 6061-T6 aluminum alloy with a wall one inch thick, which provides blast protection.

The radial inflow turbine which drives the rotor is located on the upper end of the rotor. The rotor is supported from below by an externally pressurized, gas lubricated thrust bearing. The foil journal bearings are located near the extreme ends of the rotor, and the planes of the capacitance measuring probes are located adjacent to these bearings. Each of the foils can be individually adjusted to change wrap angle, foil tension, and radial position. All of these parameters can be measured, either by micrometer motion, strain gage, or capacitance probe.

Initial testing was done with a simplified test rotor machined from Ni-Mark 300*. This material has a yield strength of over 270,000 psi. The rotor used in later testing, also of Ni-Mark 300, has fully developed blades and is quite responsive to increases in gas flow. Maximum rotational speeds attainable with air are approximately 210,000 rpm. Since helium, at room pressure and at the pressure ratio currently being used, has over eight times the adiabatic head velocity and approximately three times the sonic velocity as compared to air, we have driven the turbine and have surrounded the bearings with helium.

3.1.1 Dynamometer

The dyanamometer consists of an air supported circular plate on which are mounted the foil adjuster blocks. Figure 8 is a photograph of the bottom assembly. The dynamometer plate is located in the in the center and is kept from rotating by a calibrated cantilever spring which can be seen at the left. The torque on the dynamometer, caused by

*Trade Mark, Carpenter Steel Company

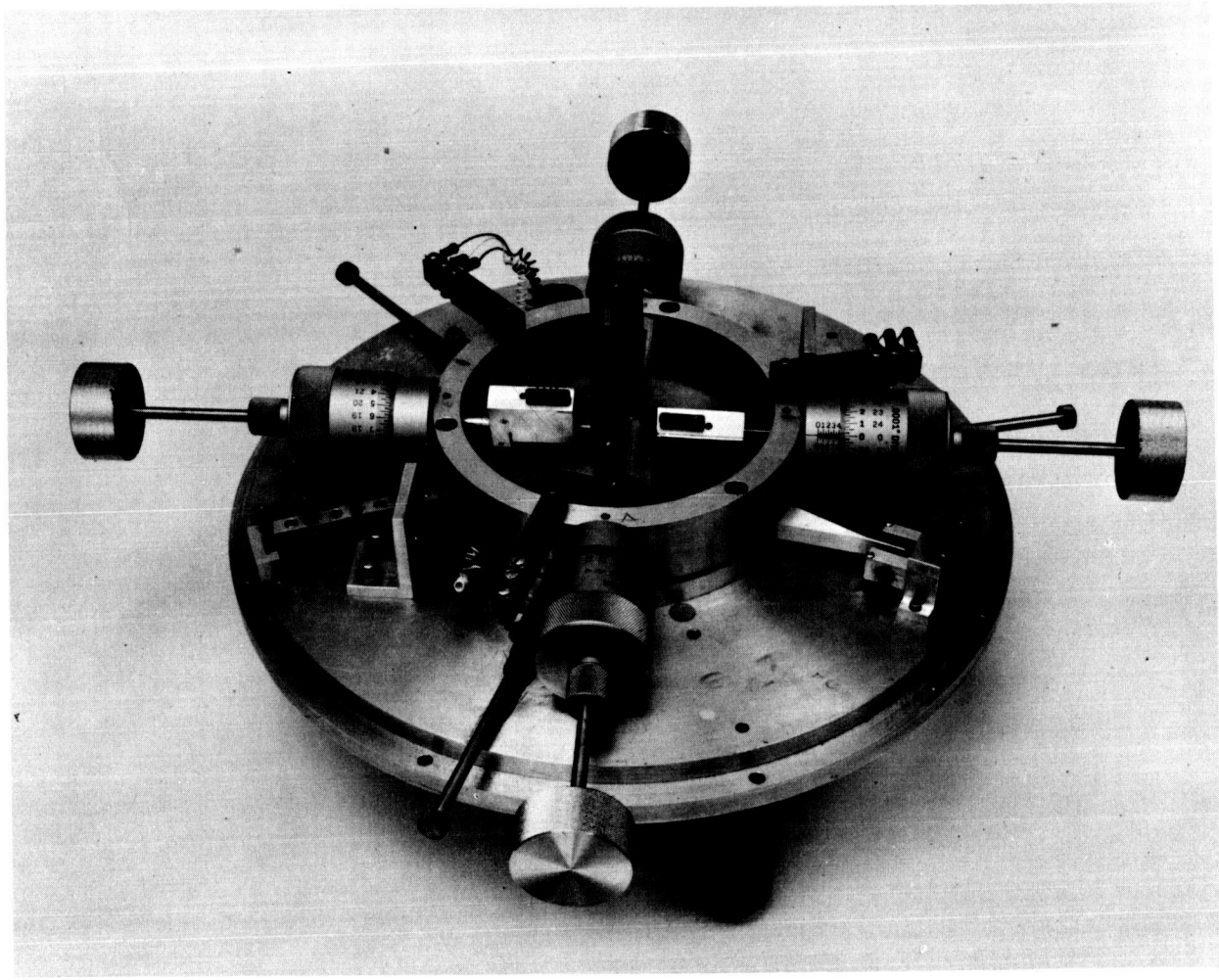

Fig. 4 High Speed Test Rig, Simplified Rotor, Dynamometer, and Lower Capacitance Probes

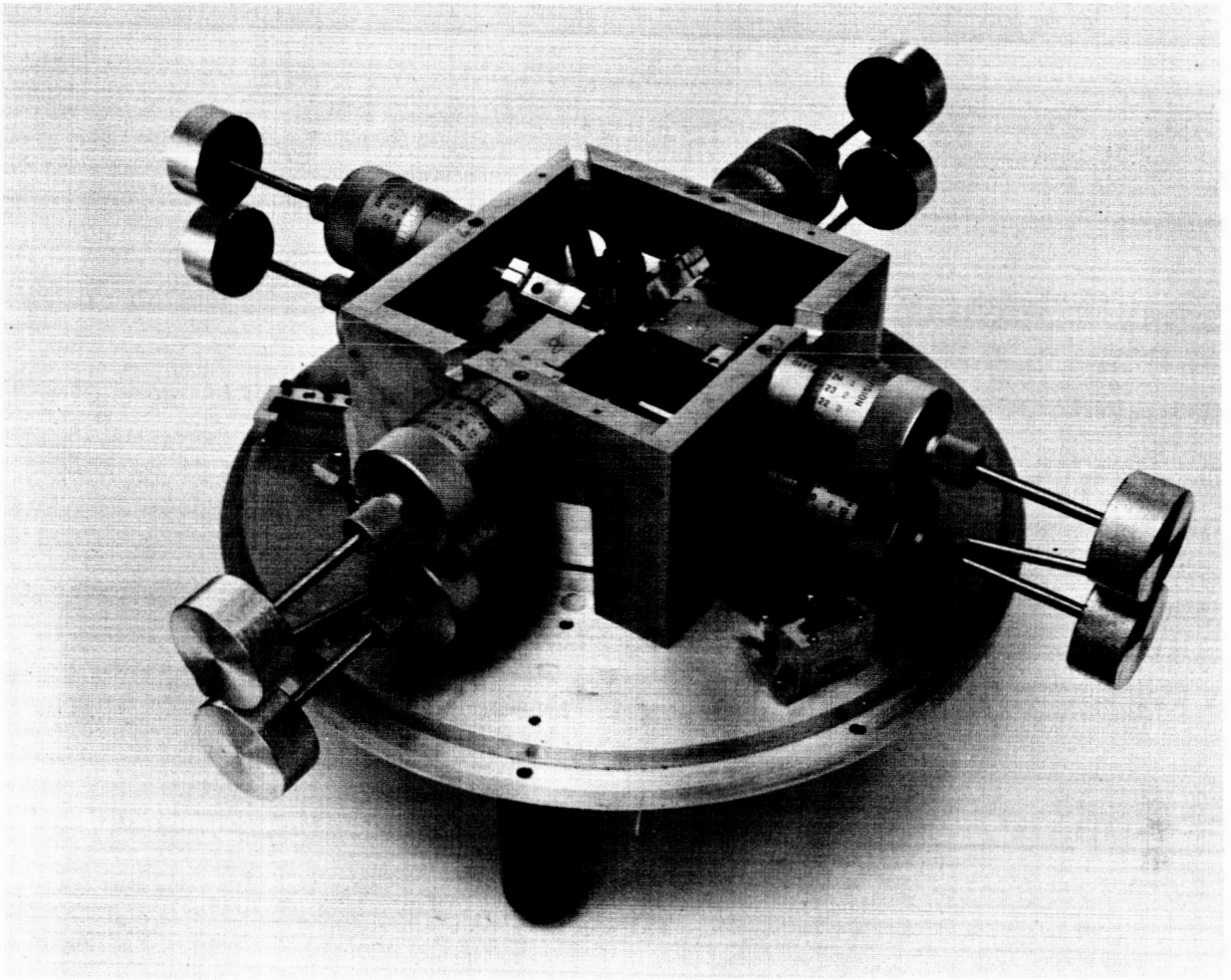

Fig. 5 High Speed Test Rig, Upper Capacitance Probes

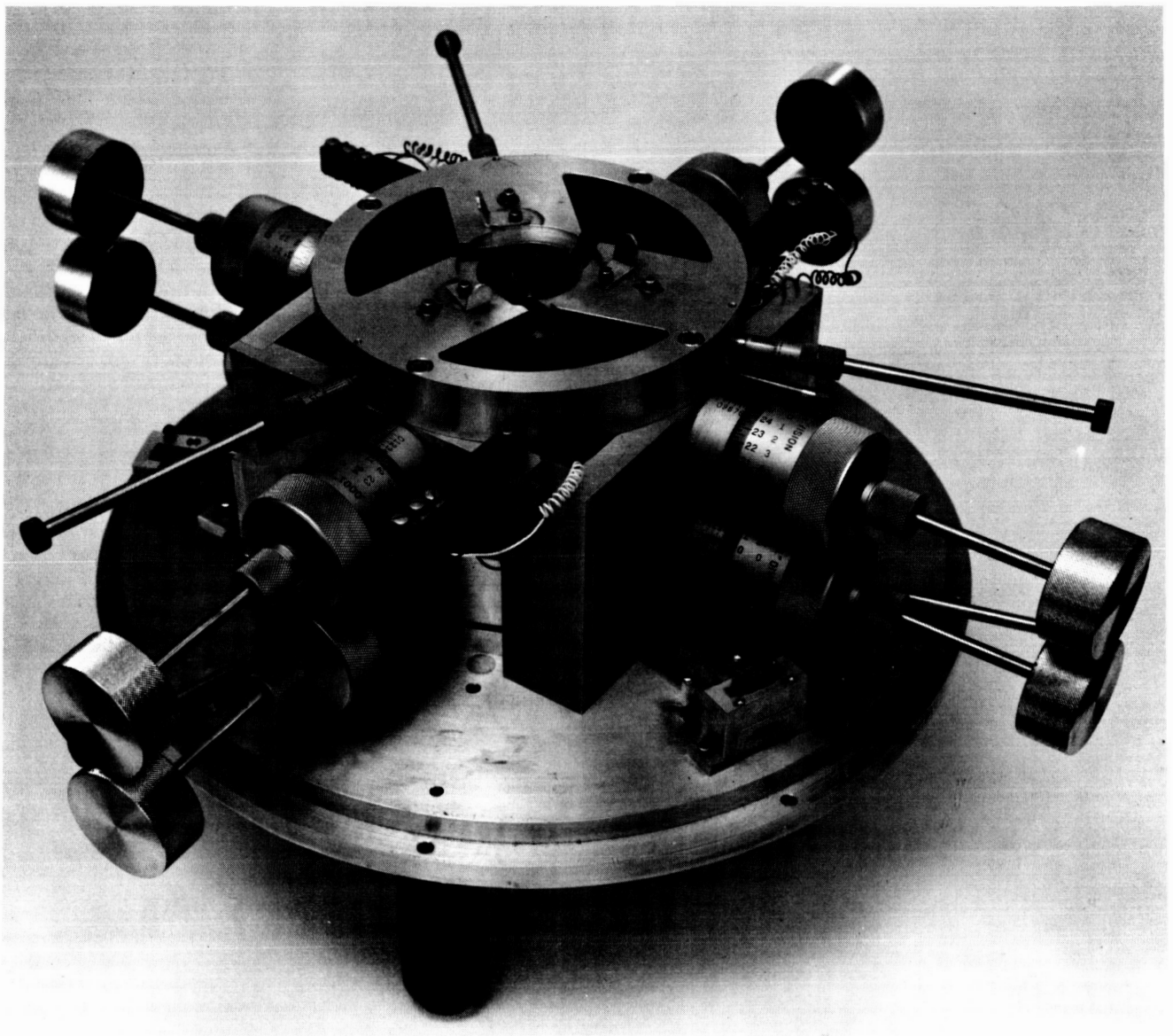

Fig. 6 High Speed Test Rig, Upper Foil Support Plate

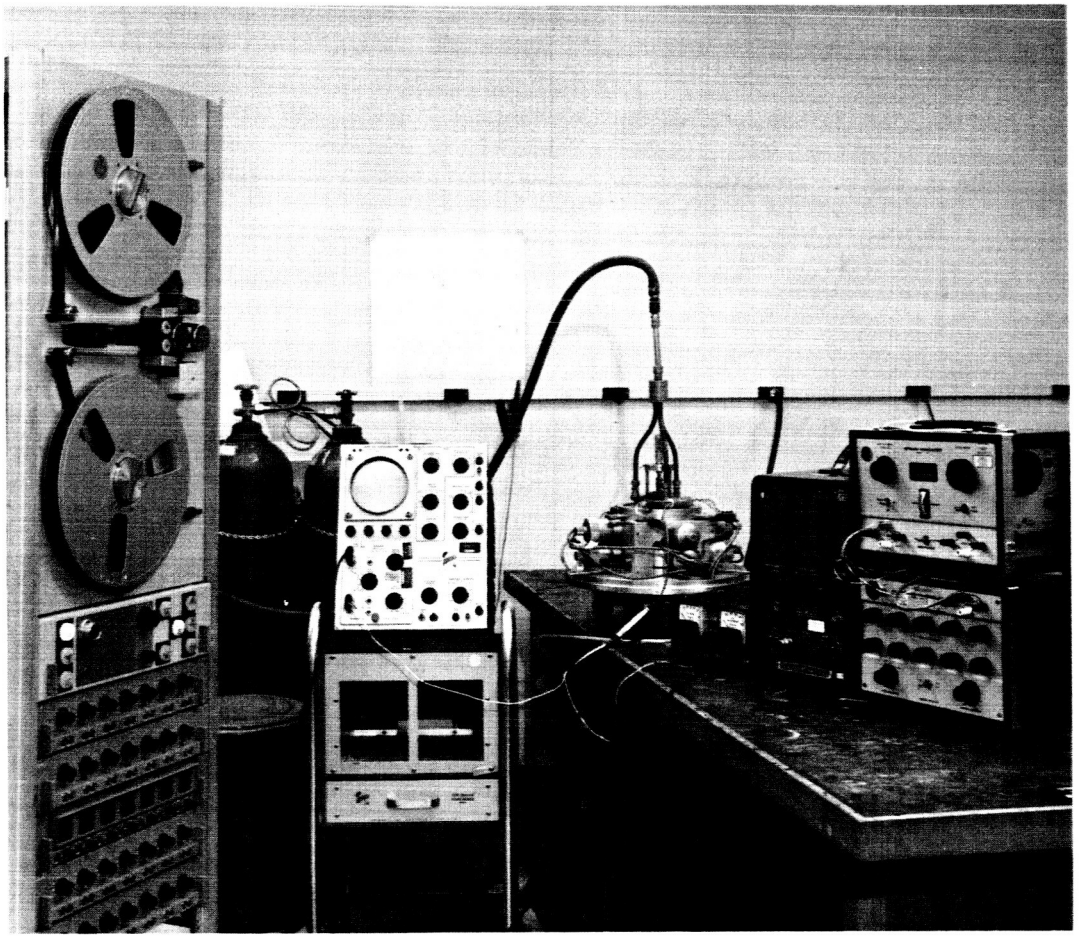

Fig. 7 High Speed Test Rig and Instrumentation - Shown with Outer Ring and Top Cover Removed

the drag on the three bottom foils, is monitored by double ended capacitance probes. These are located on the right in Fig. 8.

3.1.2 Speed Monitors

Shaft speed is monitored by a magnetic speed pickup manufactured by Pace Engineering Company, Model SV-2. The speed pickup is a magnetic device with a high-turn coil. The sensitivity of the device allows monitoring of shaft speed even though it is placed several inches from the magnetized shaft. The output of the speed pickup is fed into an electric counter which displays shaft speed in cycles per second.

Because gate time for the electronic counter only gives a speed display once every two seconds, a direct reading tachometer was constructed. This tachometer gives continuous speed readings over a range of 60,000 to 500,000 rpm. The circuit employed is a standard pulseforming network triggering a constant voltage and pulsewidth time oscillator. The integrated current is measured by a large 4-1/2 in. meter. The accuracy of the tachometer over the range 60,000 to 500,000 rpm is 6% f.s.

During the last tests conducted,the magnetic strength of the shaft was found to be short-lived, usually yielding only two runs. Then the signal deteriorated and required re-magnetization of the shaft. In future investigations a switch to a photoelectric speed sensor is planned. To obtain the necessary light-dark area, the shaft will be dulled permanently around half of the circumference. The pickup and light source will be made in plant because commercial units are too large for the available space.

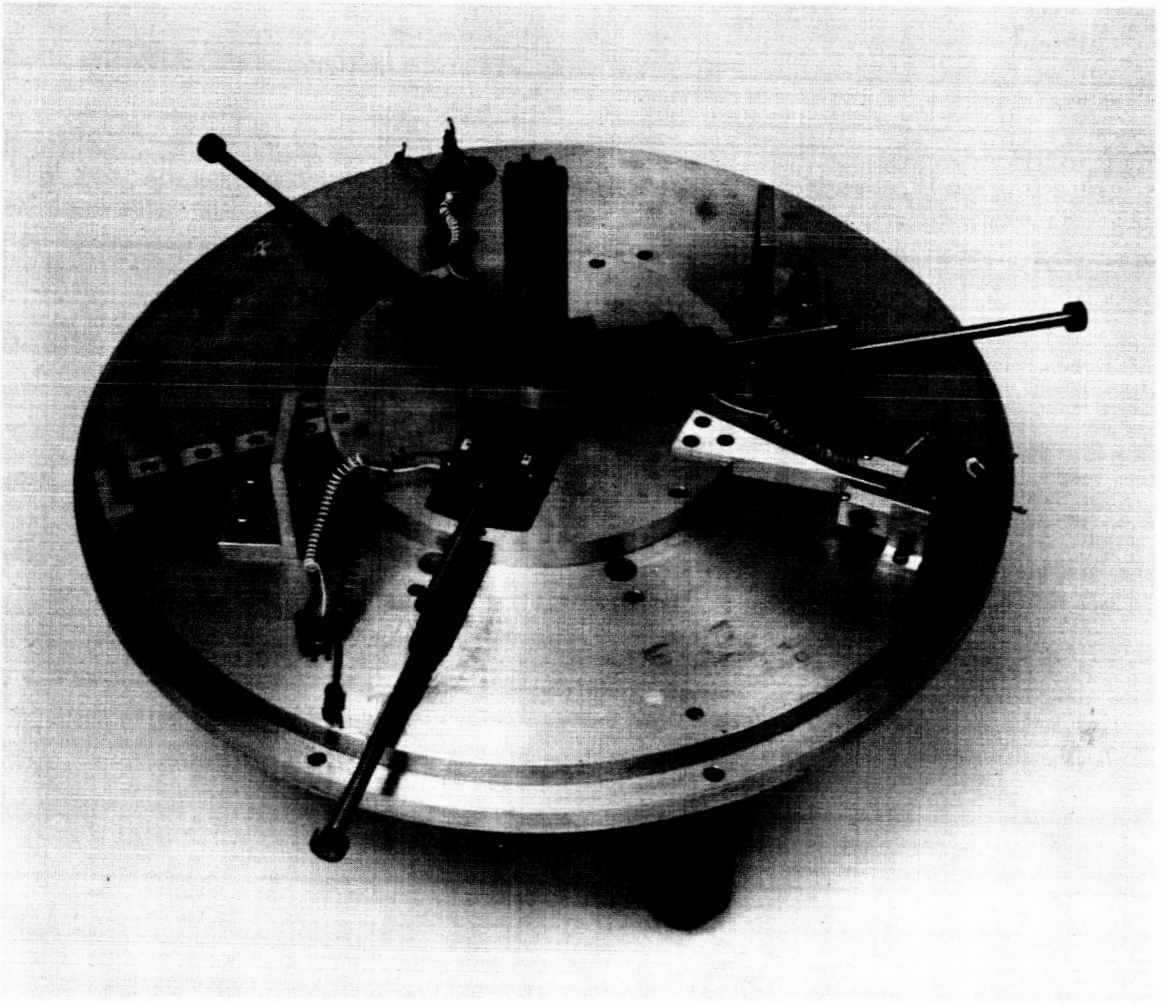

Fig. 8 High Speed Test Rig, Bottom Support Assembly

3.1.3 Capacitance Motion Measuring Instrument

The shaft orbital motion, thrust bearing motion, and dynamometer angular rotation are all measured by means of capacitance probes which detect these parameters as changes in capacitance. The requirements of this measuring system are: high sensitivity, repeatability, low noise, wide dynamic range, and calibration of the probes after they have been mounted on the final assembly. The high-speed foil bearing rotor support test rig requires a minimum of nine separate channels.

The transducer system made by the Lion Research Corporation was thought to be well suited to the present application because of the small size of the detector, the low background noise, and the low cost per channel. Figure 9 shows a calibration curve of one of the Lion units.

Figure 10 shows the measured frequency response of the Lion Research "C" Line Driver. Here it can be seen that any frequency of motion higher than 100 cycles per second is strongly attenuated. This high frequency attenuation makes the Lion unit unsuitable for monitoring orbital motion during high speed rotor tests. To overcome the difficulty, a 1.38-megacycle r-f driver and capacitance measuring probes to fit the high speed test rig were designed and built. The design of the probes was based on the material presented in reference 3.

The frequency response of the capacitance motion detector probe and its associated electronics alone as well as the frequency response of the entire system are shown in Fig. 10. The detector offers no attenuation for all practical rotational speeds, and the entire system is flat to 40 kc and drops only by 5% at 10 kc, which is the highest rotational speed which was anticipated in this test series. The probe and

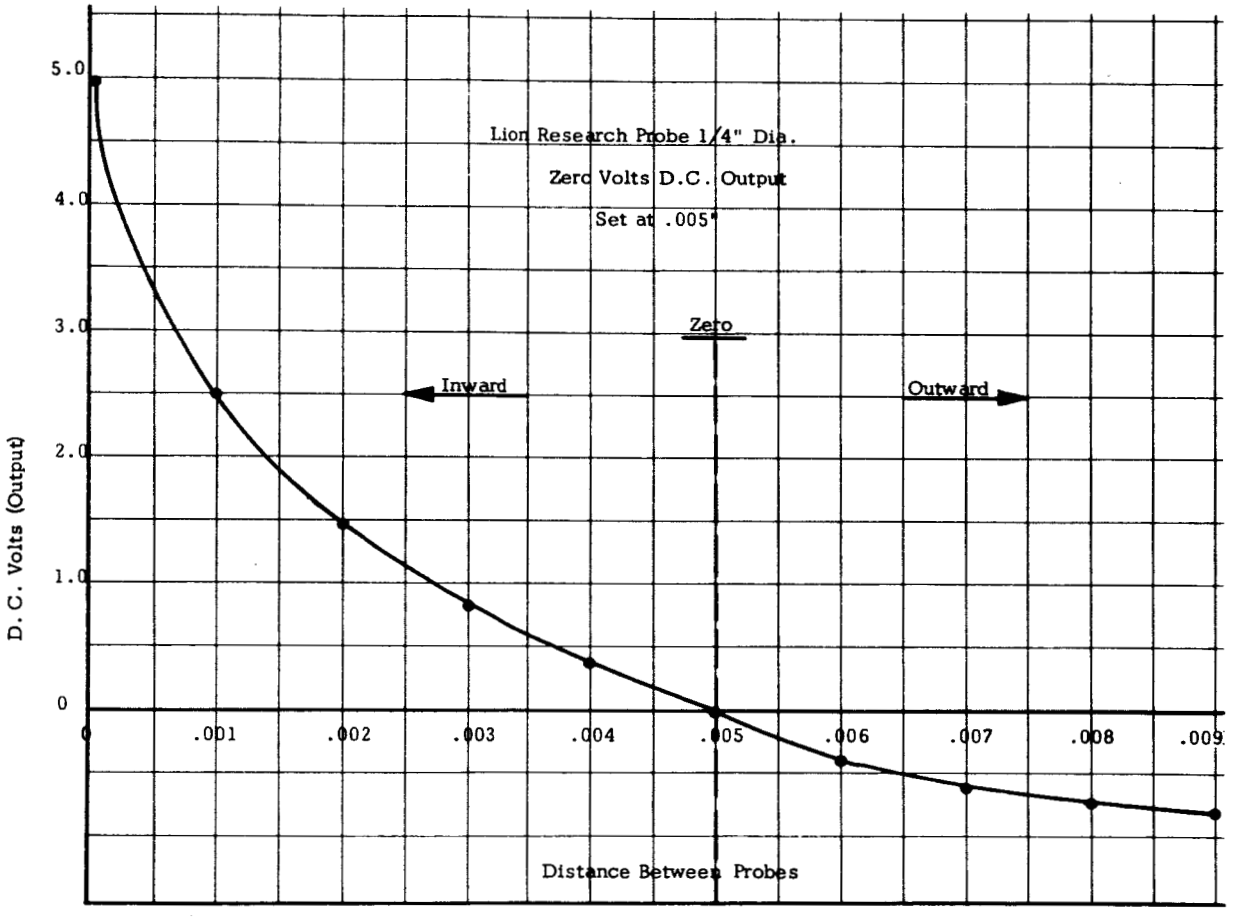

Fig. 9 Calibration Curve of Lion Research Capacitance Probe Single Ended; 0.25 Diameter; Zero Set at 0.005 in.

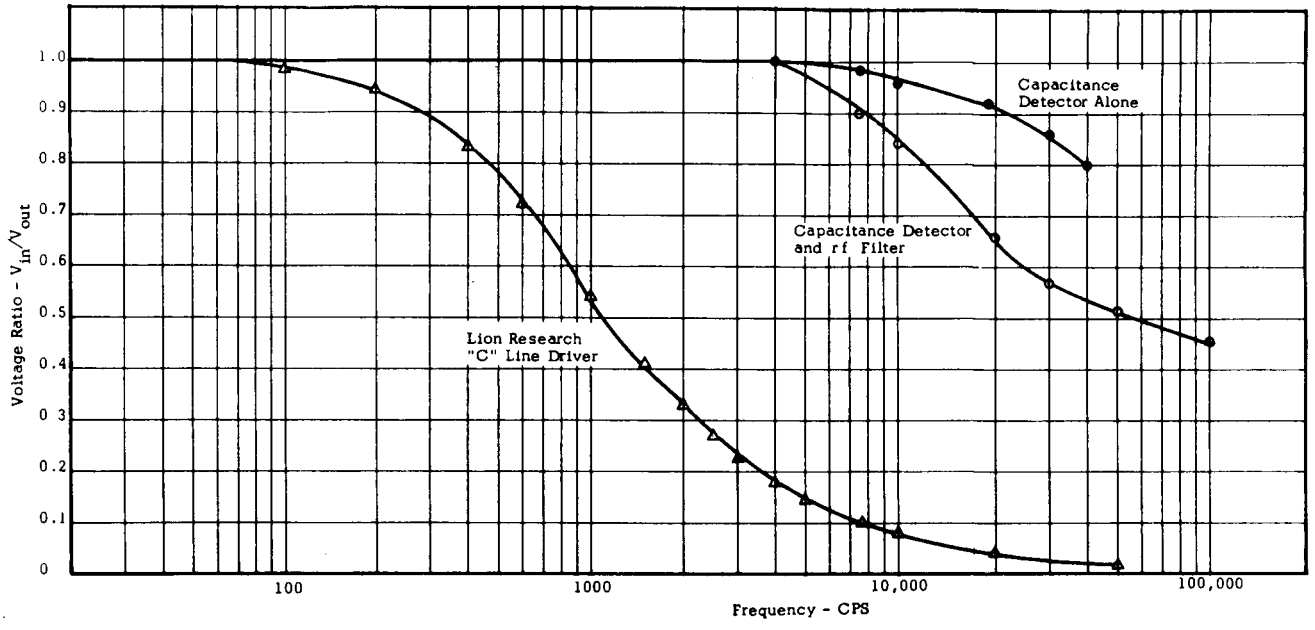

Fig. 10 Frequency Response Characteristics of Capacitance Insertion Probes

driver electronics are shown in Figs. 11 and 12. The noise level of the completed twelve-channel capacitance motion measuring system is less than 0.01 v, which corresponds to 10 μin.

Figure 13 shows the wiring diagram for the capacitance probes. These probes may be used in either a single ended or a push-pull configuration. Shifting from one mode of operation to the other requires only an exchange of wiring harnesses.

The calibration curve of the capacitance probes in push-pull operation is shown in Fig. 14.

3.2 Problems and Solutions

3.2.1 Strain gage beams

After a trial of the high-speed test rig, it was found that the original aluminum beams used to measure the foil tension had taken a permanent set. This happened when the thrust bearing failed to operate correctly because of insufficient air supply and the resultant large shaft excursion overstressed the beams. New, stronger beams were fabricated from hardened beryllium-copper. Figure 15 is a photograph of a section of the floating circular plate used as a dynamometer. In the center of the picture, the earlier aluminum strain gage beam is shown with the new one. The beryllium-copper beam is mounted on its adjuster block and with foils in place. Beryllium-copper was chosen for its characteristics of low hysteresis, low elastic modulus, and high strength. The new tension beams were installed and the strain gages calibrated. These have given good results.

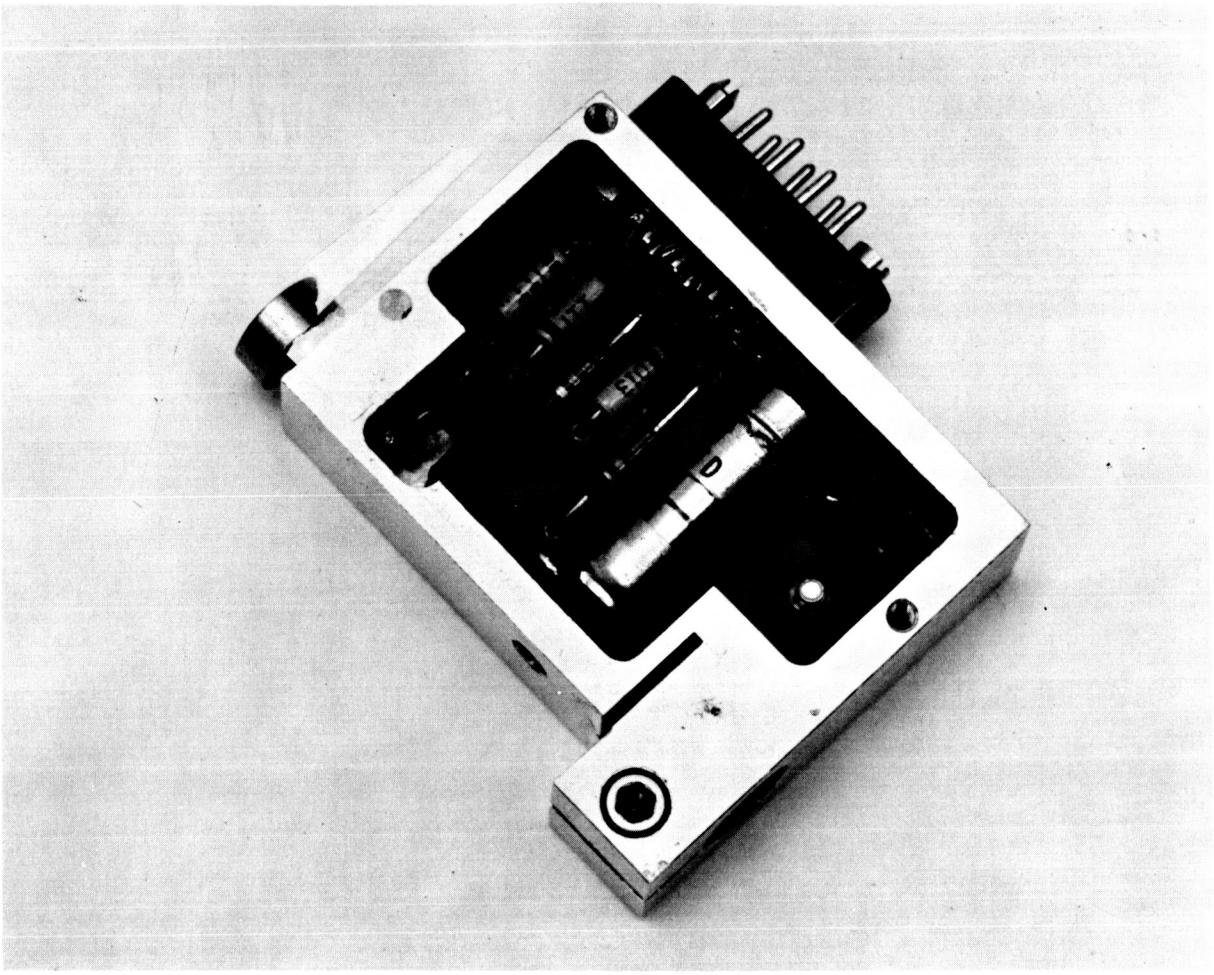

Fig. 11 Capacitance Measuring Probe and Associated Electronics

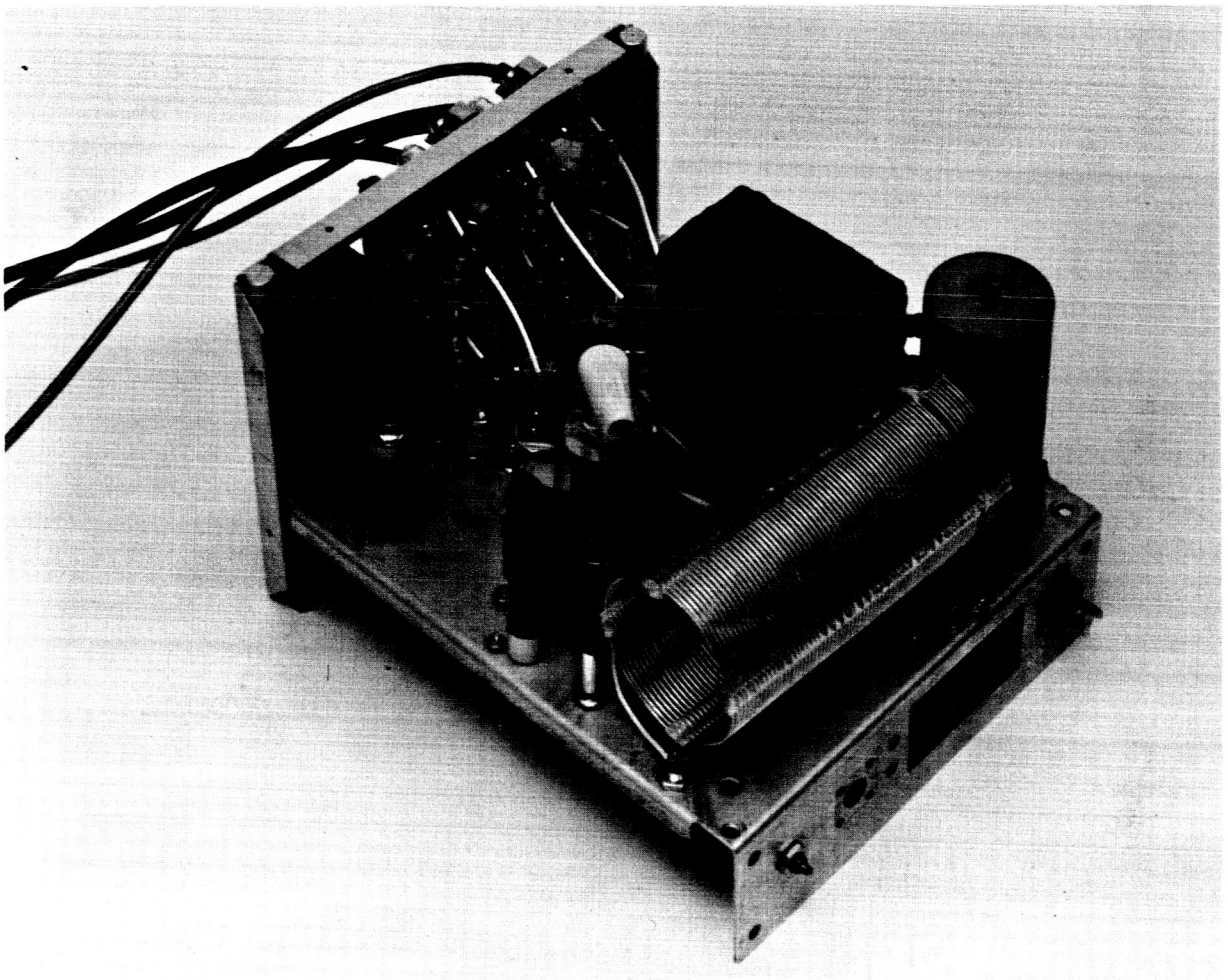

Fig. 12 Capacitance Probe Driver Electronics

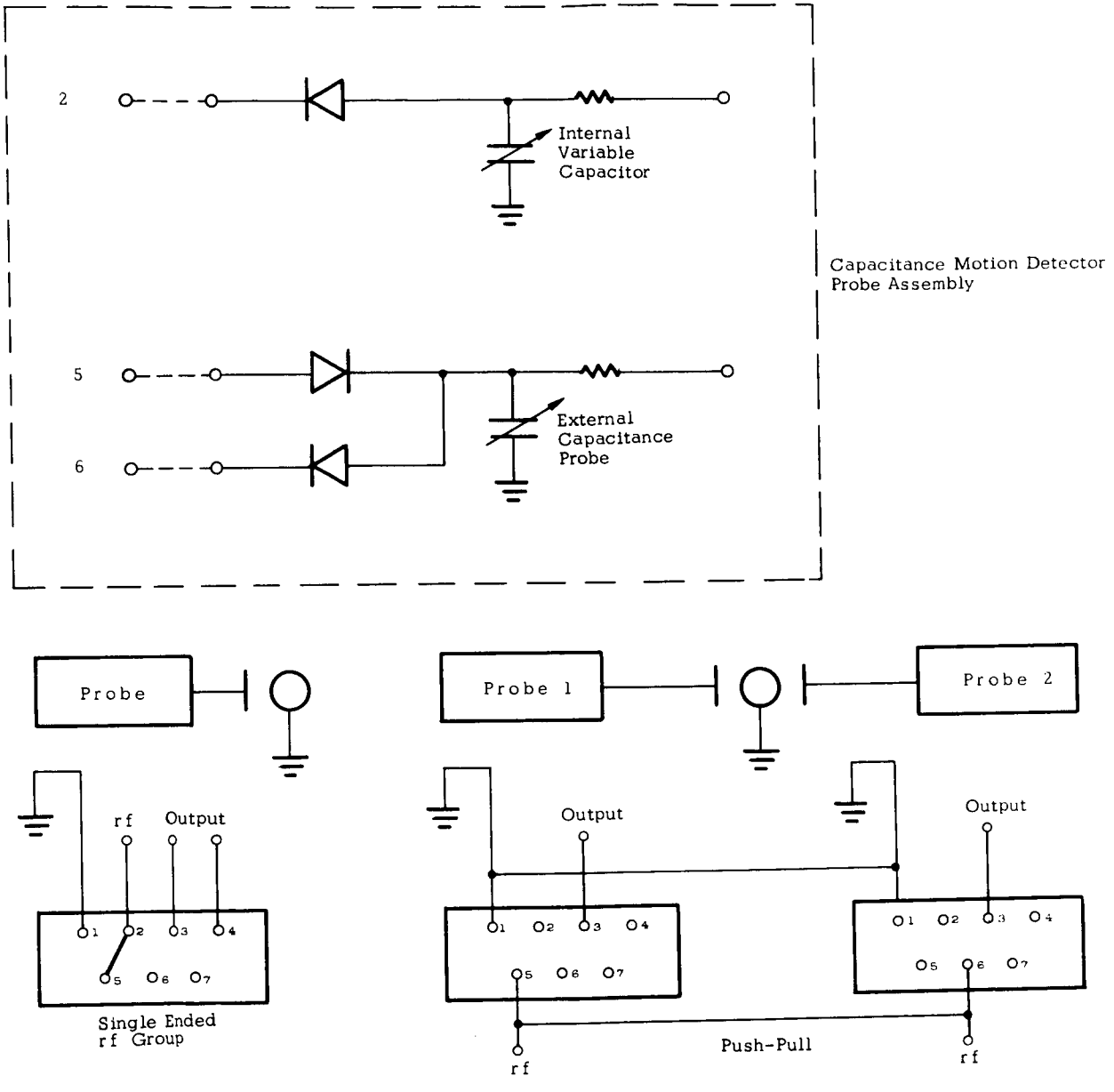

Fig. 13 Schematic Diagrams of Capacitance Motion Detector Probe and Wiring Harness

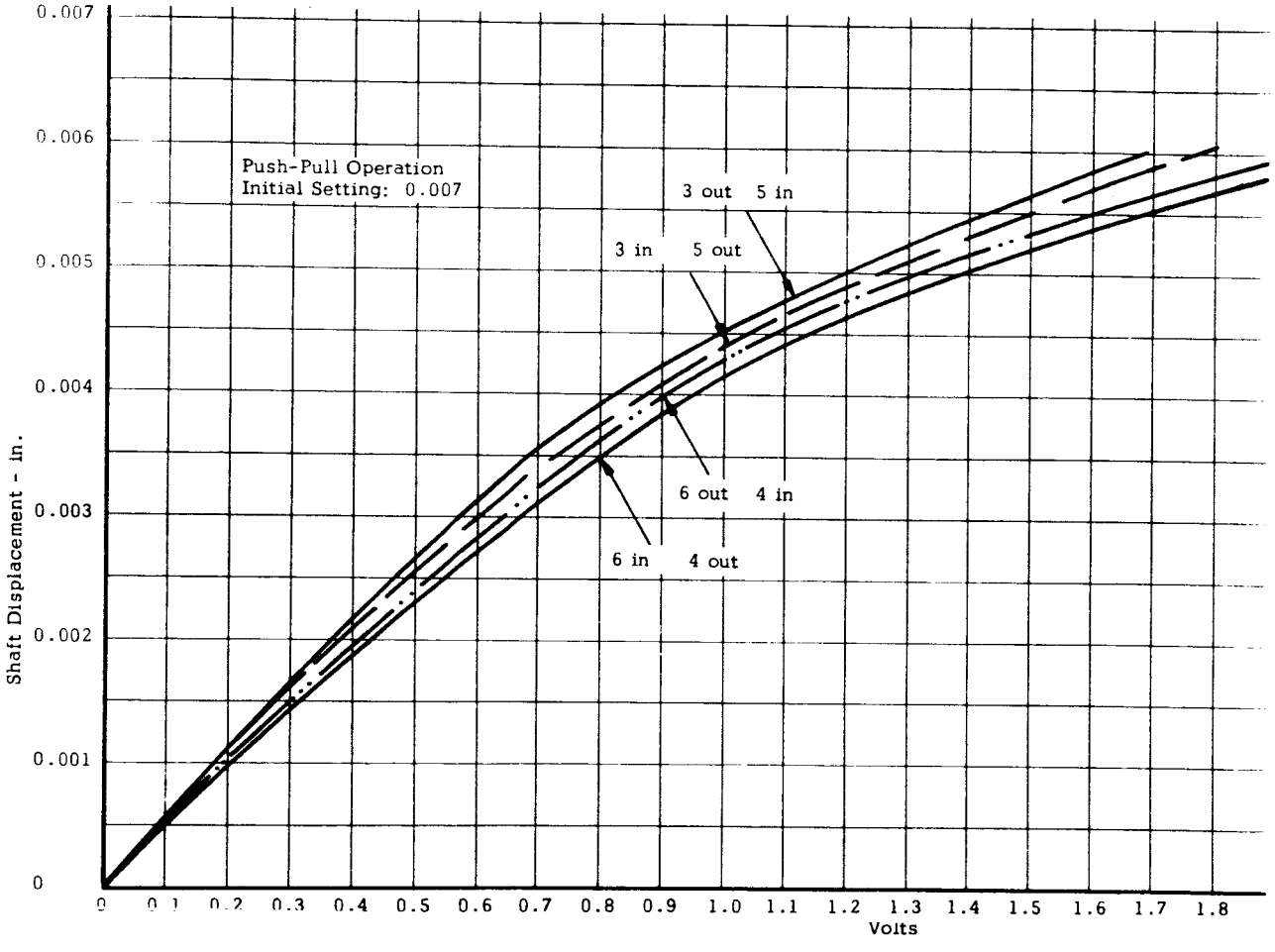

Fig. 14 Calibration Curve of the Capacitance Probes Used to Measure Shaft Motion

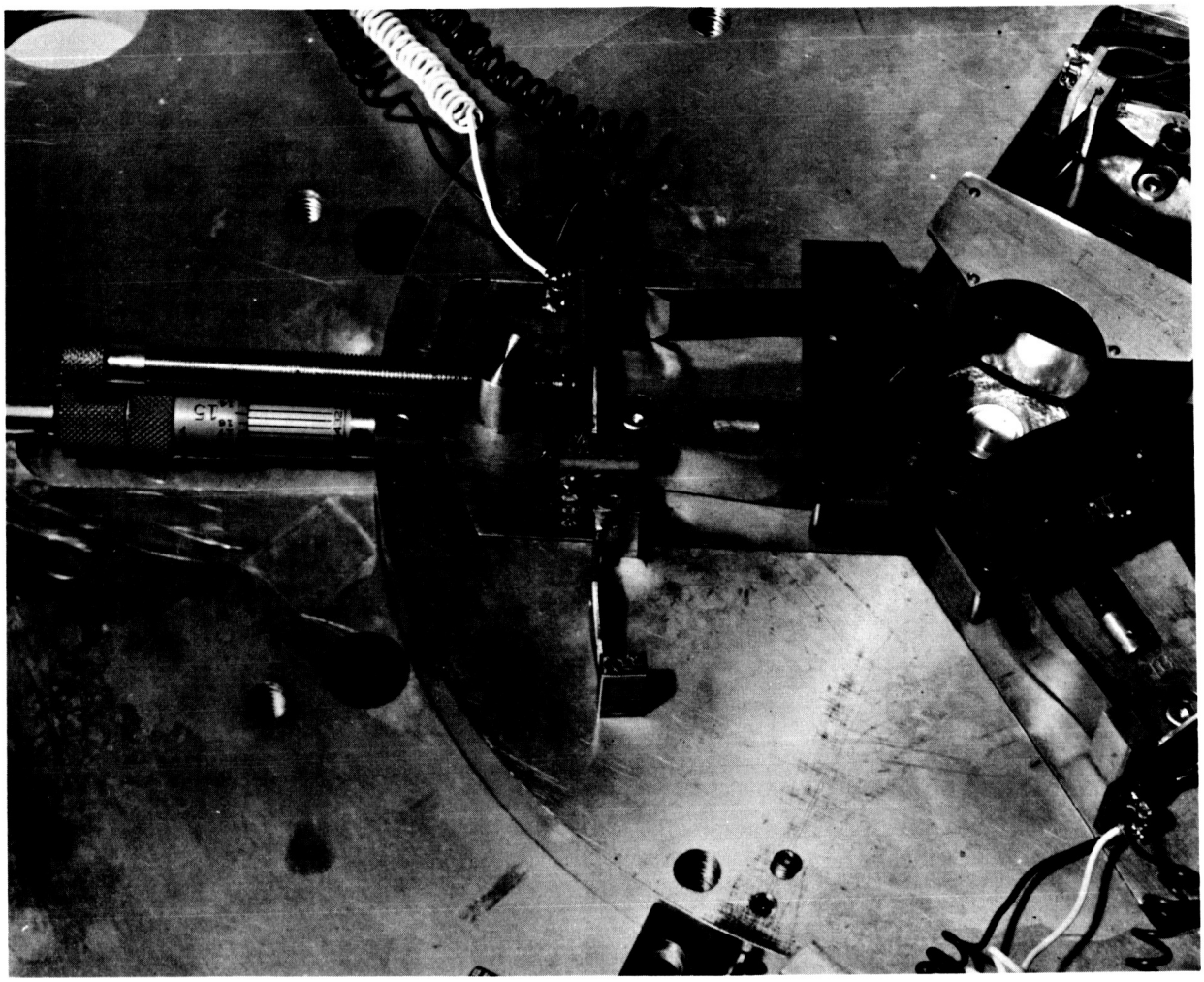

Fig. 15 High Speed Test Rig, Dynamometer, Plate Assembly

3.2.2 Thrust bearing

During preliminary testing with the high-speed test rig, rotor vibration was noticed. It was found that during the run the air pressure to the thrust bearing would drop below the level required to support the shaft. This was corrected by using an independent gas supply system for the thrust bearing. The bearing itself was modified to include a Teflon filled bronze thrust surface. Initially, speeds up to 210,000 rpm were achieved with no noticeable vibration. Figure 15 shows this modified thrust bearing surrounded by the three bottom foils. It has been found, however, that with continuous running this bearing did not operate successfully; it is believed to have been the cause of some of the low-frequency shaft motions. The Teflon-filled bronze bearing was provided with a central nitrogen supply system. The sonic velocity of nigrogen corresponds closely to the tip velocity of the shaft at 240,000 rpm; thus, supersonic flow and its attendent instabilities may have existed.

For the final quarter of the program a new thrust bearing was designed and used. This bearing is an orifice-compensated hydrostatic bearing using helium as the supporting gas. An exploded view of the thrust bearing is shown in Fig. 16. Built into the base of the bearing is a capacitance motion measuring probe. The information from the probe is recorded simultaneously with the information from other measuring probes. After approximately one hour of running at speeds above 360,000 rpm and several stop/starts, there were no signs of rubbing on the bearing or on the end of the shaft which serves as a thrust runner.

Figure 17 shows representative frequency displays of the thrust bearing. The upper forms in all photographs in Fig. 17 are the vertical variations with time of this bearing. For comparison, the lower forms shown in the photographs are the radial variations which were recorded simultaneously. Since the purpose of the thrust bearing motion

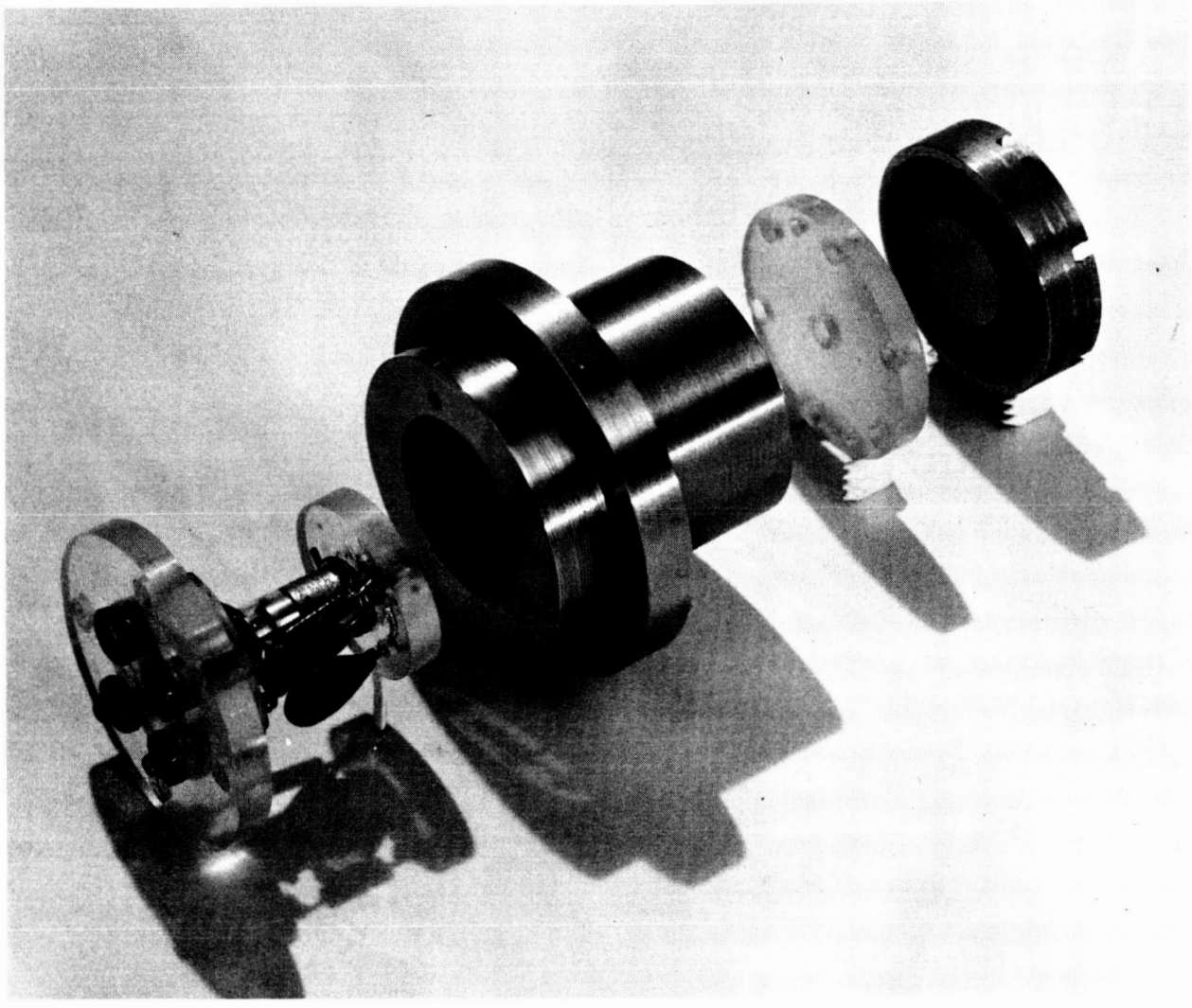

Fig. 16 Exploded View of the Thrust Bearing Showing the Capacitive Motion Measuring Insert

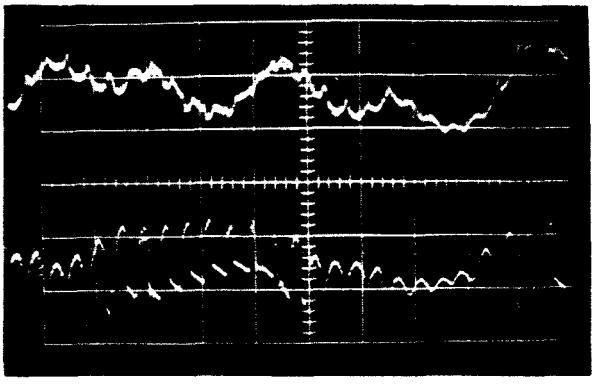

Rotational Speed = 204,000 rpm
y = 5 millisec/cm

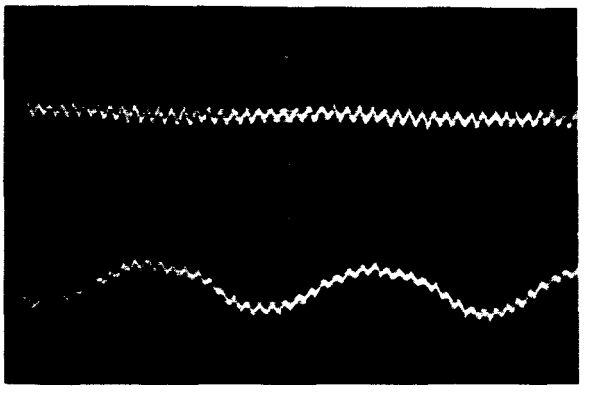

Rotational Speed = 120,000 rpm
y = 5 millisec/cm

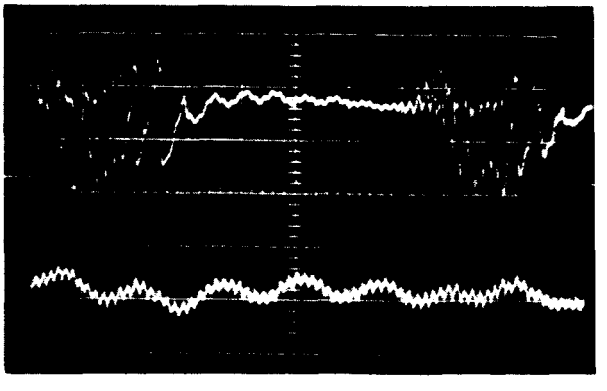

Rotational Speed = 320,000 rpm
y = 5 millisec/cm

Fig. 17 Representative Frequency Displays of Thrust Bearing (Upper Curve is Thrust Bearing; Lower Curve is the Radial Distance Probe Output)

measuring probe was to allow comparison of radial and axial frequencies, this unit was not calibrated. The hydrostatic thrust bearing capacitance probe has a design clearance of 0.0015 in. (The radial probes have 0.010 in.) At this clearance the thrust motion measuring probe is much more sensitive; therefore, the thrust bearing amplitude is assumed to be of the same order of magnitude as the radial variation.

During the next to last run the helium pressure to the thrust bearing was inadvertantly allowed to fall below the pressure necessary to support the rotor. The result was that, during coast-down, the rotor came to a violent stop and was thrown against the supporting foils and turbine shroud. The resulting blade contact broke one of the blades. The thrust runner and thrust bearing were scored and the shroud scraped. The shaft is shown in Fig. 18.

The thrust bearing pressure was returned to normal and the remainder of the tests completed. The unit ran smoothly at speed with no noticeable vibration or marked changes in shaft whirl. As the shaft would come to rest, however, the violent motions due to the scored thrust bearing would always occur. The effect on the foils is shown in Fig. 44 and described in section 3.4.

3.2.3 Starting fluid

The starting fluid used for tests conducted early in this program was methyl alcohol. When it became apparent that the probes and strain gages were adversely affected by the electrical properties of alcohol, a new starting fluid, Freon 113, was substituted. Freon, being nonconducting, has no effect on the instrumentation.

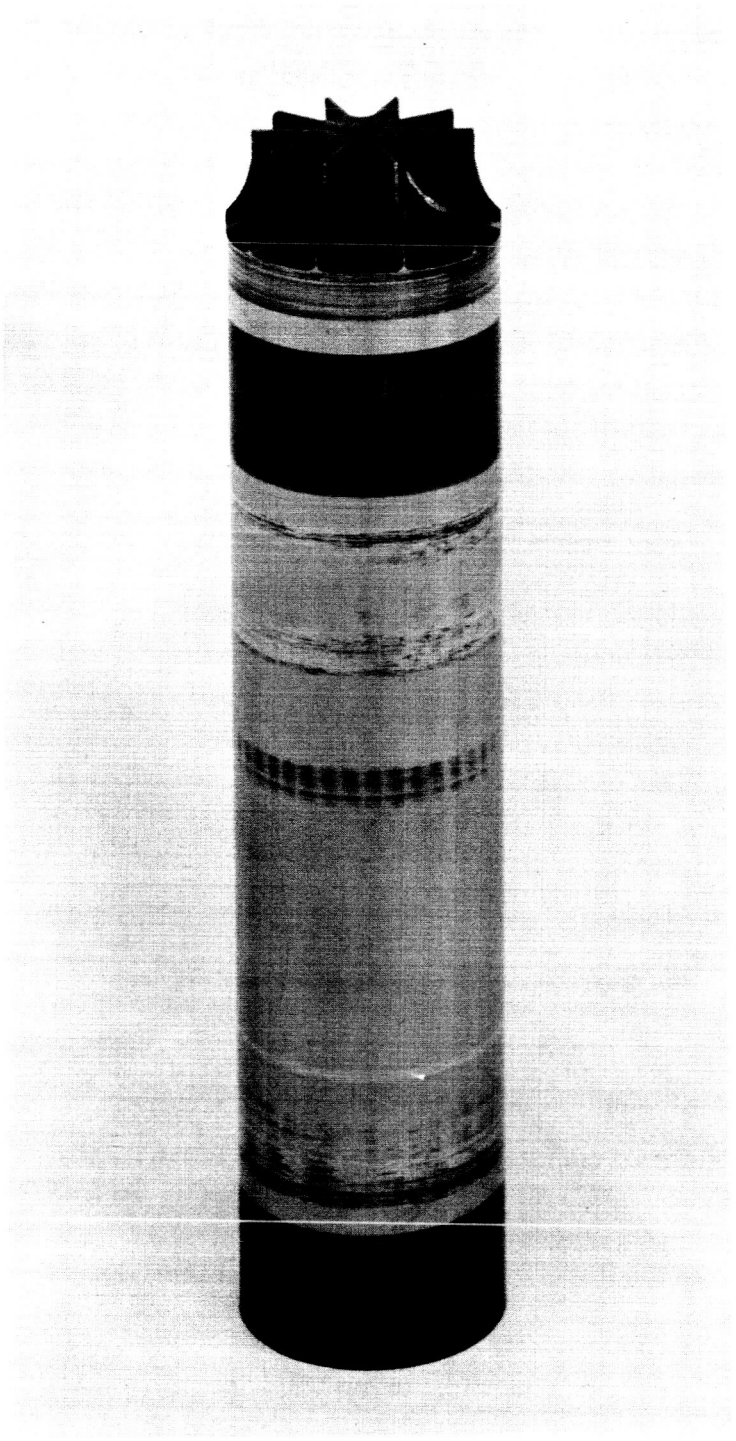

Fig. 18 One-Inch Diameter Rotor After Approximately Two Hours of Running Time and Forty Stop/Start Cycles

3.3 Flexural Critical Speed Rig Test Results

The flexural critical speed test rig was used to spin rotors supported on self-acting, gas-lubricated foil bearings. In this rig the rotor is supported axially by two externally pressurized thrust bearings and radially by two sets of three foil journal bearings. The shaft is rotated by means of gas impingement on the blading cut into the center of the shaft.

Figure 19 shows two of the three rotors used with this test rig. The two rotors shown are of stainless steel. The necked rotor has the same length and diameter as the solid rotor, except for the sections of smaller diameter. Another rotor made from magnesium was constructed to the same dimensions as the necked steel rotor shown in Fig. 19. The measured first free-free, flexural critical speed of the magnesium rotor was 90,000 rpm; the necked stainless steel rotor speed was 100,000 rpm; and the solid stainless steel rotor speed was 336,000 rpm. The free-free frequency vibration was equal to the sound frequency measured after striking shafts, hanging by silk threads, with a hammer.

Several attempts were made to accelerate these shafts through their respective flexural critical speeds. However, when the flexural critical speed of the shaft was approached, the rotor orbit grew until there was contact with the capacitance motion measuring probes. At this point, all of the shafts experienced violent low frequency oscillations. It was not possible to exceed this flexural critical speed with any of the shafts.

To accelerate the solid stainless steel rotor to its flexural critical speed (approximately 360,000 rpm) it was necessary to drive the turbine with helium gas.

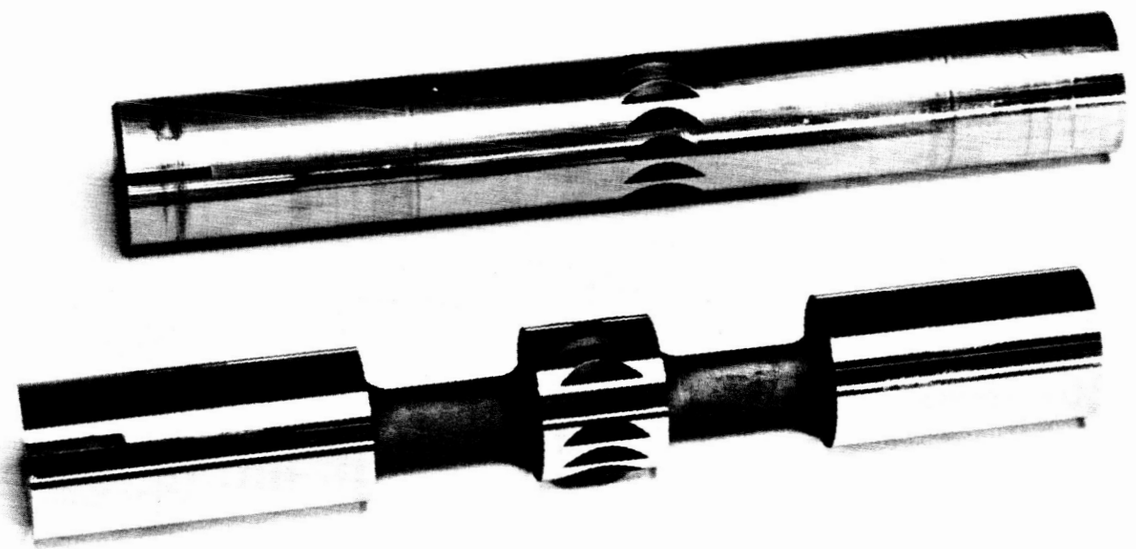

Fig. 19 Flexural Shafts with Free-Free Critical Speeds of 100,000 and 336,000 rpm

Figure 20 shows relative orbital growth of the solid rotor. Figure 21 shows the orbital motion from 121,000 to 298,000 rpm. There was no noticeable change in orbit size over this range of rotational speeds, and at no point during the tests did the orbits exhibit half-frequency whirl instability. The fractional frequency whirl at the flexural critical speed is shown in Fig. 22. This same fractional frequency whirl is shown again at lower shaft speed in Fig. 23. The frequency of this whirl is nearly constant; it is associated with the natural frequency of the mass of the rotor and the stiffness of the lubricating film and foil supports. Small frequency variations occurred which were apparently caused by foil tension changes. These changes were the result of the rubs and violent motions experienced at critical speeds. The foil tension may have varied throughout the tests in the flexural speed test rig. Due to the manner in which the foils are mounted, the tension is a nonlinear function of deflection. It would seem reasonable, therefore, to expect changes in the fractional frequency whirl as the shaft orbit varies. In Figs. 24 and 25 the fractional frequency whirl is shown for lower shaft speeds.

Figure 26 shows the orbital motions of the solid steel rotor during and after a sharp impact to the test rig. The decay record has a predominant 170-cps component. Since the experimental whirl frequencies were from 154 to 218 cps, this data further supports the hypothesis that all of the fractional frequency whirling motions were associated with the mass of the rotor and the low positional stiffness of the self-acting foil bearing used to support the rotor. This is confirmed by the data shown in Fig. 26, which was obtained after impacting the shaft-bearing assembly and observing the decaying motion. The frequency of the decay corresponds to the whirl frequency which appears during the fractional frequency whirl of the rotor bearing system.

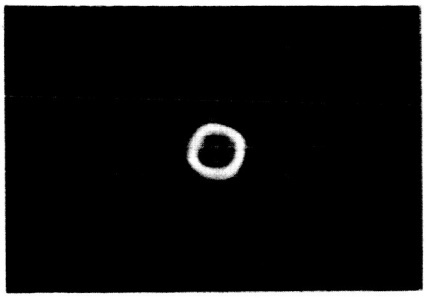

a) Rotational Speed: 120,000 rpm

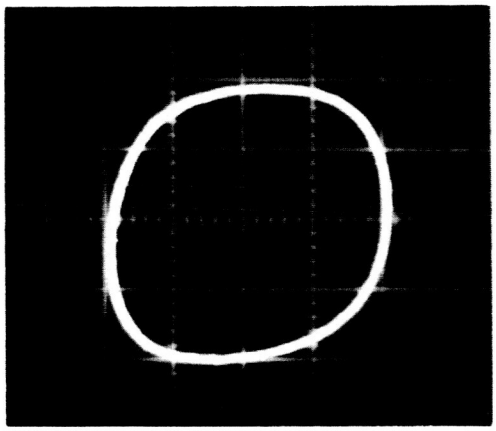

b) Rotational Speed: 347,000 rpm
(Approaching the Free-Free
Critical Speed of the Shaft)

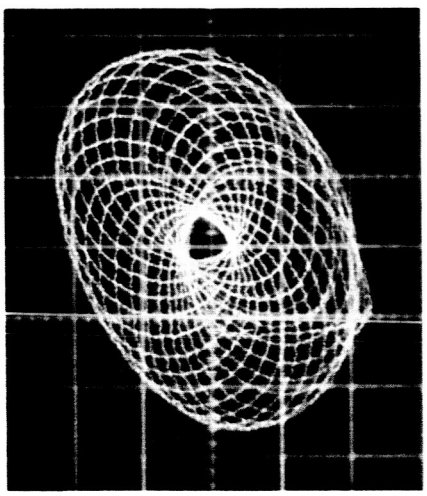

c) Rotational Speed: 347,000 rpm
(Near Shaft Free-Free Critical
Speed, Showing Subharmonic Motion)

Fig. 20 Lissajous Patterns Showing Orbits of Rotors Supported on Foil Bearings

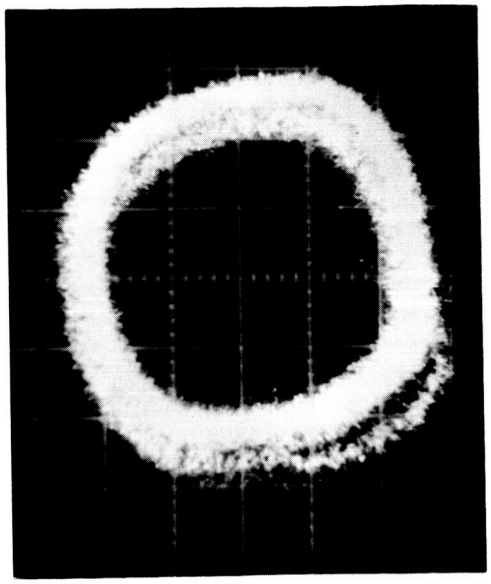

Rotational Speed = 121,000 rpm
y = 0.2 volt/cm

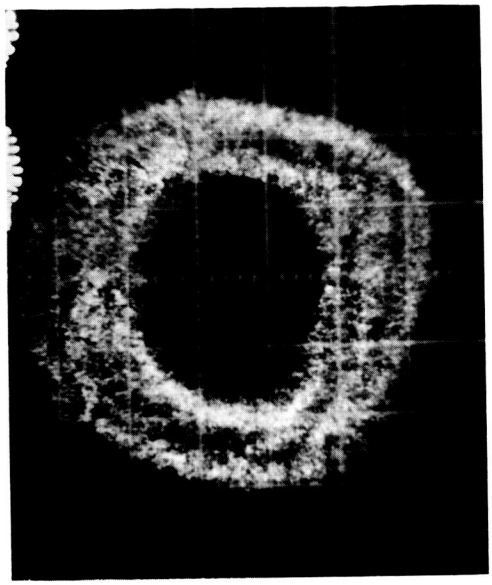

Rotational Speed = 180,048 rpm
y = 0.2 volt/cm

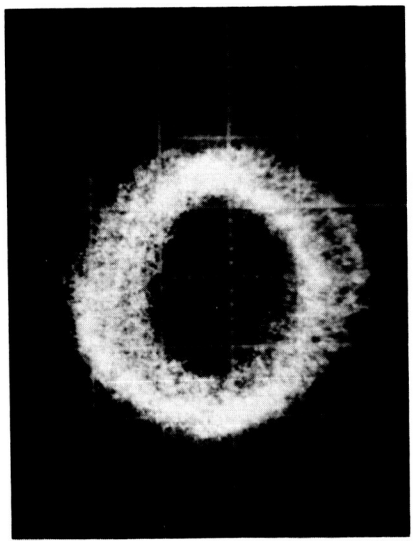

Rotational Speed = 240,216 rpm
y = 0.2 volt/cm

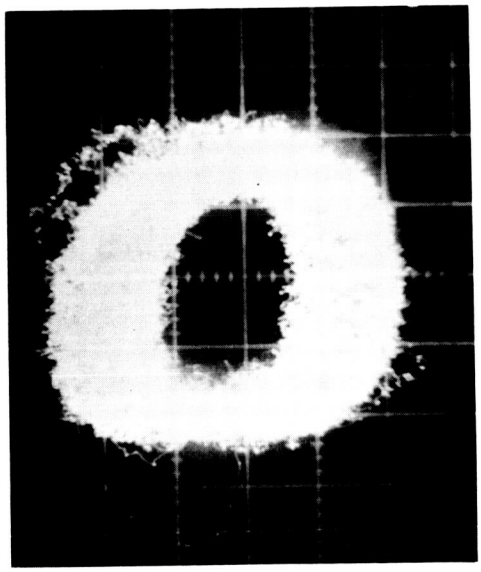

Rotational Speed = 298,800 rpm
y = 0.2 volt/cm

Fig. 21 Orbital Motion of 5/8 in. Diameter by 4.5 in. Long Shaft Supported on Helium Lubricated, Self-Acting Foil Bearings

RR 66-21

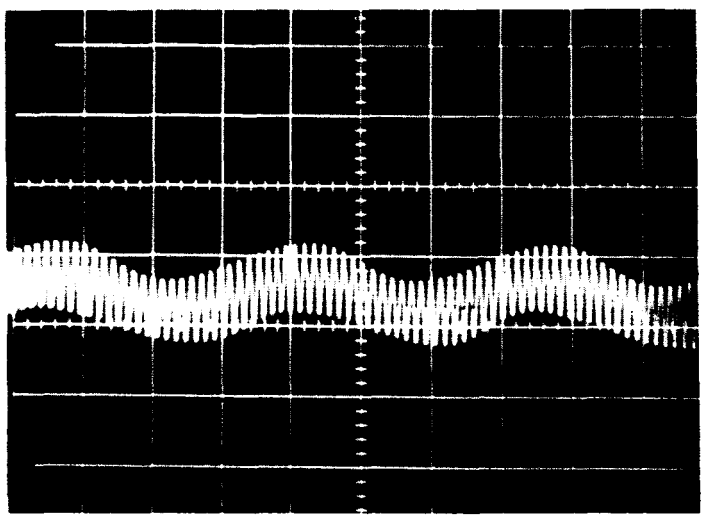

Rotational Speed = 359,000 rpm
y = 5 volts/cm
x = 10 microsec/cm
Rotational Frequency = 5968 cps
Whirl Frequency = 218 cps
Gas: Helium

Fig. 22 Shaft Motion at 359,000 rpm Showing Fractional Frequency and Synchronous Free-Free Critical Whirl

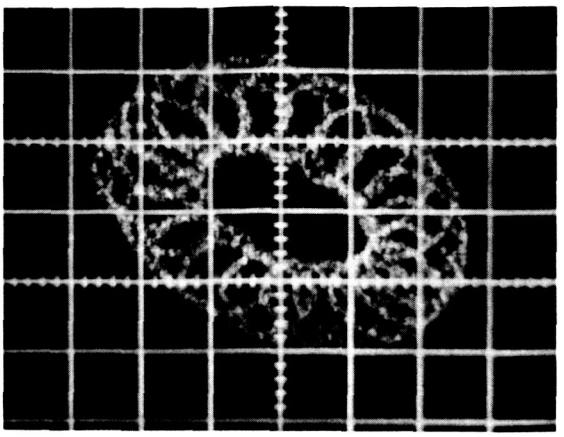

Rotational Speed = 265,000 rpm
x,y = 0.5 volt/cm
Rotational Frequency = 4408 cps
Whirl Frequency = 206 cps
Gas: Helium

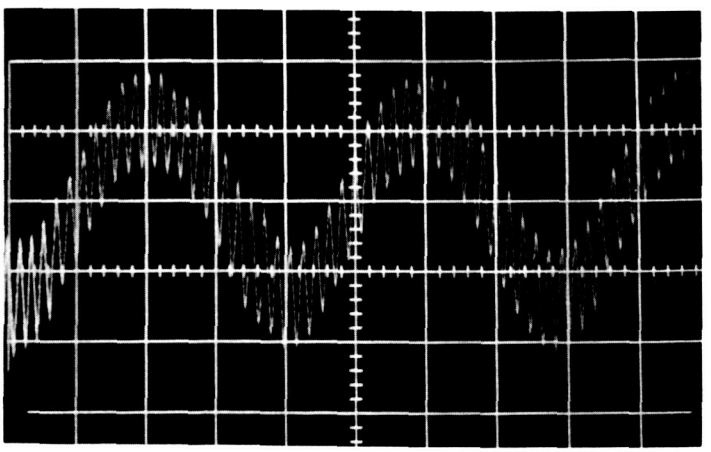

Rotational Speed = 265,000 rpm
y = 0.5 volt/cm
x = 10 millisec/cm (1/8)
Rotational Frequency = 4408 cps
Whirl Frequency = 206 cps
Gas: Helium

Fig. 23 Orbital Motion of Rotor at 265,000 rpm Fractional Frequency Critical Speed

Rotational Speed = 194,000 rpm
x,y = 0.2 volt/cm
Rotational Frequency = 3232 cps
Whirl Frequency =154 cps
Lubricant: Helium

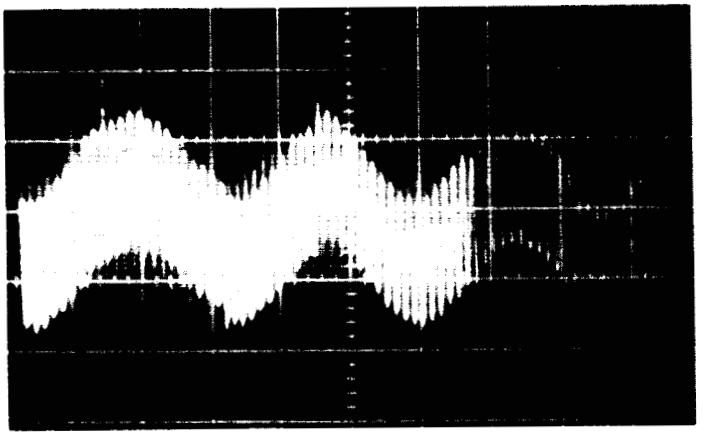

Rotational Speed = 194,000 rpm
y = 15 volt/cm
x = 10 microsec/cm (1/4)
Rotational Frequency = 3232 cps
Whirl Frequency = 154 cps
Lubricant: Helium

Fig. 24 Shaft Orbital Motion at 194,000 rpm Fractional Frequency Whirl Critical Speed

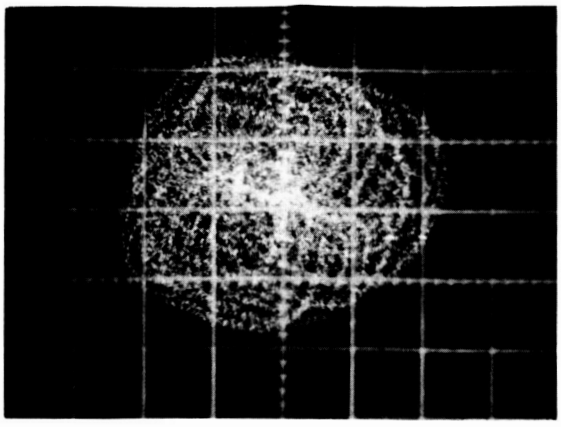

Rotational Speed = 128,000 rpm
x,y = 0.2 volt/cm
Rotational Frequency = 2129 cps
Whirl Frequency = 177 cps
Lubricant: Air

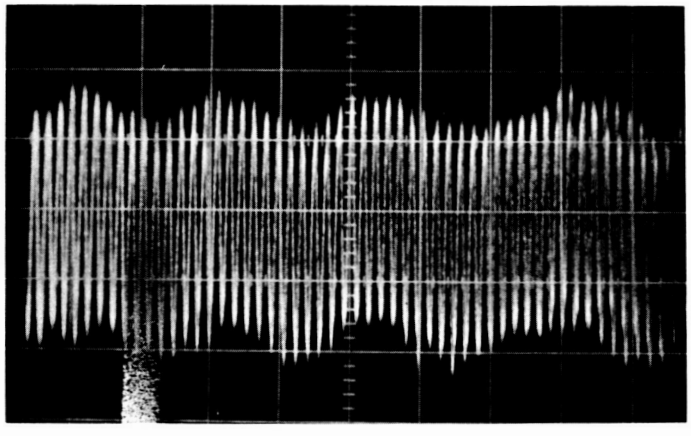

Rotational Speed = 128,000 rpm
y = 0.2 volt/cm
x = 10 millisec/cm
Rotational Frequency = 2129 cps
Whirl Frequency = 177 cps
Lubricant: Air

Fig. 25 Shaft Orbital Motion at 128,000 rpm Fractional Frequency Whirl Critical Speed

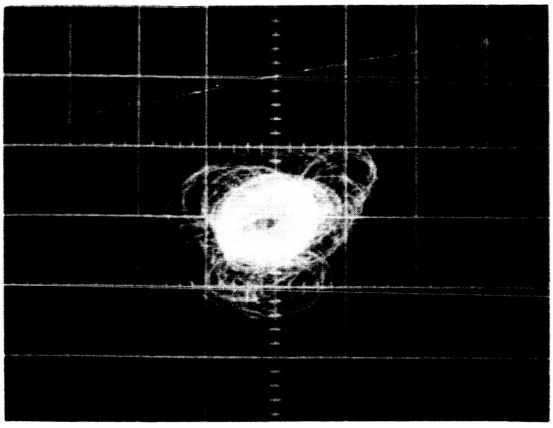

Rotational Speed = 127,000 rpm
x, y = 0.5 volt/cm
Rotational Frequency = 2129 cps
Whirl Frequency = 170 cps
Lubricant: Air

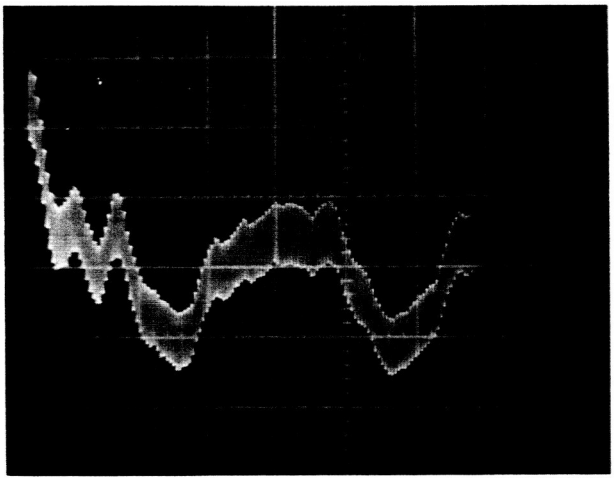

Rotational Speed = 127,000 rpm
y = 0.5 volt/cm
x = 10 millisec/cm
Rotational Frequency = 2129 cps
Whirl Frequency = 170 cps
Lubricant: Air

Fig. 26 Shaft Orbital Motion at 127,000 rpm, After Impact

For the shaft supported on a foil journal bearing, shaft-to-whirl speed ratios as high as 47:1 have been observed. These fractional frequency whirls appear to be a type of critical speed; i.e., during acceleration or deceleration of the rotor, the orbit goes from a nearly circular single frequency orbit to one containing components of shaft speed plus this fractional frequency whirl speed. The speed range over which this takes place is very narrow, usually less than 1% change in speed. The orbits have, thus far, always been bounded and not excessive. The occurrences of these fractional frequency whirl criticals are repeatable, and they can occur during acceleration of the rotor or during deceleration when the turbine driving air is disconnected. In all cases, the frequency of the subharmonic whirl has been associated with the radial support stiffness of the foil journal bearings.

Because of the sharpness with respect to speed of the occurrence of the whirl critical speeds, one would assume that a relationship should exist between the rotational speed and the occurrence of the whirl critical; i.e., with nonlinear support spring characteristics, subharmonic oscillations are possible. However, the ratio of the fundamental frequency of vibration to the subharmonic oscillation frequency is usually limited to less than 5.0. Since the whirl ratios obtained experimentally were of the order of 30:1, an experimental approach to determine the reason for the coupling of the energy associated with the high-frequency rotational speed to the low-frequency critical speed was attempted.

Figure 27 shows a three-dimensional plot of time vs frequency vs amplitude, with amplitude represented by contour lines*. The data presented in this figure is the output of one of the capacitance probes and was taken while the test rig was accelerating in speed on helium. It is representative of Figs. 20b and 20c. Frequencies are marked in KHz on

*Signatection Research, Inc., Waltham, Mass.

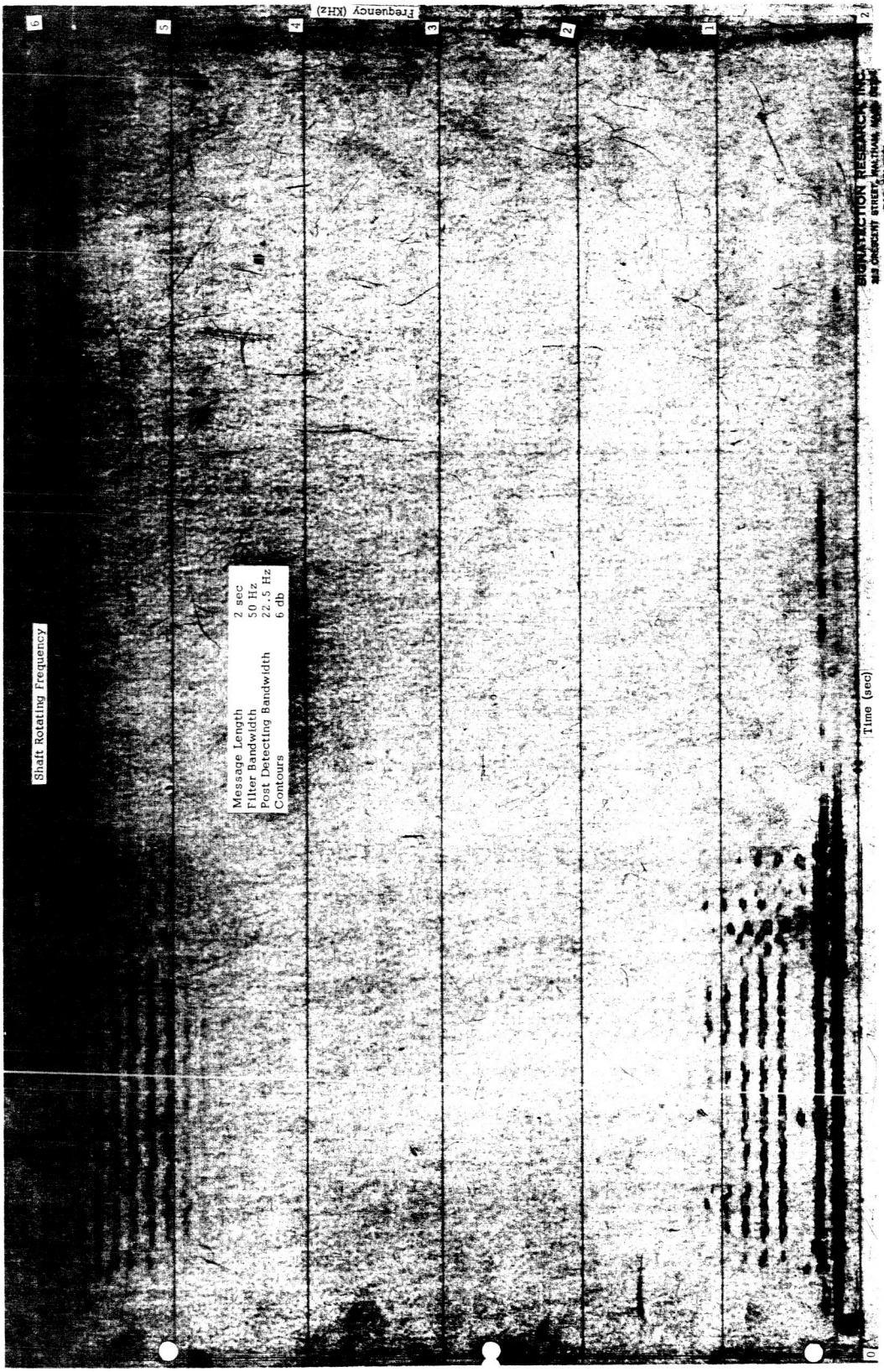

Fig. 27 Frequency-Amplitude-Time Plot of Data Used to Obtain Figs. 20b and 20c

the right side of the figure, and the sample time (the horizontal axis) represents two seconds of real time. It can be seen that there is a short period (approximately 0.3 sec) in which low-frequency motion occurs. The fundamental frequency (approximately 100 cps) and several of its harmonics appear in the lower left corner of the figure. It is readily apparent that the high-shaft-rotational speed acquires the upper and lower sidebands of this low-frequency modulation (upper left corner of Fig. 27).

Figure 28 shows the same data as Fig. 27, but with the frequency scale expanded. Here it can be seen that the appearance of the high amplitude, low frequency motion is very rapid, the frequency spectrum appearing and disappearing almost instantaneously. The upper portion of the curve in Fig. 28 shows that there was essentially no speed change associated with the appearance and disappearance of this fractional frequency whirl. Figure 29 shows similar data; the time scale presented shows acceleration of the shaft from left to right as far as the center of the figure, with deceleration shown thereafter. Here it can be seen that the fractional frequency whirl occurred on the accelerating portion of the curve with a sharp cutoff as speed was increased; then, as the turbine was disconnected and the shaft allowed to coast down, the whirl once again appeared at the same speed as the cutoff of the whirl. This shows that the shaft rotational speed associated with the occurrence of fractional frequency whirl is the determining factor for this whirl. Figure 30 gives an expanded version of the data of Fig. 29. Again, the cutoff and appearance of the whirl are very sudden.

The information presented in these frequency-spectral-contour plots shows clearly that the occurrence of fractional frequency whirl is a sudden, shaft speed dependent phenomenon and that, with the occurrence of this fractional frequency whirl, energy is transformed from

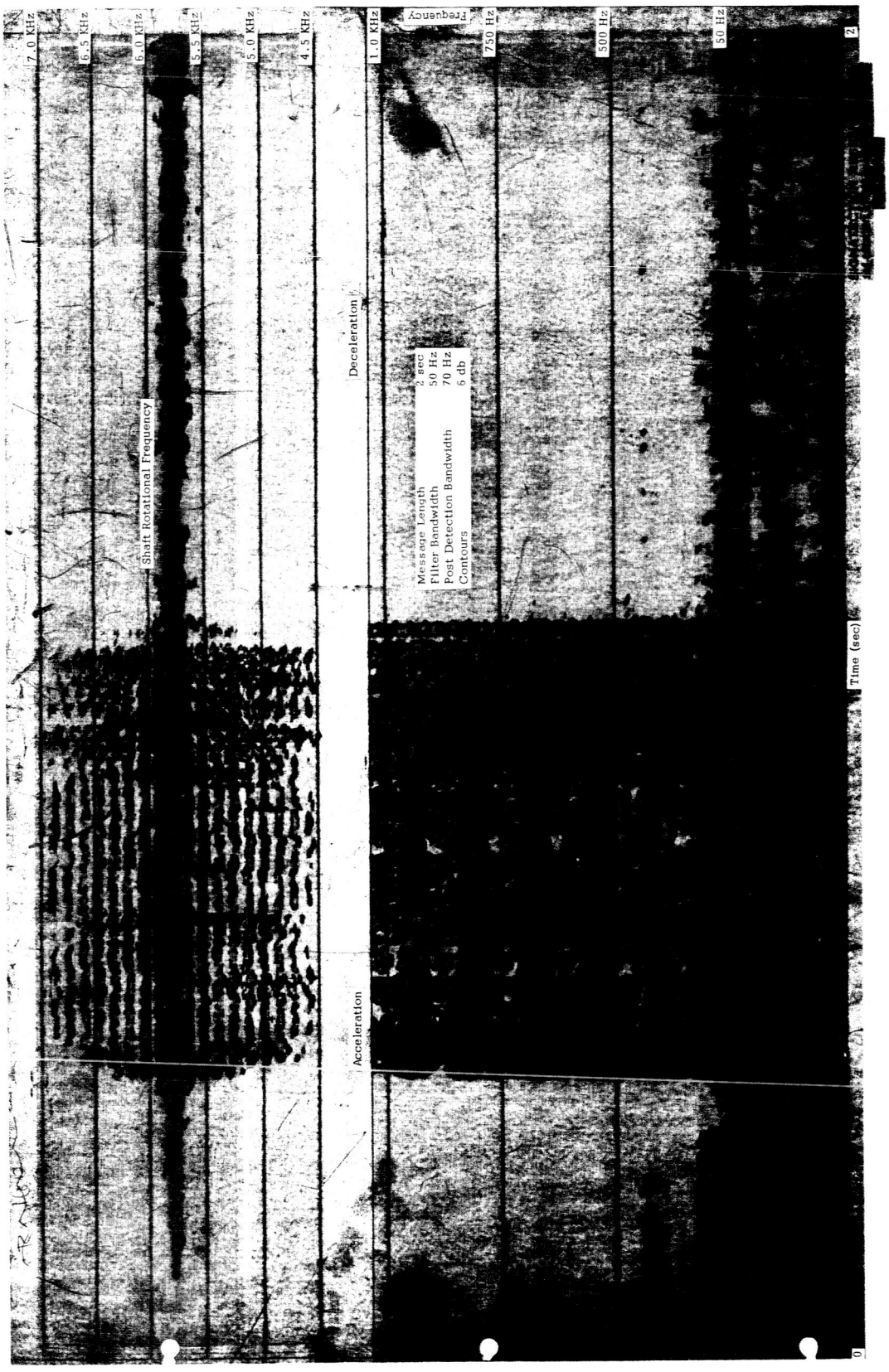

Fig. 28 Expanded Frequency Scale; Frequency-Amplitude-Time Plot of Data Used to Obtain Figs. 20b and 20c

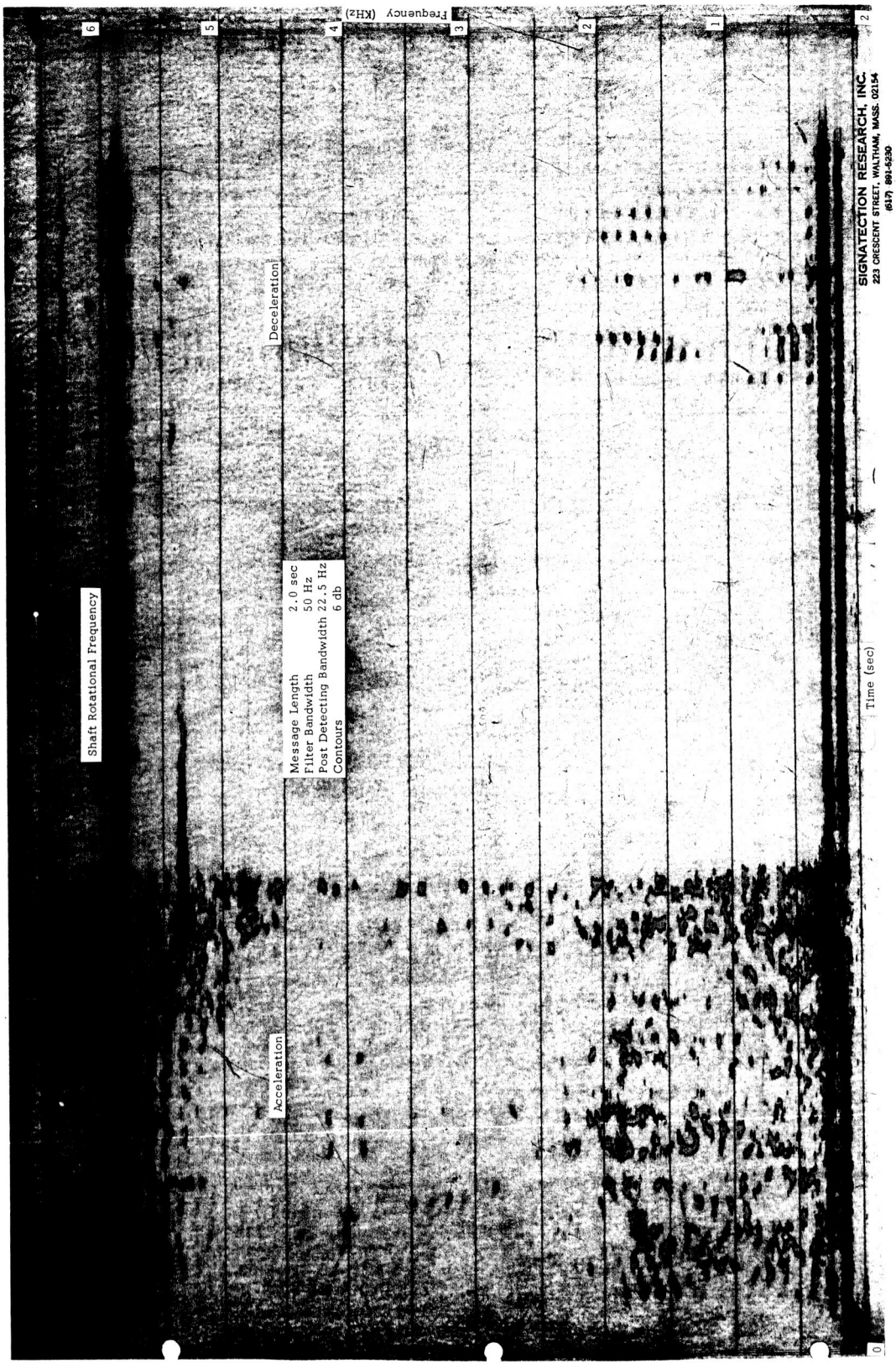

Fig. 29 Frequency-Amplitude-Time Plot Showing the Occurrence of Fractional Frequency Whirl to be Shaft Speed Dependent and Independent of Shaft Acceleration of Deceleration

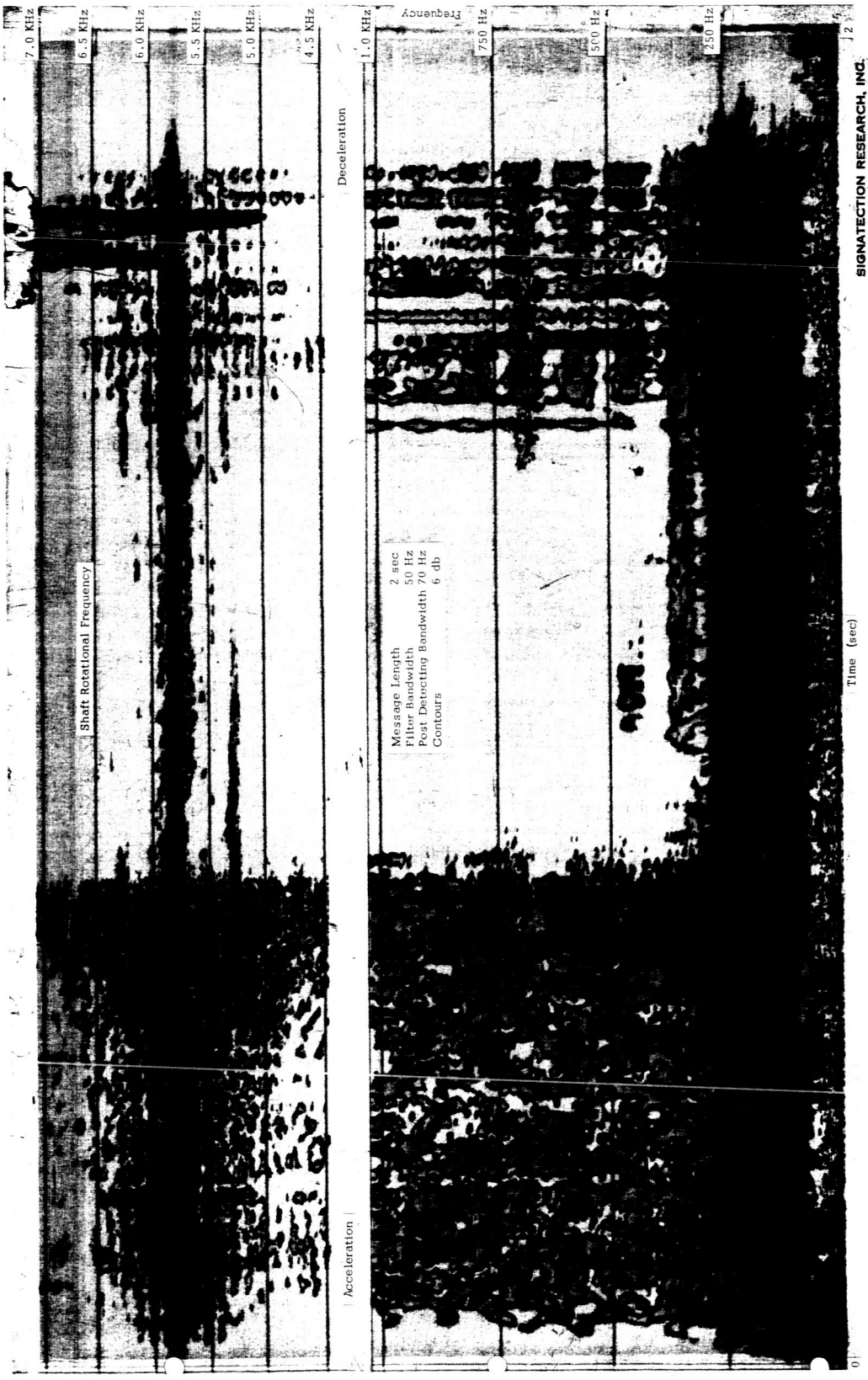

Fig. 30 Expanded Frequency Scale. Frequency-Amplitude-Time Plot Showing Fractional Frequency Whirl to be Shaft Speed Dependent and Independent of Shaft Acceleration or Deceleration

the high-frequency shaft rotational speed to the low-frequency whirl speed. The mechanism and cause of the sudden transfer of energy over such a large frequency span is presently not known. Since fractional frequency whirl appears to be a characteristic of rotors supported on self-acting foil bearings, future work on these bearings should include analytic investigations into this phenomenon to determine its exact cause.

3.4 High-Speed Rig Test Results

Figures 31 through 33 are photographs of orbits and shaft motions taken from the high-speed rig. During a given run, the foil tension and wrap angle were held constant and the speed varied. Foil tension was adjusted while the shaft was rotating at approximately 60,000 rpm. There was no noticeable change in foil tension as speed was increased. Foil tensions of 2.2, 3.1, and 4.0 lbs/in. were used. Wrap angles were 150° and 210°. With 150° wrap, it was possible to make runs with all of the foil tensions. With 210° wrap, however, it was very difficult to start at 3.1 lbs/in. tension, and starts could not be made at all at 4.0 lbs/in. Foil material used throughout this phase of testing was 0.001 in. Havar.

The outputs of the capacitance probes, the dynamometer and rotational speed were all recorded on magnetic tape. The tape speed was always 60 ips when recording. The speed may then be reduced to 30, 15, or 7-1/2 ips when the data is being reproduced.

Figure 31 shows shaft orbits at two speeds with air lubrication and whirl frequencies at high speed with helium. The magnitude of the excursions may be found from the vertical scale. At 240,000 rpm the maximum radial excursion is approximately 0.001 in. Figure 32 shows orbital motions with whirl frequencies displayed alongside for comparison. As in Fig. 31, the predominant whirl frequency is approximately 108 cps.

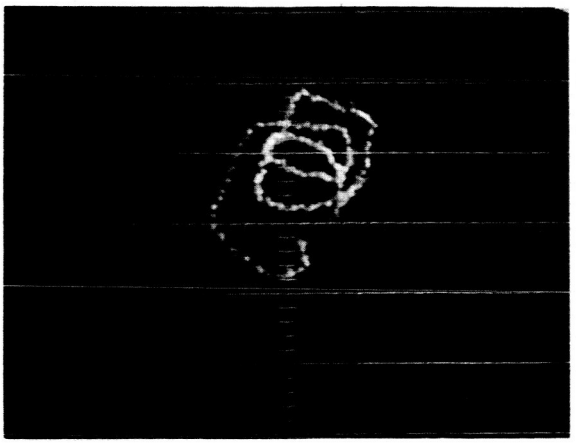

Rotational Speed = 34,000 rpm
x,y = 50 microin/cm
Lubricant: Air

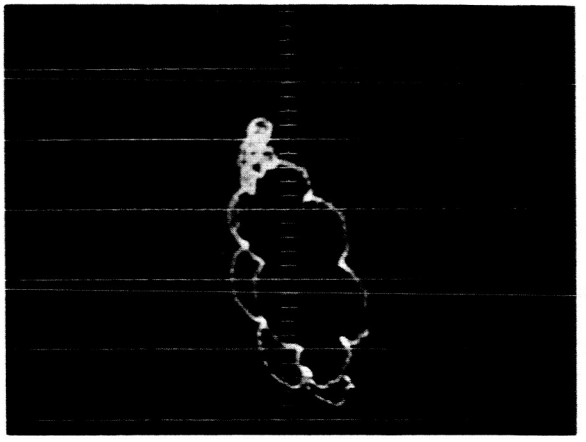

Rotational Speed = 97,000 rpm
x, y = 250 microin/cm
Lubricant: Air

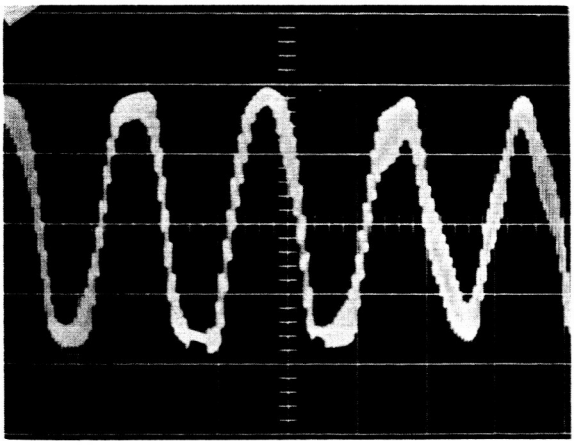

Rotational Speed = 240,000 rpm
x = 20 millisec/cm
y = 500 microin/cm
Whirl Frequency = 108 cps
Turbine On
Lubricant: Helium

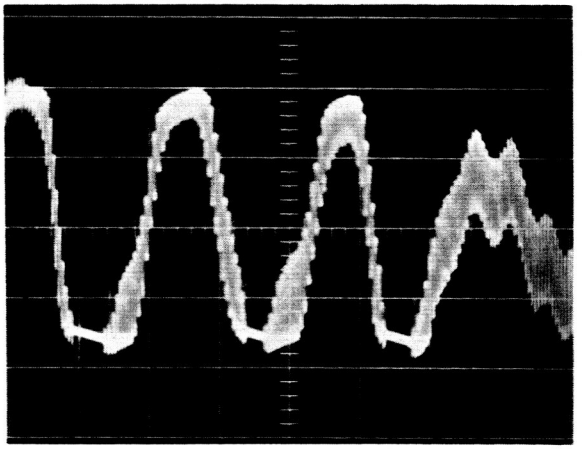

Rotational Speed = 240,000 rpm
x = 20 millisec/cm
y = 500 microin/cm
Whirl Frequency = 108 cps
Turbine Off
Lubricant: Helium

Fig. 31 Orbital Motion of 1 in. Diameter Shaft Supported on Air and Helium Lubricated Self-Acting Foil Bearings. Wrap Angle = 210°, Foil Tension = 2.20 lb/in.

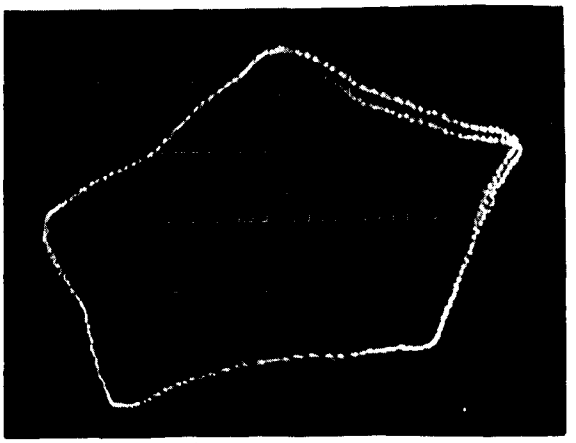

Rotational Speed = 25,600 rpm
x, y = 100 microin/cm
SR/W = -4

Rotational Speed 26,200 rpm
x = 10 millisec/cm
y = 100 microin/cm
Whirl Frequency = 108 cps

Rotational Speed = 71,500 rpm
x,y = 100 microin/cm
SR/W = -4

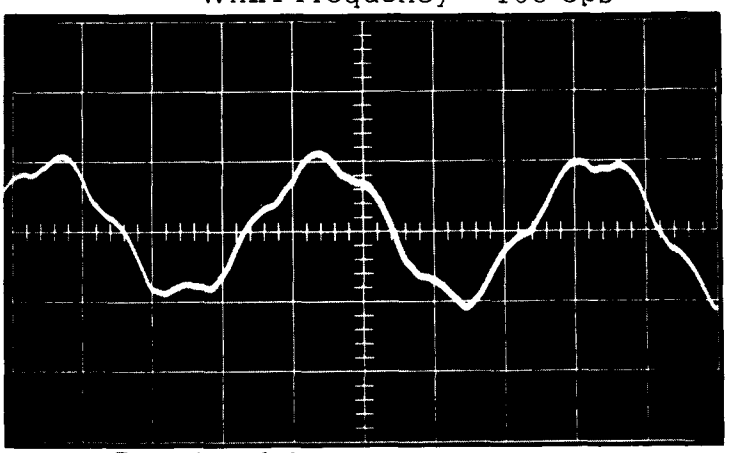

Rotational Speed = 71,500 rpm
x = 10 millisec/cm
y = 250 microin/cm
Whirl Frequency = 107 cps

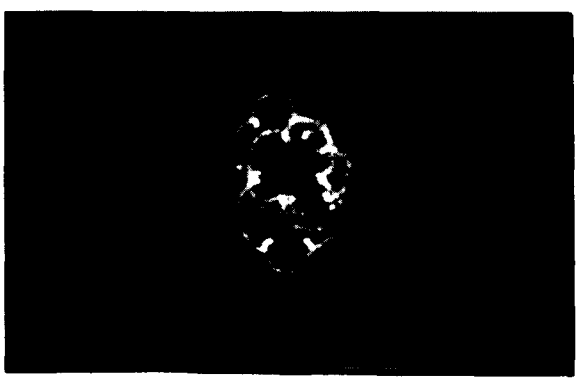

Rotational Speed = 97,000 rpm
x, y = 250 microin/cm
SR/W = 7

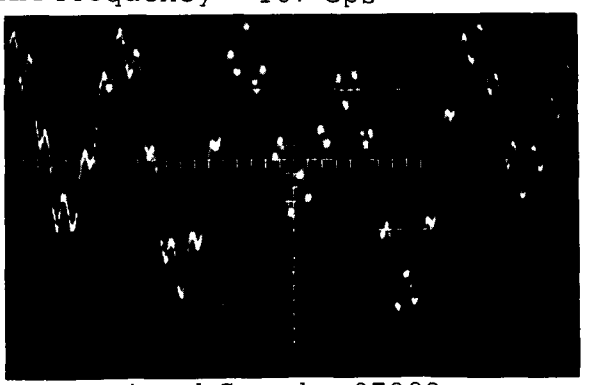

Rotational Speed = 97000 rpm
x = 10 millisec/cm
y = 100 microin/cm
Whirl Frequency = 240 cps

Fig. 32 Orbital Motion of 1 in. Diameter Shaft Supported on Air Lubricated, Self-Acting Foil Bearings. Wrap Angle = 210°, Foil Tension = 2.20 lb/in.

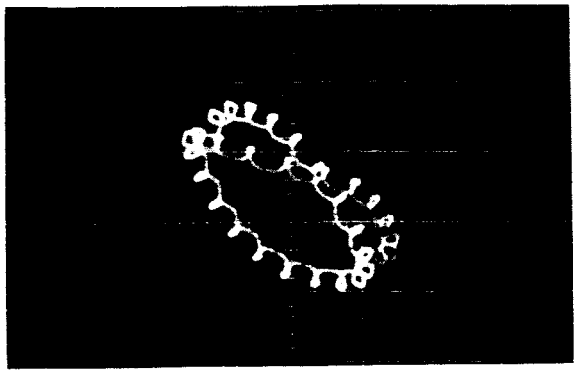

Rotational Speed = 71,600 rpm
x,y = 250 microin/cm
150° Wrap, 2.2 lb/in. tension
SR/W = -18

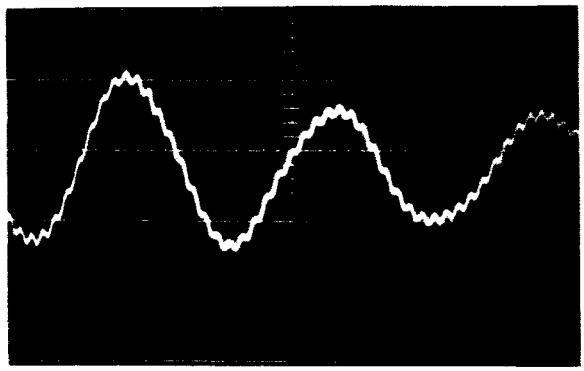

Rotational Speed = 71,600 rpm
x = 20 millisec/cm; y = 500 microin/cm
Whirl Frequency = 68 cps
150° Wrap, 2.2 lb/in. tension

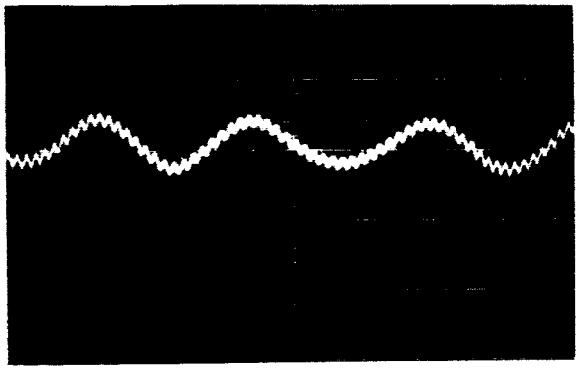

Rotational Speed = 89,500 rpm
x = 20 millisec/cm; y = 500 microin/cm
Whirl Frequency = 84 cps
150° Wrap, 3.1 lb/in. tension

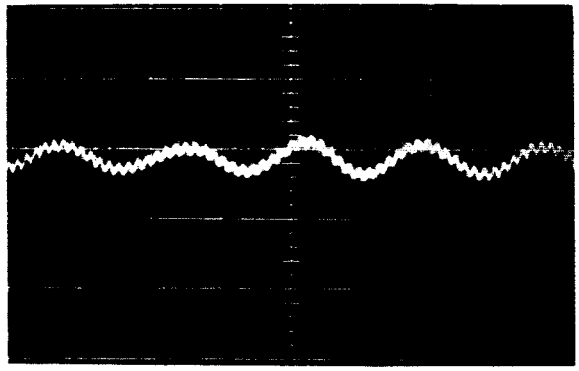

Rotational Speed = 89,300 rpm
x = 20 millisec/cm; y = 500 microin/cm
Whirl Frequency = 116 cps
150° Wrap, 4.0 lb/in. tension

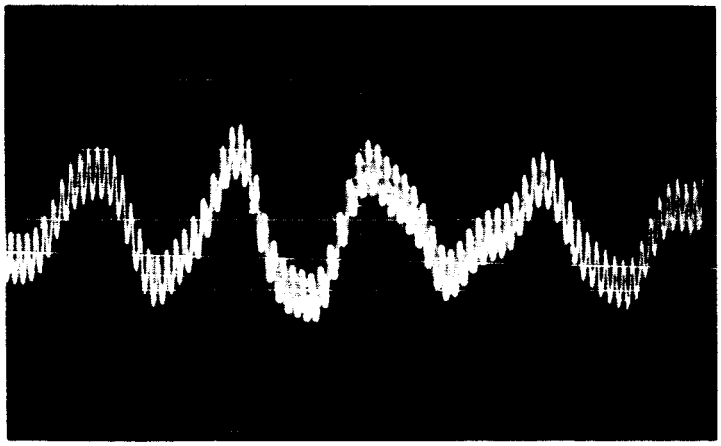

Rotational Speed = 94,000 rpm
x = 20 millisec/cm; y = 500 microin/cm
Whirl Frequency = 92 cps
210° Wrap, 2.2 lb/in. Tension

Fig. 33 Impact Response of 1 in. Diameter Shaft, Varying as a Function of Foil Wrap Angle and Foil Tension.

Figure 33 is a comparison of the impact response at various wrap angles and foil tensions. As would be expected, as foil tension and wrapping increase, so does the frequency at which the system whirls after impact. The orbit shown in Fig. 33 is typical of those for all conditions immediately after impact.

Figures 34 through 37 are from test data taken during the last quarter. The data was taken only while the foils were operating in a helium atmosphere. As shown in earlier test results, the largest amplitude whirl orbit occurs at approximately 100 cps. This fractional frequency seems to be a basic system frequency and is a function of the rotor mass and of the stiffness of the lubricating film and foil supports.

During the last quarter of this investigation a computer program was made up that plotted Lissajous patterns as a function of the ratio of shaft speed to whirl speed (SR/W) and the ratio of amplitude (AR). Lissajous patterns are the result of plotting $x = a \sin \omega_s t + b \sin \omega_r t$ and $y = a \cos \omega_s t + b \cos \omega_r t$ where a and b are the geometric and whirl amplitudes, respectively, and ω_s and ω_r are the shaft and whirl rotational frequencies, respectively. Figure 39 shows three x-y plot Lissajous patterns corresponding to those in Fig. 32. The first two plots shown in Fig. 39 are negative whirls, i.e. whirl rotation opposite to shaft rotation, and are characterized by outside loops and SR/W + 1 number of loops. The negative whirls shown are very likely generated by the contact of shaft and foil during the relatively high-amplitude fractional-frequency whirl. This is not a steady state phenomenon. Figure 40 shows a computed plot of the orbit shown at the top of Fig. 33. The orbit shown in Fig. 33 is the result of impact of a small hammer on the exterior of the test rig, and the negative whirl would be expected. Figure 34 is the orbital motion, including the computed plots, of the 1 in. diameter shaft on helium; the ratio of geometric eccentricity to whirl orbit is approximately 0.14.

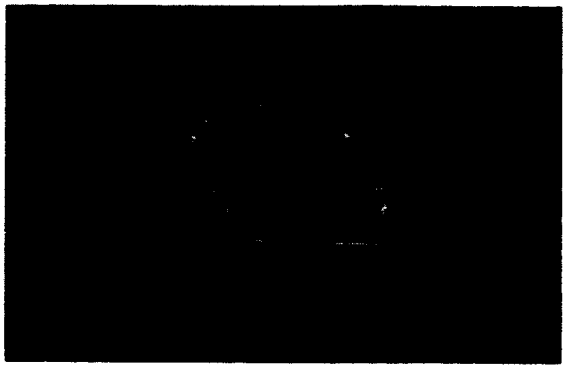

Rotational Speed = 133,000 rpm
x, y = microin./cm
Whirl Frequency = 139 cps

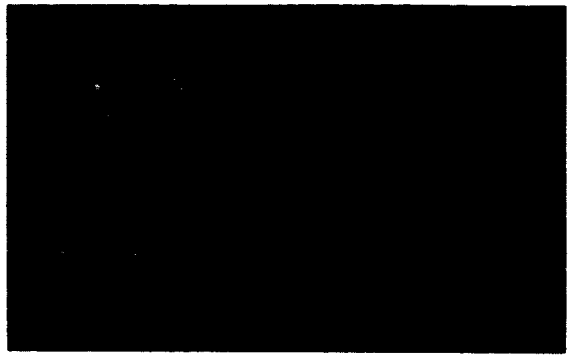

Rotational Speed = 133,000 rpm
x = 10 millisec/cm
SR/W = 16

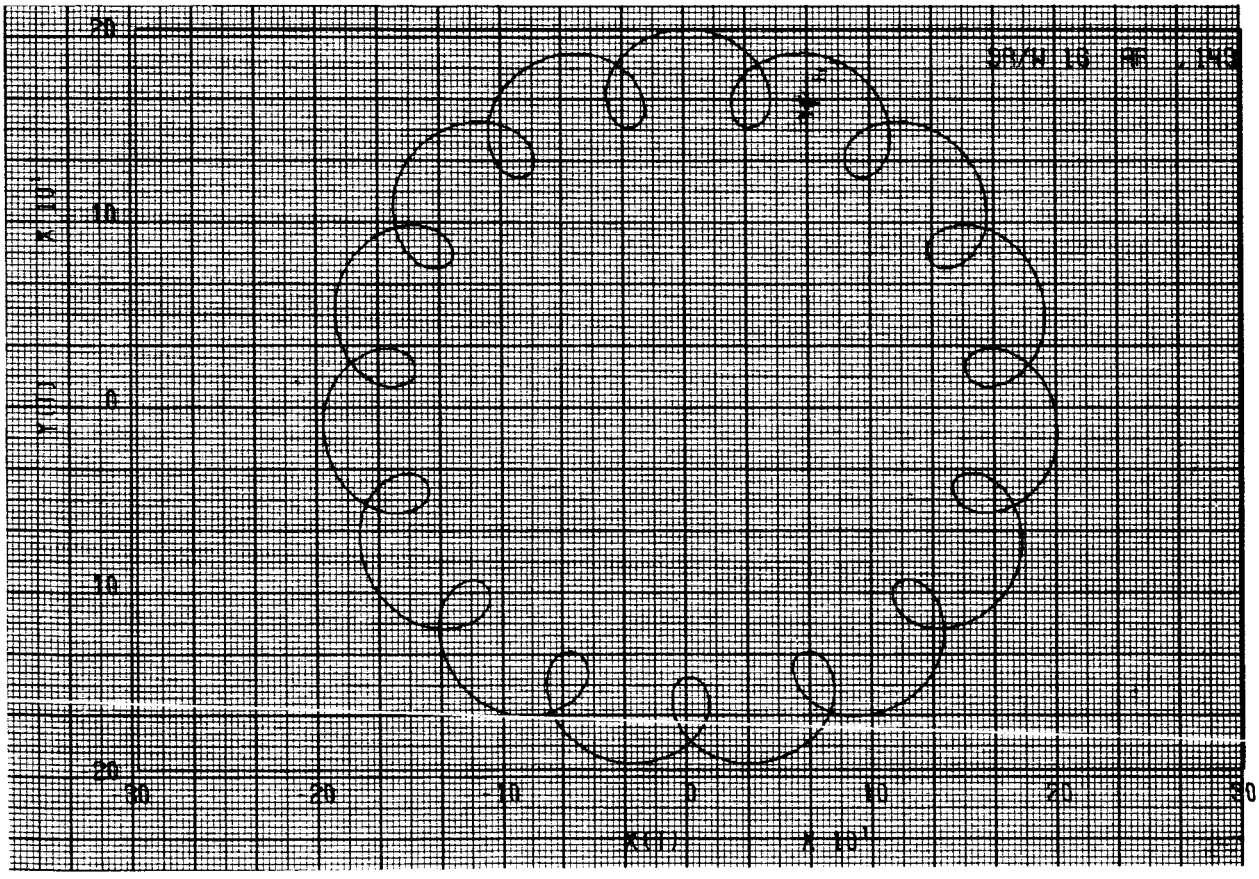

Rotational Speed = 133,000 rpm
x = 10 millisec/cm
SR/W = 16

Fig. 34 Orbital Motion of 1 in. Diameter Shaft Supported on Helium Lubricated, Self-Acting Foil Bearing; Wrap Angle = 150°; Foil Tension = 2.2 lb/in. (Corresponding Computer Plot Included)

RR 66-21

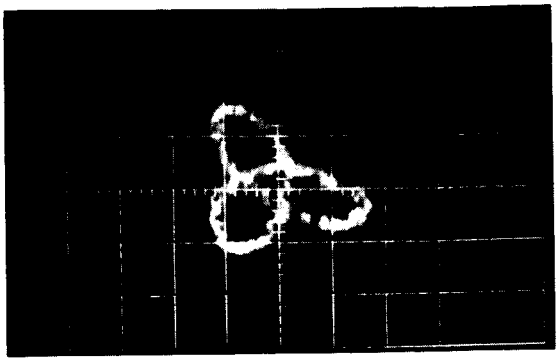

Rotational Speed = 120,000 rpm
x,y = 300 microin./cm
Whirl Frequency = 179 cps

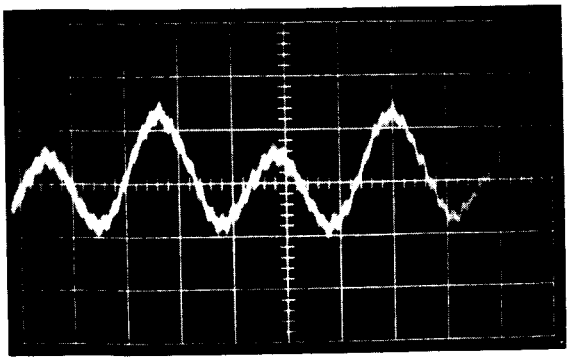

Rotational Speed = 120,000 rpm
x = 10 millisec/cm
SR/W = 11

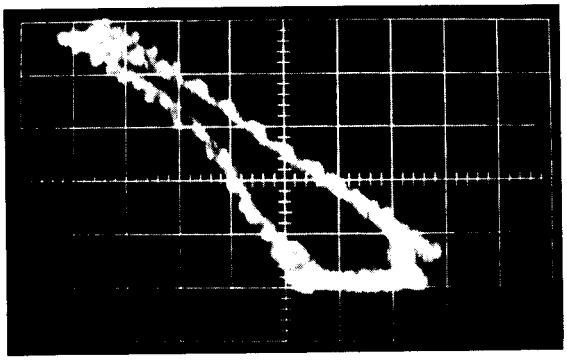

Rotational Speed = 278,000 rpm
x,y = 275 microin./cm
Whirl Frequency = 74 cps

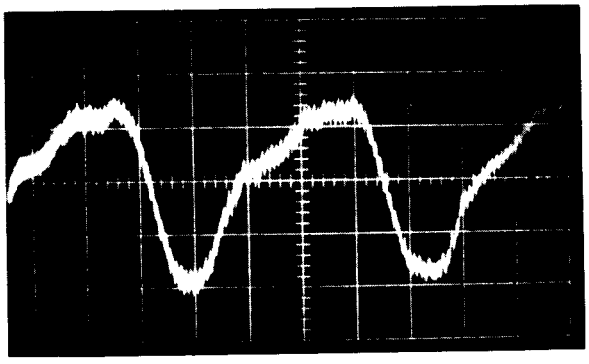

Rotational Speed = 278,000 rpm
x = 10 millisec/cm
SR/W = 62.5

Fig. 35 Orbital Motion of 1 in. Diameter Shaft Supported on Helium Lubricated, Self-Acting Foil Bearing; Wrap Angle = 150°; Foil Tension = 3.1 lb/in.

Rotational Speed = 320,000 rpm
x,y = 275 microin./cm
Whirl Frequency = 102 cps

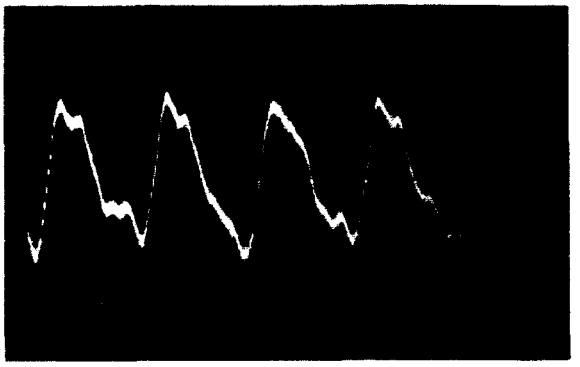

Rotational Speed = 320,000 rpm
x = 10 millisec/cm
SR/W = 42

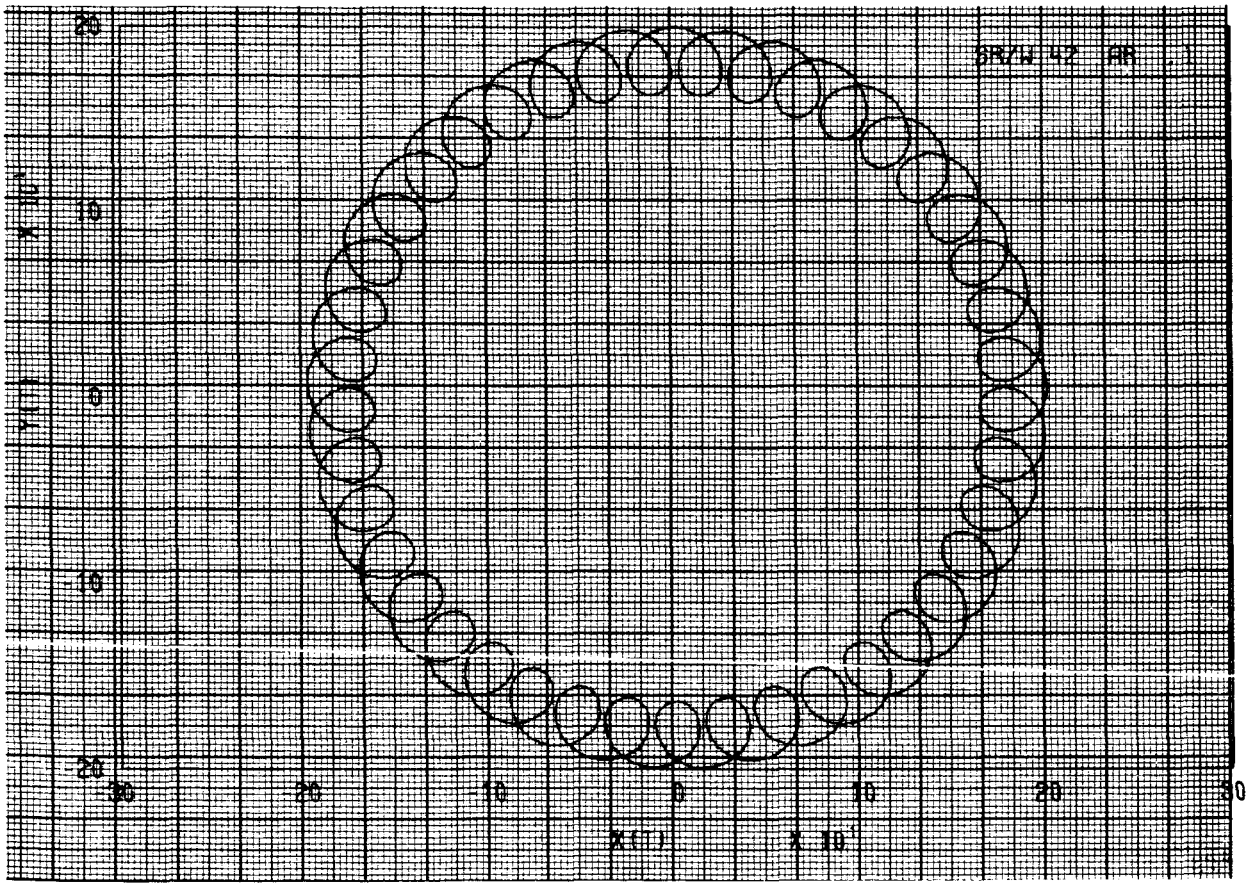

Fig. 36 Orbital Motion of 1 in. Diameter Shaft Supported on Helium Lubricated, Self-Acting Foil Bearing; Wrap Angle = 150°; Foil Tension = 3.1 lb/in. (Corresponding Computer Plot Included)

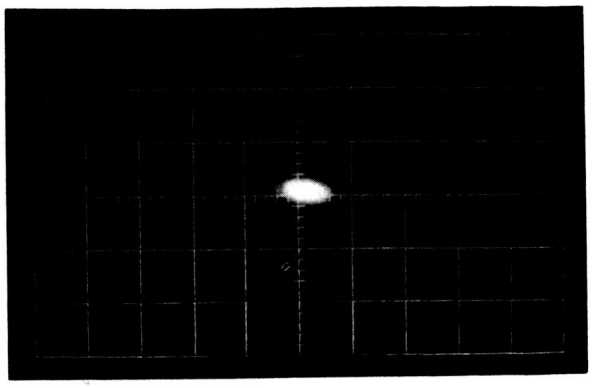

Rotational Speed = 353,000 rpm
x, y = 400 microin./cm

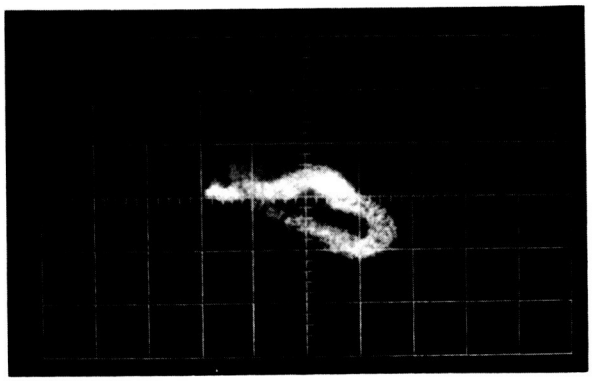

Rotational Speed = 358,000 rpm
x, y = 300 microin./cm
Whirl Frequency = 97

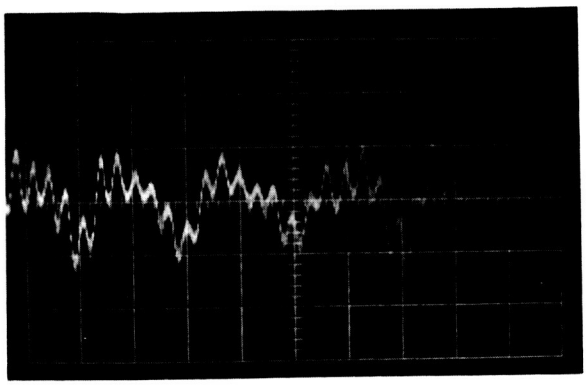

Rotational Speed = 358,000 rpm
x = 10 millisec/cm
SR/W = 62

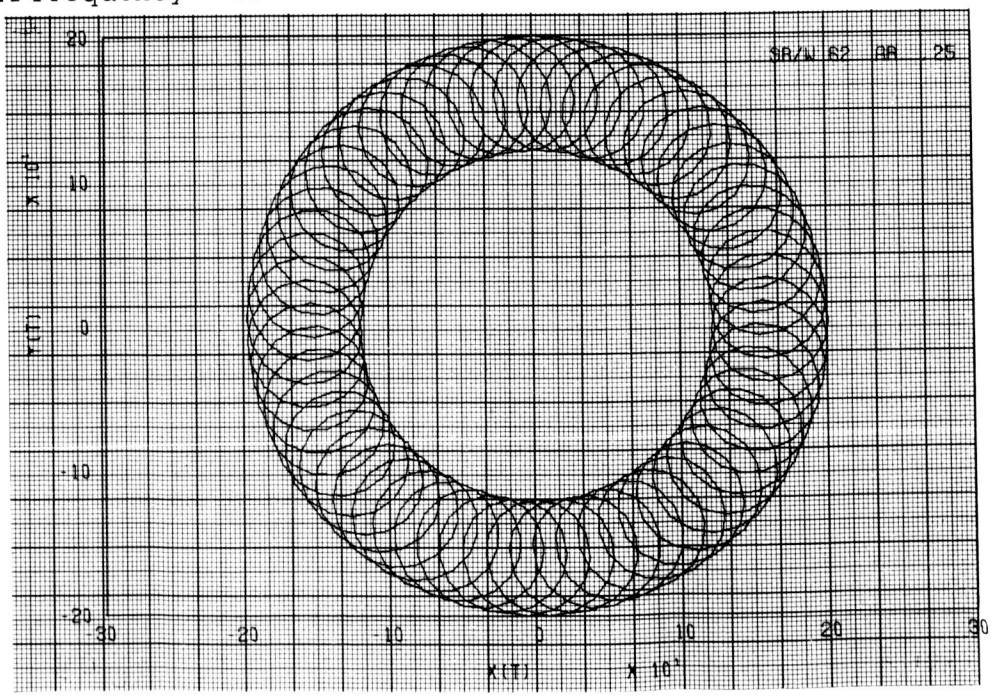

Fig. 37 Orbital Motion of 1 in. Diameter Shaft Supported on Helium Lubricated, Self-Acting Foil Bearing; Wrap Angle = 150°; Foil Tension = 4.0 lb/in. (Corresponding Computer Plot Included)

RR 66-21

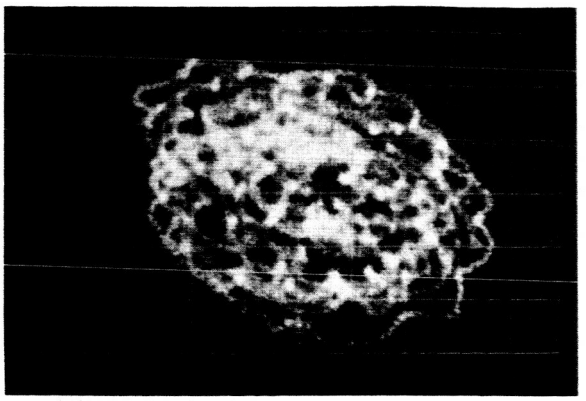

Rotational Speed = 204,000 rpm
x, y = 300 microin./in.
Whirl Frequency = 238 cps

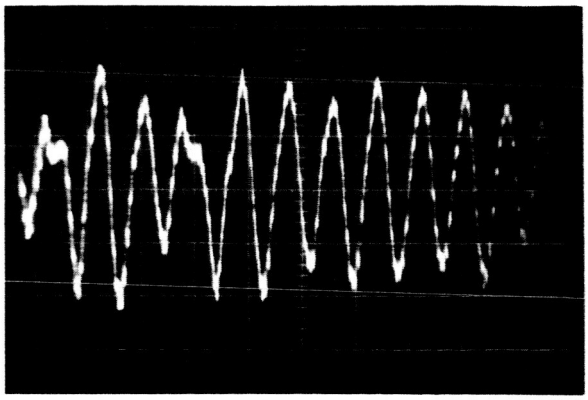

Rotational Speed = 204,000 rpm
x = 10 millisec/cm
SR/W = 16

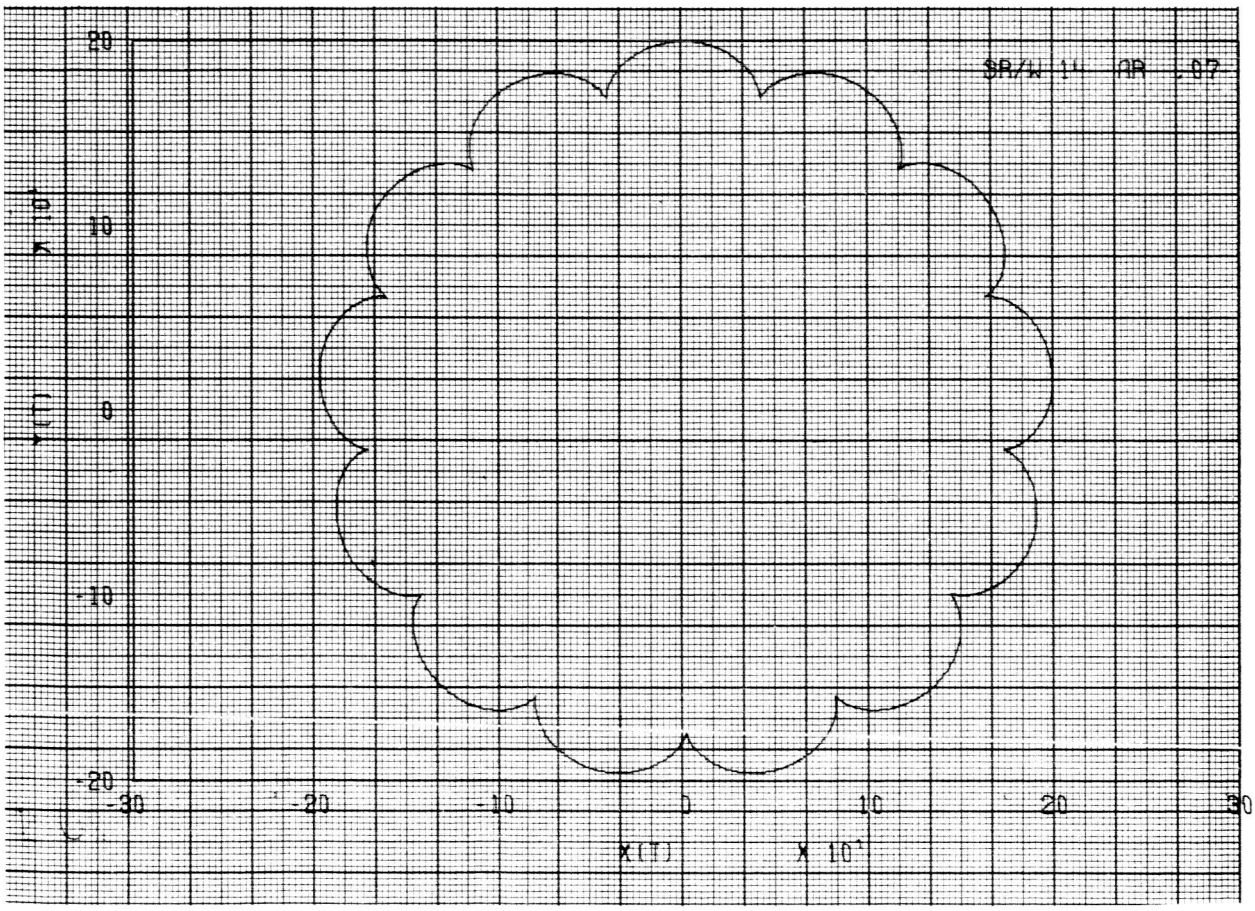

Fig. 38 Orbital Motion of 1 in. Diameter Shaft Supported on Helium Lubricated, Self-Acting Foil Bearing; Wrap Angle = 150°; Foil Tension = 4.0 lb/in. (Corresponding Computer Plot Included)

RR 66-21

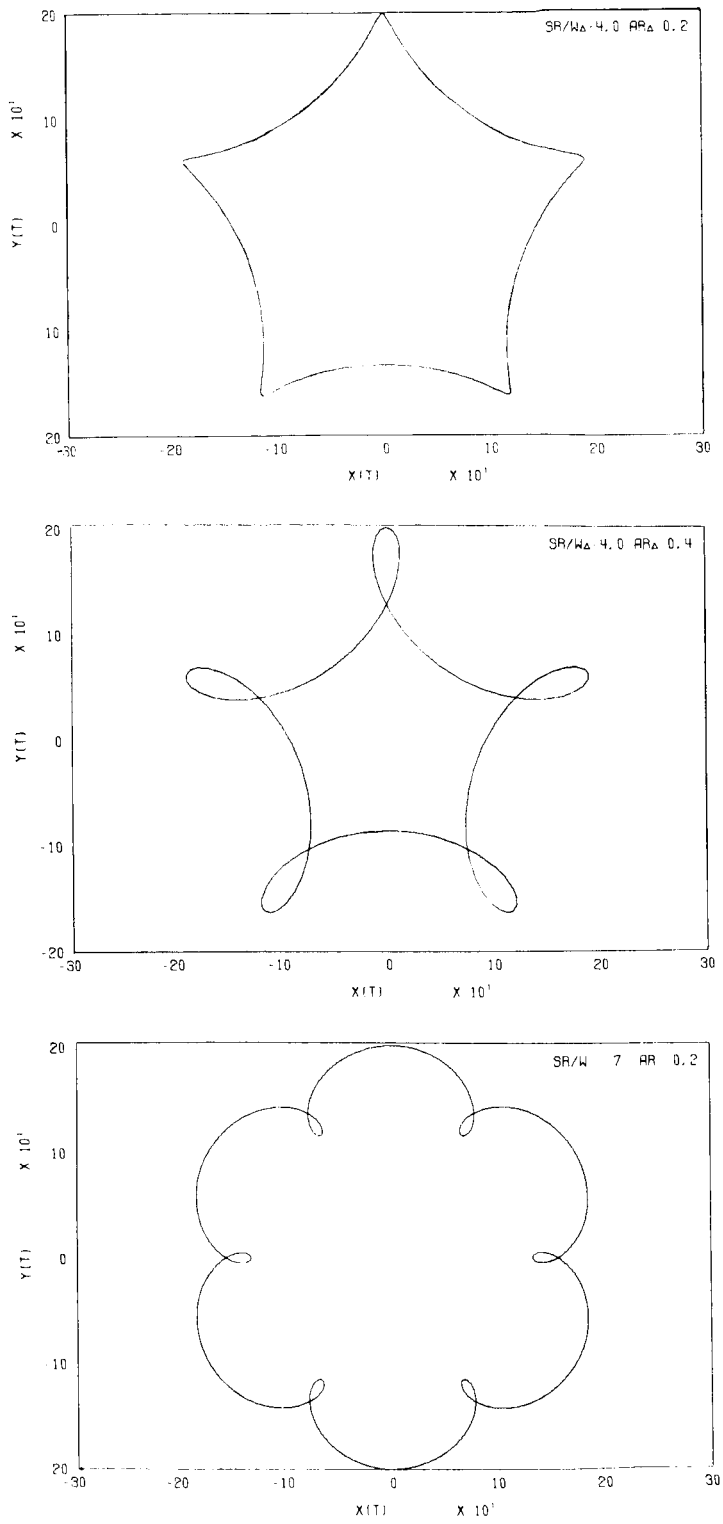

Fig. 39 Computed Lissajous Patterns Corresponding to Those Shown in Fig. 31

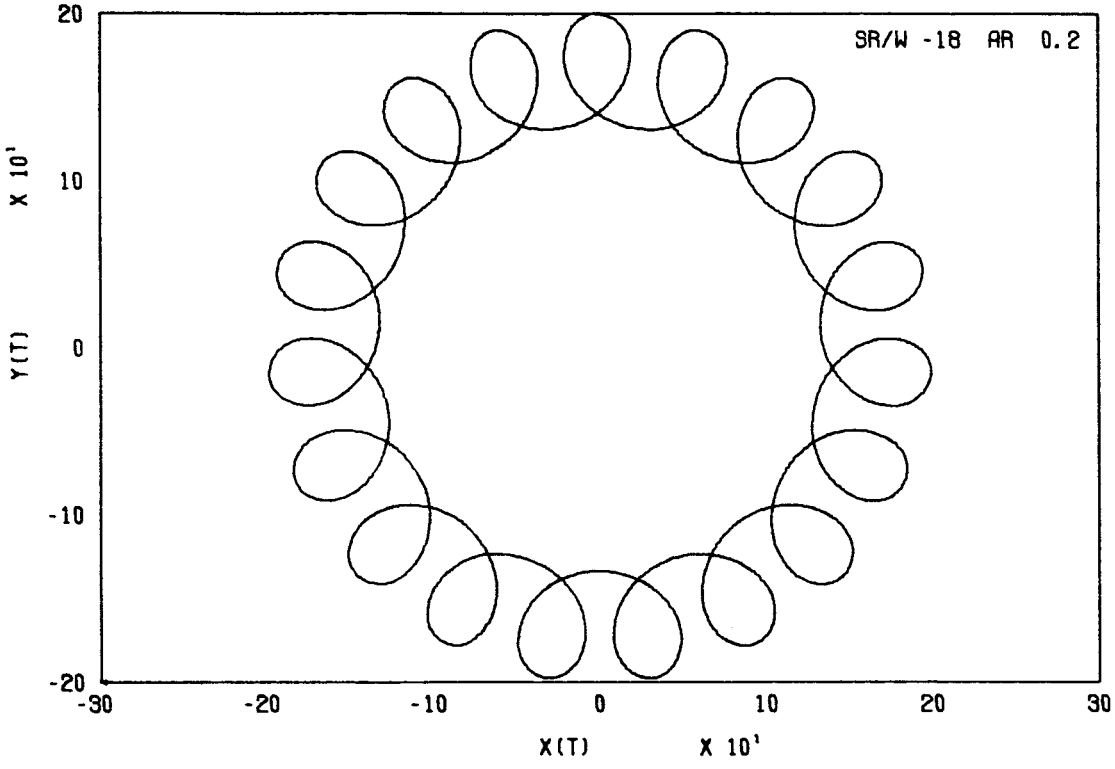

Fig. 40 Computed Lissajous Pattern Corresponding to That Shown at the Top of Fig. 32

Figures 34 through 37 are orbits, some with computed plots, of the 1 in. shaft with various foil tensions, supported on helium lubricated foil bearings.

It is worth noting that the orbit of approximately 0.002 in. shown in Fig. 35 is larger than any shown in Fig. 37 or Fig. 38. These two figures present recorded information taken after the thrust bearing had failed, causing one of the turbine blades to break. It is believed that the higher foil tensions of Figs. 37 and 38 nullified the runout due to the unbalance caused by the broken blade.

Figure 41 is a set of curves showing the variation in torque as a function of speed with various wrap angles and foil tensions. The results shown in Fig. 41 were taken from runs made in air. Figures 42 and 43 are comparisons of theoretical and experimental viscous torques. In all cases, measured torques were higher than those predicted by theoretical analysis. The theoretical torque equation is based on laminar flow in all regions of the foil bearings. As can be seen from Fig. 43, the foil drag is Reynolds number dependent. In bearing configurations tested, the entrance and exit regions were turbulent. However, the Taylor critical Reynolds number was not exceeded in the constant gap region. The film thickness was calculated under the laminar flow assumption of reference 4. From this reference it can be shown that over the angle of wrap required to build the film pressure up to T/R the film thickness undergoes a ten-to-one reduction, yielding a thirty-fold increase in Reynolds number at the entrance. This sufficient to cause turbulent flow. Under these conditions the film thickness will be reduced throughout the wrap, and the foil drag will increase due to the reduced gap and turbulent flow.

During the last quarter of this program the analysis in reference 4 was modified to include the effects of compressibility, and Figs. 42 and 43 reflect these effects.

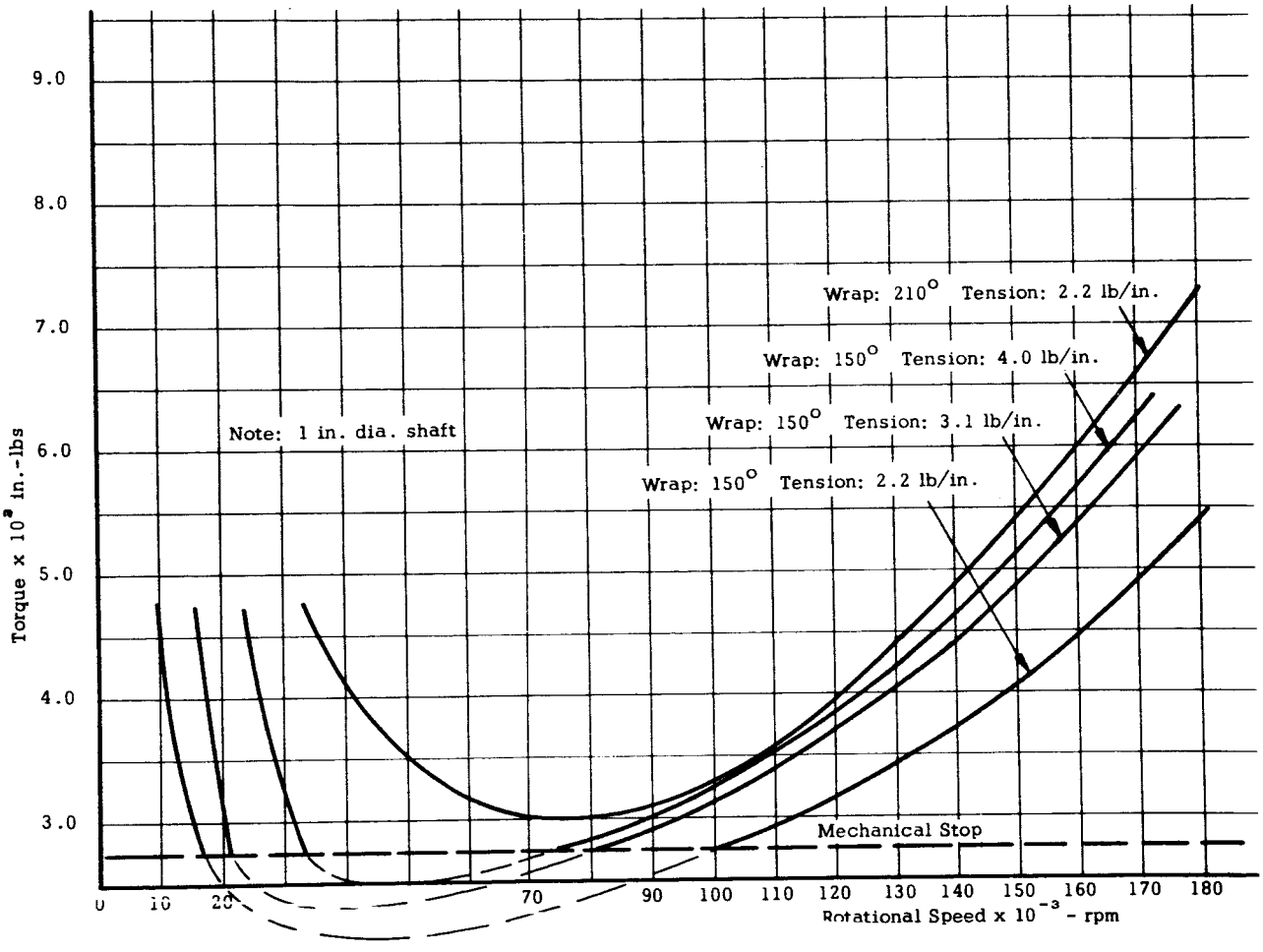

Fig. 41 Torque Variations with Speed, Wrap Angle, and Foil Tension

RR 66-21

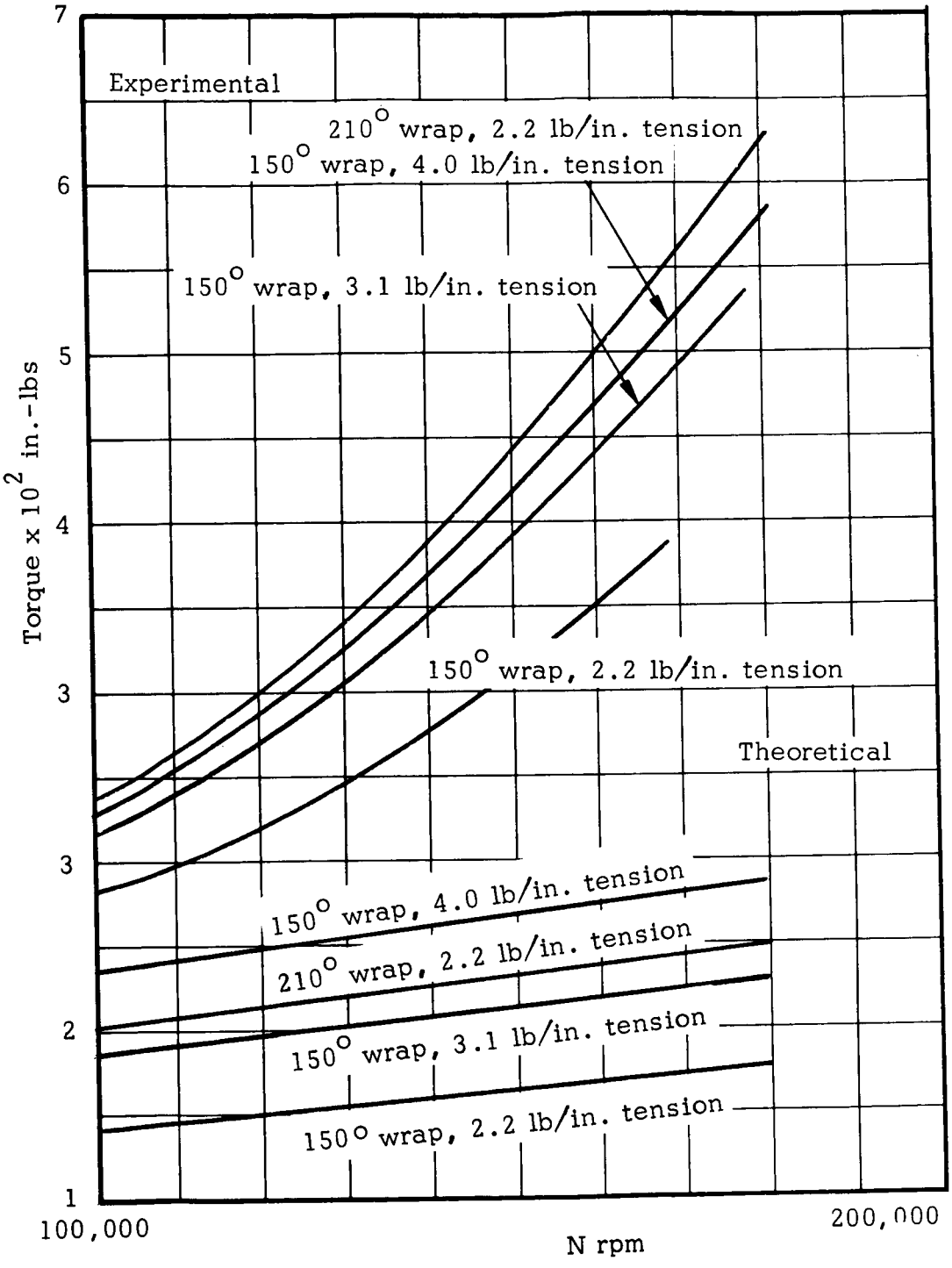

Fig. 42 Comparison of Experimental and Theoretical Foil Bearing Drag Results

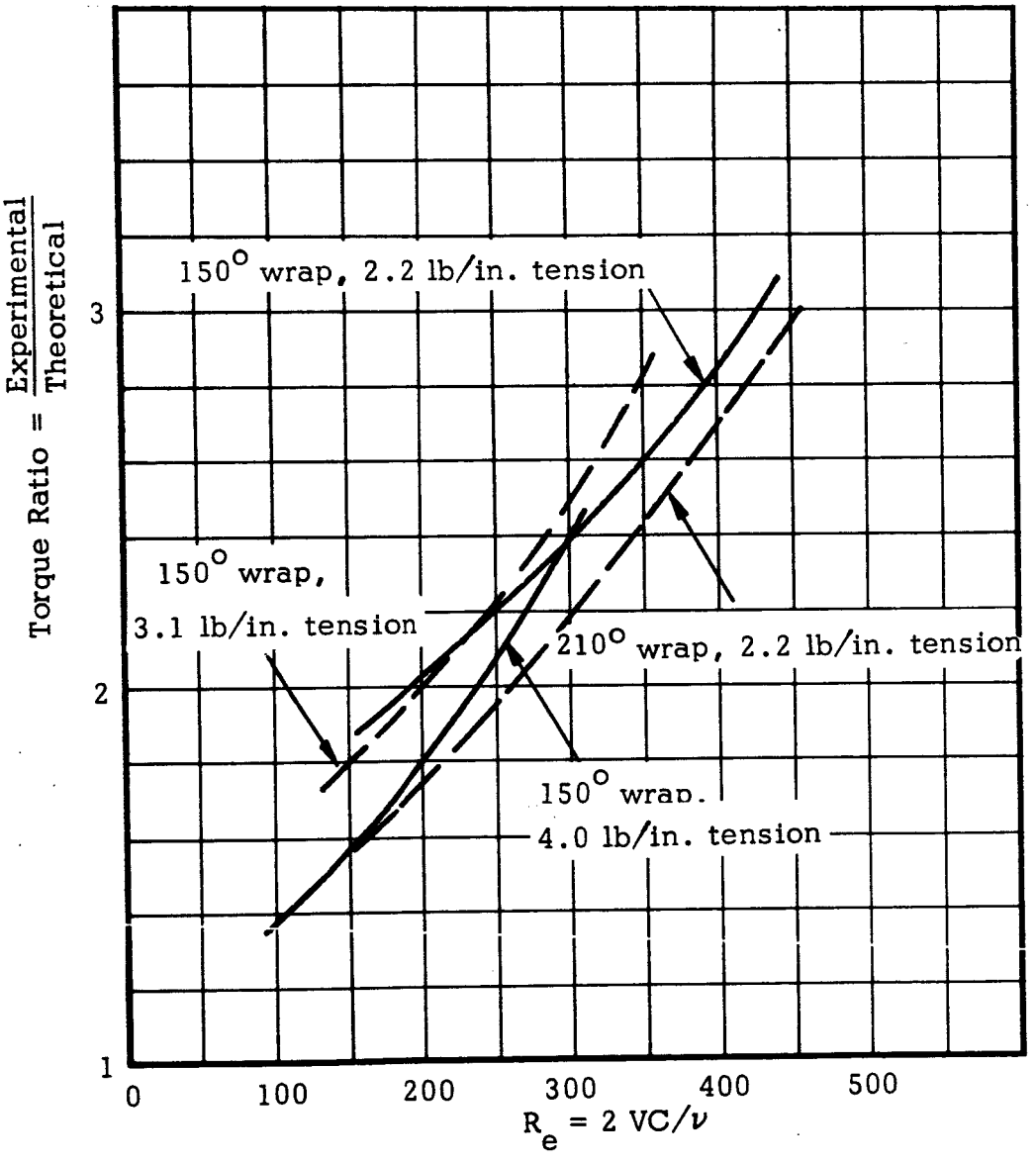

Fig. 43 Comparison of Experimental and Theoretical Foil Bearing Drag Results as a Function of Reynolds Number

Figure 44 shows photographs of samples taken from the foils after approximately two hours of running. These foils were used at various wrap angles and at speeds up to 240,000 rpm. The figure also shows a section of unused foil material for comparison. As shown in the figure, the entrance region gives evidence of the most contact. This is assumed to be due to start/stop conditions. At low speeds, the shaft tends to run along the foil pushing the foil against the supports.

Figure 45 shows the 0.001 in. thick Havar foils used in tests during the last quarter of this program. Running time for the lower foils was approximately two hours and for the upper foils, one hour, and there were approximately 40 stop/start cycles. The thrust bearing failure described in section 3.2.2 resulted in abnormal load on the foils due to the violent stops. The debris from contact of the turbine with the shroud and from the rotor rubbing the seal and scraping the probes could have entered the entrance regions and caused rubbing.

Figure 45 also shows the foils in their respective positions in the high-speed test rig. In all cases, the region where the metal has been removed is within the exit region and appears to be fatigue failure. Due to the negative pressure in a portion of the exit region, the foil tends to make a reverse curve to maintain equilibrium. The fluid forces causing reverse curvature in the exit region become stronger as the rotational speed increases. Therefore, both the magnitude of the reverse radius and the angular position of the region of minimum separation are speed dependent. The fluid film forces appearing to cause reverse curvature are a steady state phenomenon and, as such, will not cause fatigue. One explanation of what seems to be fatigue failure in the exit region is that instabilities in the Cuette flow against the flexible foil may be causing foil flutter. Reference 5 shows that critical Reynolds numbers vary from

Unused

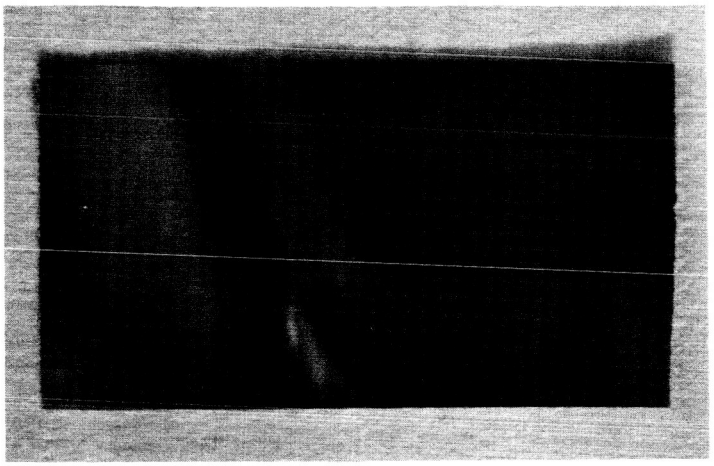

Leading Edge

Bottom Foil

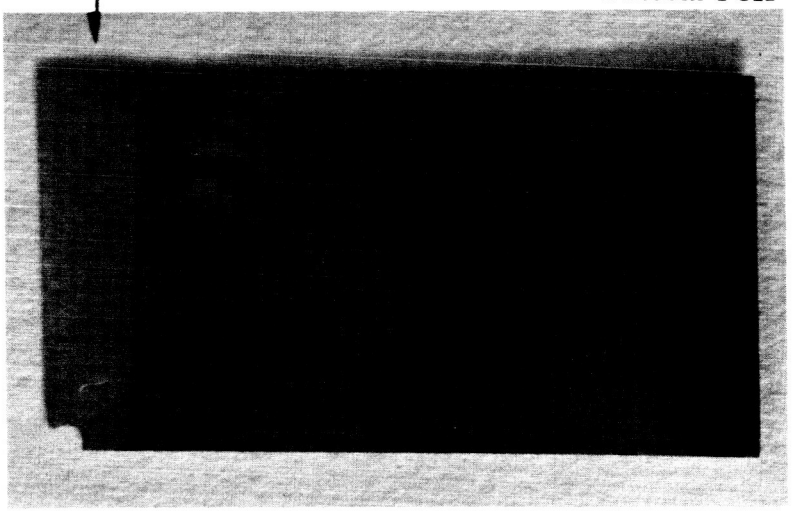

Top Foil

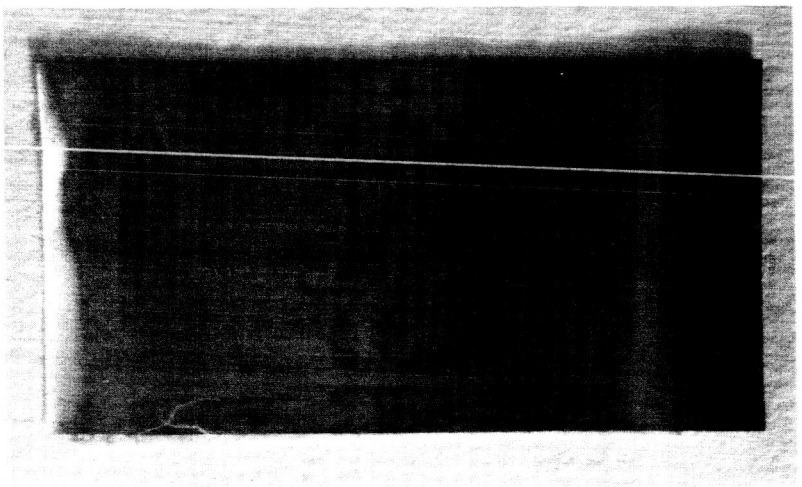

Fig. 44 Foil Condition After Approximately Two Hours of Running Time and Forty Stop/Start Cycles; Peak Speed = 240,000 rpm

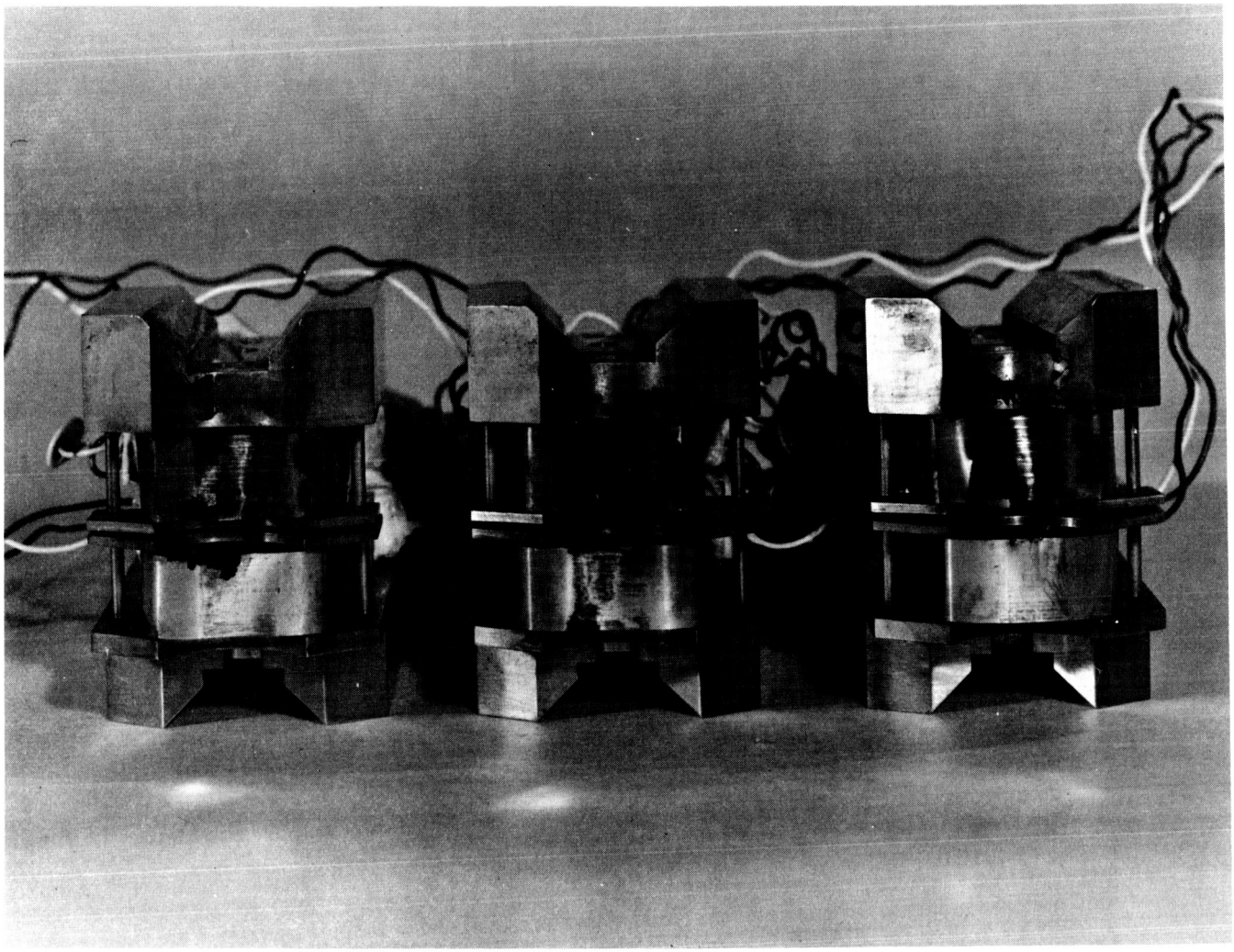

Fig. 45 Foil Condition After Tests Made During Fourth Quarter; Total Running Time for Upper Foils = 1 hr; for Lower Foils, 2 hr; Peak Speed = 381,000 rpm

1000 to 10,000 based on the somewhat arbitrary standards used by the author. A Reynolds number of 1000 is reached when the film thickness in the exit region reaches 0.010 in. for helium and 0.013 in. for air. These values were calculated using a rotational speed of 350,000 rpm.

The value of the critical Reynolds number decreases as the amplitude of the disturbances is increased. In the future, experimental and analytical studies will determine the failure mode, inherent limitations, and possible remedies for this situation.

4.0 CONCLUSION

The objectives of this study were to determine by analytical and experimental means the characteristics of a rotor supported on gas-lubricated foil journal bearings and determination of the maximum speed at which the rotor can be operated without encountering self-excited "whirl" instabilities.

During this study a self-acting, gas-lubricated, foil journal bearing system was designed and fabricated. The foil mounting fixtures were made such that wrap angle and foil tension could be varied. In addition, the lower foil fixtures were mounted on a gas-lubricated plate that allowed the bearing torque on the lower foils to be recorded. Shaft motion was measured by push-pull capacitance probes mounted in two planes axially located along the shaft. The output of the magnetic speed pickup and that of the capacitive motion measuring probes were simultaneously recorded on a tape recorder. The one-inch diameter test rotor was machined from a high strength steel, Nimarc 300, with a radial inflow turbine on one end.

The peak speed recorded during this study was 381,000 rpm. This rotational speed does not represent the limiting speed of the test unit or of the foil bearings, but it was the highest speed recorded before the thrust bearing failed. Throughout the series of tests made during this study limited amplitude, fractional frequency whirl was frequently observed. However, fractional frequency whirl does not seem to represent a serious limitation to the operation of foil bearings since it is sharply speed dependent and of relatively small amplitude. The observed whirls were bounded, and there was no apparent loss in load capacity and no failure related to this phenomenon. As expected, at no time during any of the runs was half-frequency whirl instability observed.

In the experiments performed with the foil bearing test units, it was not possible to accelerate a rotor through its flexural critical speed. When the flexural critical speed of the shaft was approached, the rotor orbit grew until there was contact with the capacitance motion measuring probes. The ability of the foils to damp and restrain a rotor under radial acceleration is a function of wrap angle and foil tension. As would be expected, the higher foil tensions gave lower amplitude runout when the test unit was impacted.

Comparison of theoretical calculations[4] and experimental test results on foil drag shows the data obtained experimentally to be two to three times higher than the calculated data. There is probably experimental error due to the rotating field of gas caused by the rotating shaft impinging on the dynamometer plate and foil support structures, causing an exaggeration of the actual bearing torque. The theoretical analysis assumes laminar flow while, in reality, the foil is operating in the turbulent region. Under turbulent conditions the film thickness is reduced throughout the wrap and the foil drag increased.

As part of this study of a foil bearing rotor support system, an analysis was made on the attitude angle of a self-acting gas-lubricated foil bearing. While it was originally assumed that the attitude angle of a foil bearing was less than 5°, it can be shown theoretically that the attitude angle is a function of system geometry. In a perfectly symmetrical and frictionless three-foil system, the attitude angle is zero. However, in a single-foil system, where the foil bearing centerline remains fixed, the attitude angle is -47.8°.

Because of the "capstan effect" due to the flexibility of the foils, the dry friction forces between the rotor and foil are very high during starting. Means of reducing this objectionably high starting torque

might be provided by: (1) temporary reduction of foil tension; (2) temporary external pressurization; or (3) solid or boundary lubricants. Quantitative data on these and other possible methods of reducing starting torque would permit selection of the most effective method for use in designing practical foil bearings.

There are several areas that require further study before the self-acting foil bearing can become a widely used device.

An investigation should be made on the effect of foil stiffness on the behavior of a rotor supported by self-acting foil bearings. Since the foil bearing derives its freedom from half-frequency whirl instability from the co-linearity between the displacement and force vectors, foil flexibility is necessary; yet the foil must be stiff enough to center the rotor under varying loads. An investigation which would reveal the most desirable tradeoffs between the values of these two parameters could be conducted on the existing test equipment.

Further study of the dynamic behavior of foil bearings should also be conducted. While the foil supported rotor appears to be free from self-excited vibrations, there is little known about the response of such a bearing to external vibrations. The low radial stiffness of the foils results in a low natural frequency, through which the rotor has to be accelerated during start, and which can easily be excited from external inputs. Possibly by mounting the foils on energy absorbing mountings, the low-frequency oscillations due to the foils can be damped. The dynamic behavior of foil bearings can be investigated experimentally on the existing test equipment.

APPENDIX 1

The Support of a Rotor on Self-Acting Gas-Lubricated Foil Journal Bearings

The self-acting gas lubricated foil journal bearing can be used to support a high-speed rotor. This type of journal bearing has been shown to be free from the self-excited half-frequency whirl instability that limits the speed of conventional gas lubricated bearings. The only limitation to rotational speed of a rotor supported by a foil journal bearing is the occurrence of the first flexural critical speed of the rotor.

The foil journal bearing is free from self-excited half-frequency whirl because of the flexibility of the foils. However, this flexibility coupled with the elasticity of the supporting foils often results in a rotor support with a relatively low radial or positional stiffness. Due to this low positional stiffness there are low frequency, rigid body, critical speeds through which the rotor bearing system must be accelerated. These critical speeds are associated with the mass, length and polar moment of inertia of the rotor and the location and geometry of the supporting foils. The occurrence of these critical speeds and the low positional stiffness of the foil journal bearing often precludes its use in many practical applications.

The object of this analysis is to present the support characteristics of self-acting, gas-lubricated foil journal bearings in terms of the physical quantities involved. With this information, the designer can then manipulate these several parameters to obtain a self-acting foil journal bearing that is compatible with the particular rotor support application.

Figure A-1 shows a schematic of a self-acting foil journal bearing used to support a rotating shaft. Figure A-2 shows the equivalent mass-spring representation of the foil bearing rotor support. In this case, the rotor is centered within the supporting structure by three foils each of which is wrapped about the rotor with an angle θ. These foils have a tension of T lbs. per unit width of foil. When the shaft rotates with tangential velocity U, the surrounding gas lubricant is brought into each of the foil bearings and the lubricating film thickness can be expressed as[5]

$$\frac{h}{R}\left(\frac{T}{6\mu U}\right)^{2/3} = .643 \quad * \qquad \text{(A-1)}$$

Equation (A-1) gives the lubricating film thickness in the constant gap region of the foil bearing. The clearances at the inlet and exit regions differ from that in a constant gap region; however, Baumeister[7] has shown that the extent of these regions is approximately 20 times the lubricating film thickness, which is usually an insignificant distance compared to the bearing length. For this preliminary analysis, the entrance and exit regions will be ignored.

The relationships of foil tension, rotational speed, and air film thickness for a self-acting foil journal bearing operated in a gas with a viscosity of 0.26×10^{-8} reyns is shown in Fig. A-3. Note that the air film thickness is not a function of the wrap angle of the foil. The radial centering force F, however, decreases with the decreasing wrap angle,

$$F = 2T \sin\frac{\theta}{2} \qquad \text{(A-2)}$$

*Equation A-1 is based on the assumption of incompressibility. When compressibility effects are included, the constant 0.643 is modified as a function of the parameter $T/P_a R$ (see reference 9). This dependence is incorporated in Figs. A-3 and A-5.

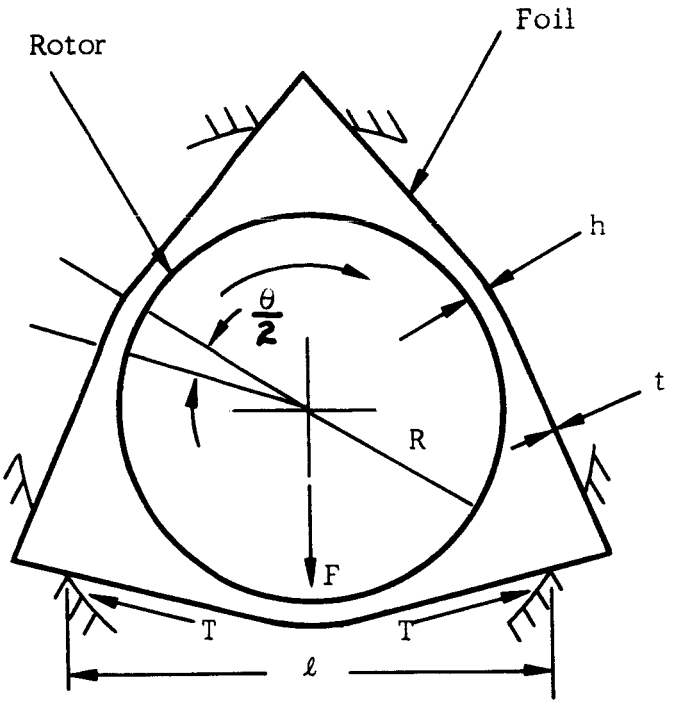

Fig. A-1 Schematic Representation of a Rotor Supported on Self Acting Foil Journal Bearings

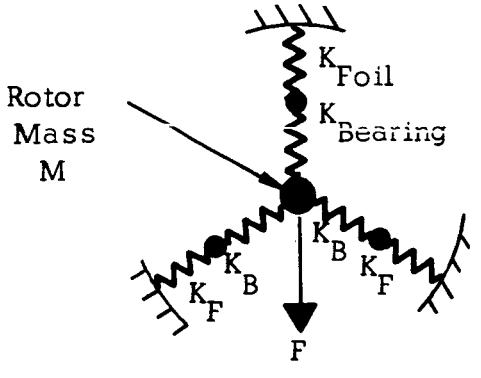

Fig. A-2 Mass-Spring Equivalent of Foil Bearing Rotor Support

This equation is shown in Fig. A-4. The radial stiffness $\left(\frac{dF}{dh}\right)$ of a lubricating film of a single self-acting foil journal bearing can be obtained by substitution of Eq. (A-1) into Eq. (A-2) and differentiating with respect to h,

$$K_B = \frac{dF}{dh} = -3 \times .643^{3/2} (6\mu U) \frac{R^{3/2}}{h^{5/2}} \sin\frac{\theta}{2} \quad \text{(A-3)}$$

$$\mu = .26 \times 10^{-8} \text{ reyn}$$

$$\left(\frac{dF}{dh} \times \frac{1}{U}\right) = -2.41 \frac{R^{3/2}}{h^{5/2}} \sin\frac{\theta}{2} \times 10^{-8} \quad \text{(A-4)}$$

Equation (A-4) with $\theta = \pi$ is shown in Fig. A-5 as a function of radius R. The relationship between the stiffness per unit speed, speed, and radial stiffness for a 180° wrap foil are shown in Fig. A-6

The gas film is formed between the shaft and the foil and the foil is connected at its extremities to the supporting structure. In general, a foil that is sufficiently flexible to conform to the self-acting pressure distribution within the lubricating film over the shaft will be elastic and extensible. The support stiffness of this elastic foil is

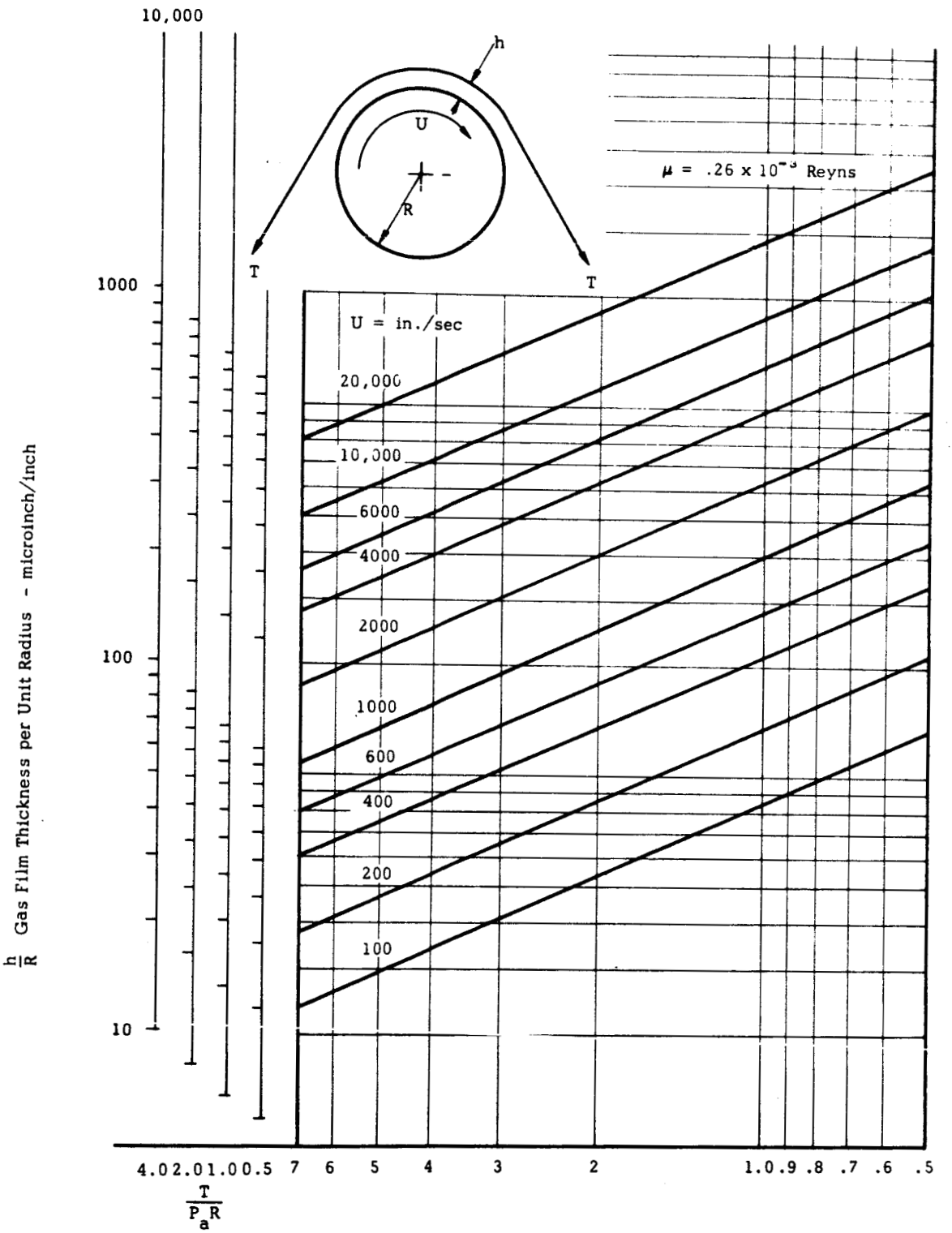

Fig. A-3 Characteristics of a Self-Acting Gas Lubricated Foil Journal Bearing

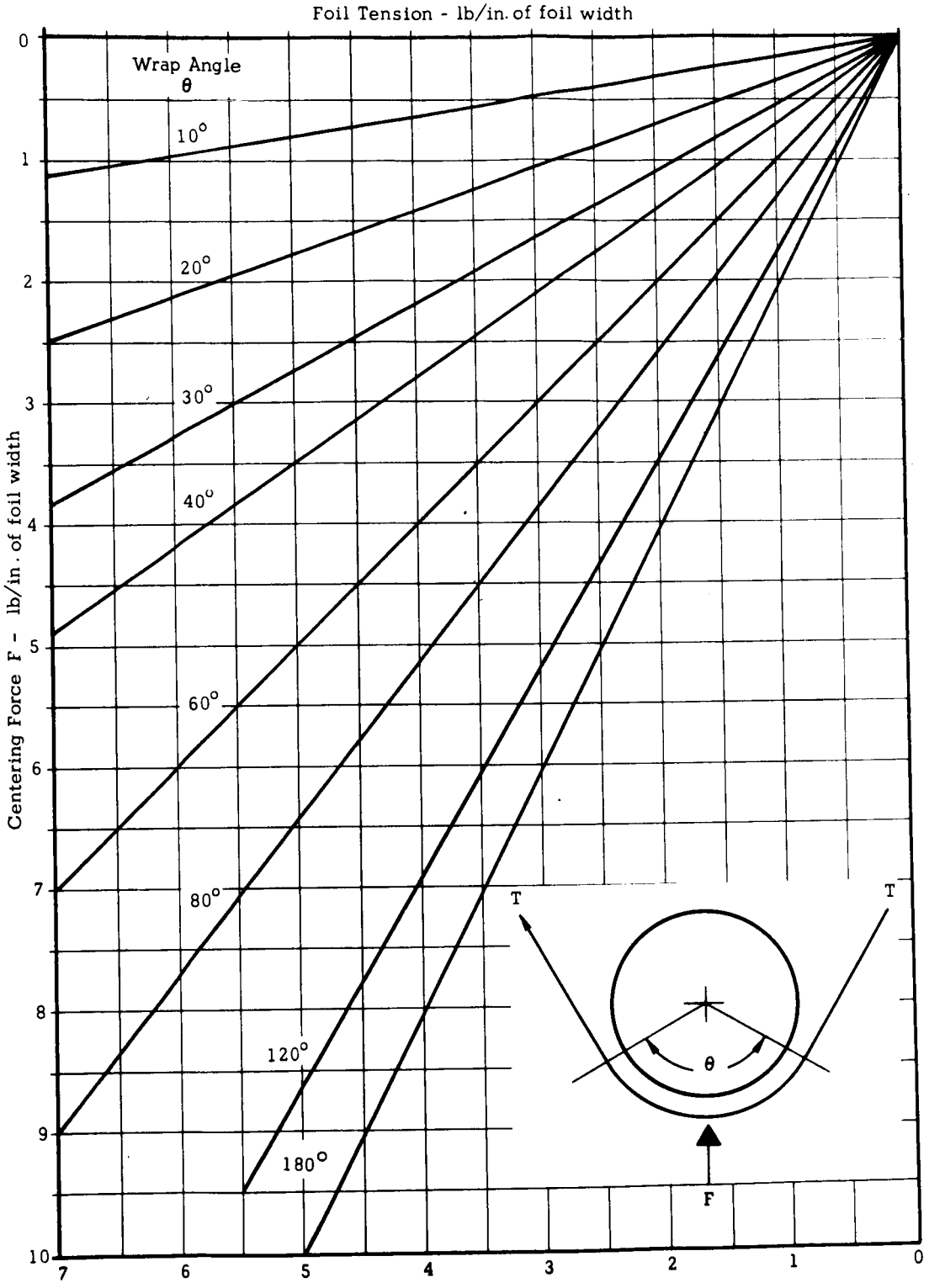

Fig. A-4 Centering Force of a Foil Journal Bearing as a Function of Wrap Angle and Foil Tension

$$K_F = \frac{2ET \sin\frac{\theta}{2}\,\dfrac{\dfrac{l}{\sin\frac{\theta}{2}} - \dfrac{R}{\cos^2\frac{\theta}{2}} + R}{\dfrac{l}{\cos^2\frac{\theta}{2}} - 2R\tan\frac{\theta}{2} + R\theta} + T\cos\frac{\theta}{2}}{\dfrac{l}{4\cos^2\frac{\theta}{2}} - \dfrac{R\sin\frac{\theta}{2}}{2\cos^2\frac{\theta}{2}}} \qquad (A\text{-}5)$$

Specific Cases

1. $R = 0$

$$K_F = \frac{\dfrac{ET\sin^2\frac{\theta}{2}}{\cos\frac{\theta}{2}} + T\cos\frac{\theta}{2}}{\dfrac{l}{4\cos^2\frac{\theta}{2}}}$$

2. $R = 0$; Low initial tension or normal wrap angle

$$K_F = \frac{4ET}{l}\sin^2\frac{\theta}{2}\cos\frac{\theta}{2}$$

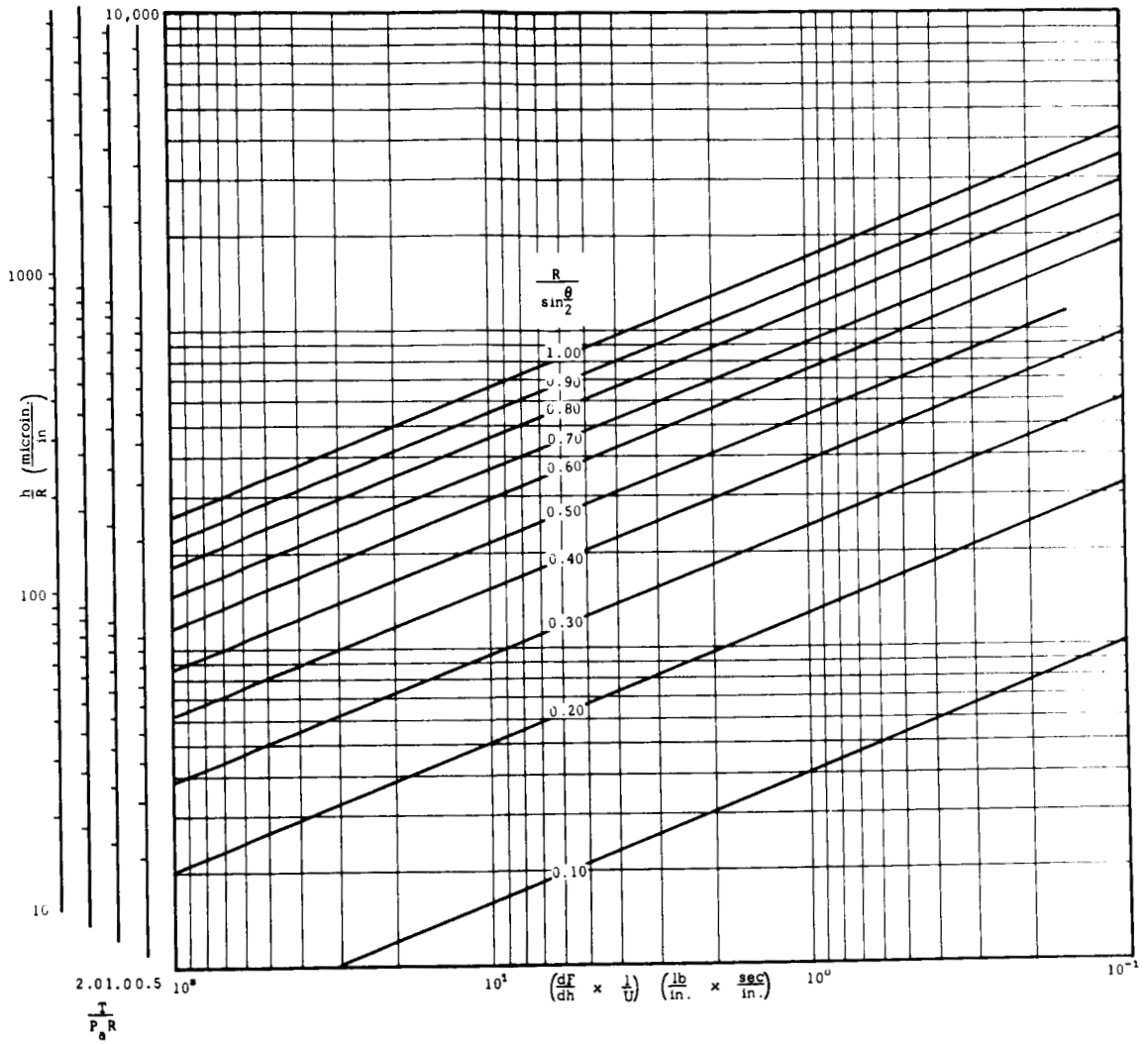

Fig. A-5 Radial Stiffness of Self-Acting Foil Journal Bearings

RR 66-21

The overall radial stiffness of each portion of the foil journal bearing can be obtained by treating the gas film and the foil stiffness as two springs connected in series as represented in Fig. A-2.

$$K = \frac{K_F K_B}{K_F + K_B} \tag{A-6}$$

The total radial stiffness of a particular foil bearing rotor support can be obtained from Eq. (A-6) multiplied by one-half the number of individual foils in the bearing.

The viscous frictional force exerted on the foil over the constant gap region per unit width of each foil journal bearing can be expressed as in reference 8.

$$f = \mu U \frac{R}{h} \Theta \tag{A-7}$$

With a given set of rotor bearing conditions, ie. U, R, μ, θ, T, t, E, 1, these equations and graphs can be used to obtain the radial stiffness and frictional drag of a foil bearing rotor support system. The information, however, is not sufficient to describe these parameters over a wide range of speeds. This limitation is imposed by the conflicting requirements of Eqs. (A-1) and (A-5). Equation (A-1) requires an increasing lubricating film thickness with increasing rotational speed, but this increased film thickness can only be obtained through stretching of the supporting foil, which increases the foil tension. The support characteristics of the self-acting foil journal bearing, therefore, requires the simultaneous solutions of Eqs. (A-1) and (A-5) with particular geometry of foils and support under consideration.

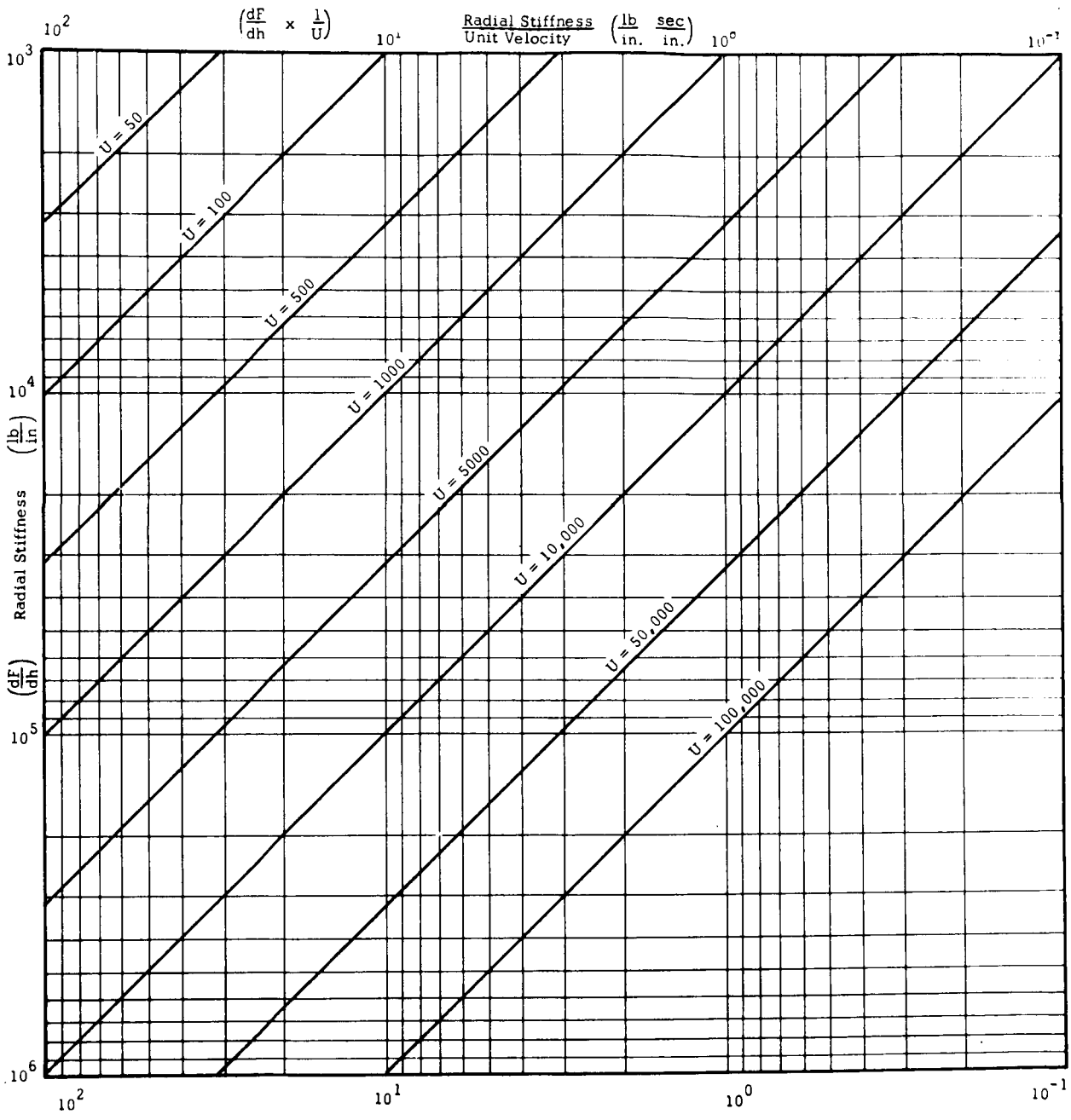

Fig. A-6 Radial Stiffness per Unit Velocity of Self-Acting Foil Journal Bearings

APPENDIX II

On the Attitude Angle of Foil Bearings*

1. INTRODUCTION

The stability of a bearing is closely related to the attitude angle (the measured angle from the load vector to the displacement vector, positive when in the direction of rotation and negative when not). It is of interest, therefore, to investigate this angle for foil bearings. For brevity, let the direction of the load be termed vertical and the direction of its normal horizontal. The investigation will be restricted to steady state conditions.

The horizontal component of the load depends on the foil-fluid system and on the horizontal mobility of the supports of the foil. The vertical component of the displacement depends on the foil-fluid system, on the vertical mobility of the foil through its supports (i.e., the mechanism, if any, for collecting slack), and on the extension of the foil.

In reference 4 it is shown (see Fig. A-7) that

$$h_e = r_o H_e \left(\frac{6\mu U}{T}\right)^{2/3} < O; \; h_i = r_o H_i \left(\frac{6\mu U}{T}\right)^{2/3}; \; h^* = r_o H^* \left(\frac{6\mu U}{T}\right)^{2/3}$$ where

H_e, H_i, and H are constants given in reference 5. If no slack is collected, the length of the foil between the supports ℓ is related to its initial length ℓ_o by $\ell = \ell_o \left(1 + \frac{T}{Et}\right)$. When the load on the shaft is changed while steady state conditions prevail, the change in tension modifies h_i, h_e, h^* as well as the length of the foil. The combination

*This section was done by Abe Eshel.

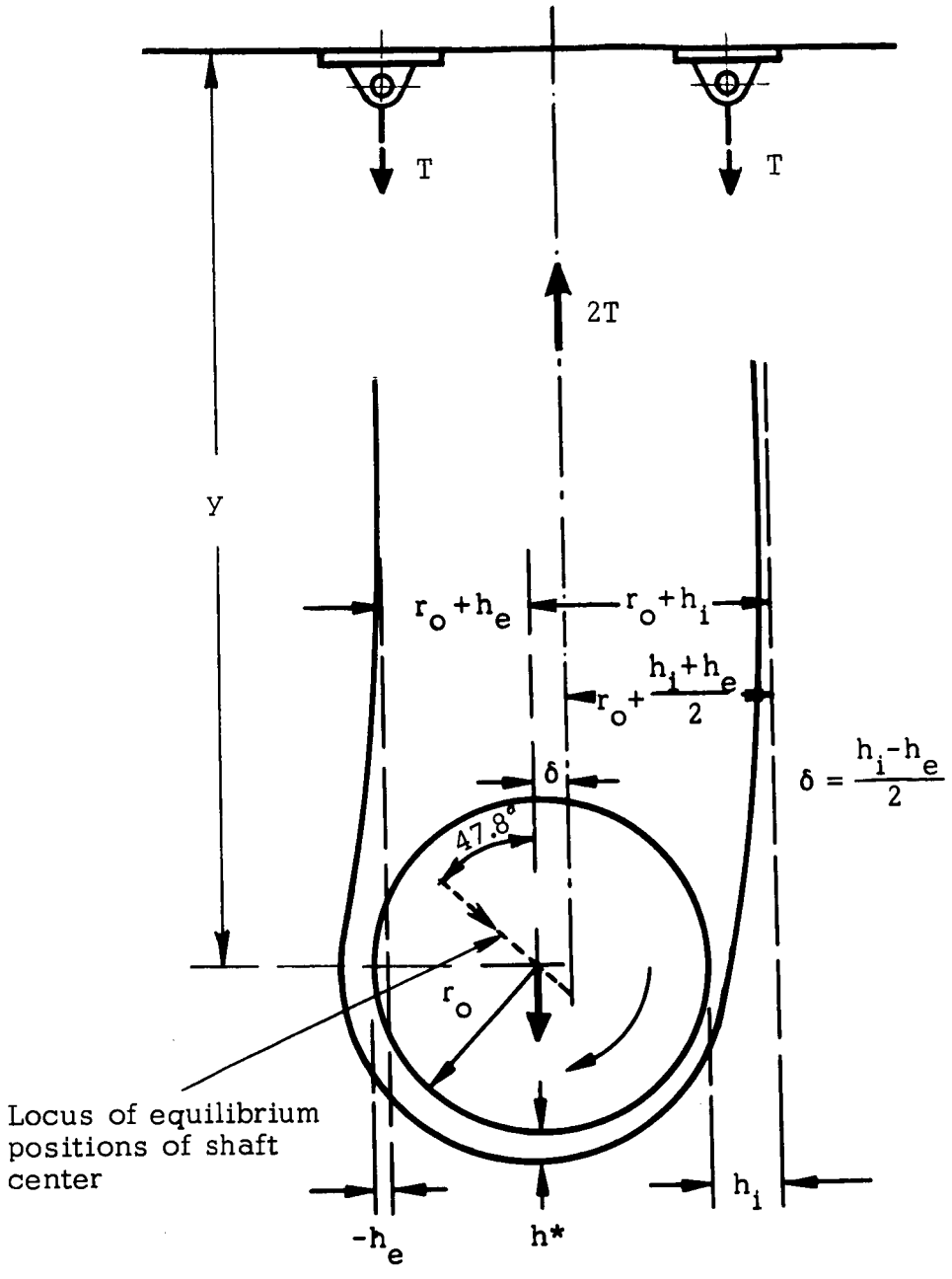

$$h_e = r_o H_e \left(\frac{6\mu U}{T}\right)^{2/3};\quad h_i = r_o H_i \left(\frac{6\mu U}{T}\right)^{2/3};\quad h^* = r_o H^* \left(\frac{6\mu U}{T}\right)^{2/3}$$

$$H_e = -0.646\,H^* \qquad H_i = 2.820\,H^* \qquad H^* = 0.643$$

Fig. A-7 Single Foil System with 180° Wrap Angle

of these factors, geometrical considerations, and the mobility of the supports, determines the equilibrium locus of the center of the shaft under load. In the following some specific cases are considered.

2. Single Foil System with 180-degree Wrap

Case 1: Load parallel to asymptotes; foil free to move normal to the asymptotes

In this case the static response of the shaft to load is motion parallel to the asymptotes (vertical). Thus, the attitude angle is zero.

Case 2: Load parallel to asymptotes; centerline of foil bearing* remains fixed

In this case the distance of each foil from the centerline is $r_o + \frac{h_i + h_e}{2}$. The distance of the center of the shaft from the center line is $\delta = \frac{h_i - h_e}{2}$.

The horizontal distance δ may be evaluated also in a different manner. The overall equilibrium of the fluid system requires

$$W = 2T \qquad \text{(balance of forces)} \tag{A-1}$$

$$W \cdot \delta = \oint (\tau_s - \tau_r)\, r_o^2\, d\theta \qquad \text{(balance of moments)} \tag{A-2}$$

*The centerline of the foil bearing is defined here as the line of action of the resultant of the two foil tensions.

where τ_s and τ_f are the shears of the shaft and the foil on the fluid respectively. According to the Reynolds approximation:

$$\tau_s - \tau_f = \left(\frac{\partial p}{\partial s}\frac{h}{2} - \mu\frac{v}{h}\right) + \left(\frac{\partial p}{\partial s}\frac{h}{2} + \mu\frac{v}{h}\right) = \frac{\partial p}{\partial s}h \qquad \text{(A-3)}$$

Substituting in Eq. (A-3)

$$\frac{dp}{ds} = 6\mu v\,\frac{h - h^*}{h^3} \qquad \text{(A-4)}$$

$$h = r_0 H \left(\frac{6\mu v}{T}\right)^{2/3} \qquad \text{(A-5)}$$

$$ds = r_0\, d\xi \left(\frac{6\mu v}{T}\right)^{1/3} \qquad \text{(A-6)}$$

$$p - p_a = \frac{T}{R} = T\left(\frac{1}{r_0} - \frac{1}{r_0^2}\frac{d^2h}{d\theta^2}\right) \qquad \text{(A-7)}$$

one finds from Eq. (A-2).

$$W\cdot\delta = -\frac{T}{r_0}\oint \frac{d^3h}{d\theta^3}\,h\,d\theta = -T r_0 \left(\frac{6\mu v}{T}\right)^{2/3}\left[H\frac{d^2H}{d\xi^2}\right]_{-\infty}^{\infty}$$

$$+ \frac{T r_0}{2}\left(\frac{6\mu v}{T}\right)^{2/3}\left[\left(\frac{dH}{d\xi}\right)^2\right]_{-\infty}^{\infty} \qquad \text{(A-8)}$$

With the boundary conditions[4],

$$H(\infty) \sim \frac{\xi}{2} + H_a$$
$$H'(\infty) \sim \xi \qquad \text{(A-9)}$$
$$H'' \sim 1$$

hence

$$W\cdot\delta = (2\pi)\, r_0 \left(\frac{G\nu U}{T}\right)^{2/3} \frac{H_i - H_e}{2} = (2\pi)\,\frac{h_i - h_e}{2} \qquad \text{(A-10)}$$

or: $$\delta = \frac{h_i - h_e}{2}$$

It is thus found that a moment $W\cdot\delta$, independent of wrap angle, acts on the fluid system. In order to find the attitude angle, it is necessary to find the vertical displacement. For the inextensible foil,

$$2y + (r_0 + h^*)\pi = l_0$$
$$\delta y = -\frac{\pi}{2}\delta h^* \qquad \text{(A-11)}$$
$$tg|\phi| = \frac{\delta h_i - \delta h_e}{2\left(\frac{\pi}{2}\delta h^*\right)} = \frac{H_i - H_e}{\pi H^*} = \frac{2.820 + 0.646}{\pi} \cong \frac{2\sqrt{3}}{\pi}$$

$$\phi = -47.8^\circ \qquad \text{(A-12)}$$

3. Single Foil System With Θ-Wrap

Case 1: Foil supports free to move perpendicularly to the asymptotes

As in the 180° wrap case, the angle between the displacement vector and the load is zero.

Case 2: The centerline of the foil is fixed

Since the value of $\oint r_o^2 (T_s - T_f)\, ds$ is independent of Θ, it follows that (see Fig. A-8 for notation)

$$W \cdot \delta = T r_o \left(\frac{6\mu v}{T}\right)^{2/3} (H_i - H_e) \qquad \text{(A-13)}$$

But

$$W = 2T \sin\frac{\Theta}{2} \qquad \text{(A-14)}$$

hence

$$\delta = \frac{r_o \left(\frac{6\mu v}{T}\right)^{2/3} (H_i - H_e)}{2 \sin\frac{\Theta}{2}} \qquad \text{(A-15)}$$

$$y = x \sin\frac{\Theta}{2} - (r_o + h^*) \cos\frac{\Theta}{2} \qquad \text{(A-16)}$$

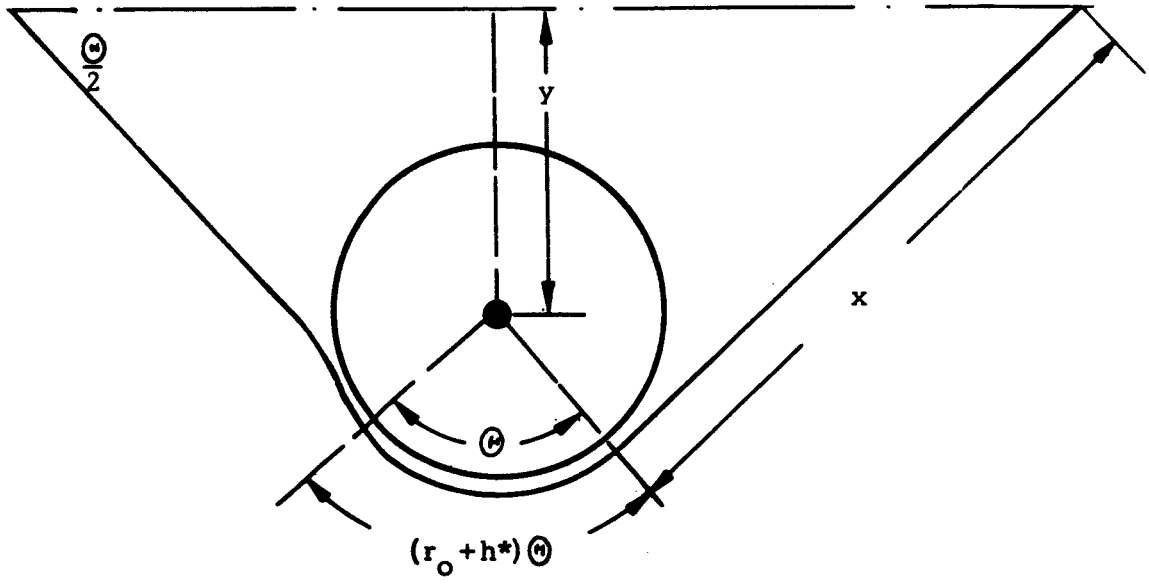

Fig. A-8 Single Foil System with Θ Wrap

$$x + (r_o + h^*)\frac{\Theta}{2} = \frac{l_o}{2} \tag{A-17}$$

$$\delta y = -\delta h^* \left(\frac{\Theta}{2}\sin\frac{\Theta}{2} + \cos\frac{\Theta}{2}\right) \tag{A-18}$$

$$tg\,|\phi| = \frac{H_i - H_e}{2H^*\sin\frac{\Theta}{2}\left(\frac{\Theta}{2}\sin\frac{\Theta}{2} + \cos\frac{\Theta}{2}\right)} \cong \frac{\sqrt{3}}{\sin\frac{\Theta}{2}\left(\frac{\Theta}{2}\sin\frac{\Theta}{2} + \cos\frac{\Theta}{2}\right)} \tag{A-19}$$

4. Three Foil System with Θ Wrap

Consider first a stationary, frictionless, three-foil system, each of wrap angle Θ. Each foil is assumed to be initially under tension T_o, but the shaft is not loaded. Each foil exerts a resultant reaction of magnitude $2T_o \sin\frac{\Theta}{2}$ passing through the center of the shaft.

Let the origin of the system of coordinates be located at the center of the shaft in the above condition. Suppose that rotation at an

angular velocity ω starts now, while the shaft is still load-free. The load on each foil by virtue of the initial tension is $P_o = 2T_o \sin \frac{\theta}{2}$. Since each foil has its own inlet and exit region, there is a net moment on the fluid within each foil of magnitude $T_o r_o \left(\frac{6\mu U}{T_o}\right)^{2/3} \left(H_i - H_e\right)$, and the resultant foil force on the fluid (of magnitude P_o) cannot act through the shaft center but must be displaced by an amount δ (see Fig. A-9) where

$$P_o \cdot \delta = T_o r_o \left(\frac{6\mu U}{T_o}\right)^{2/3} \left(H_i - H_e\right)$$

The summation of the three-foil reactions on the fluid gives no net force but a couple of magnitude $3P_o\delta$. By symmetry, the center of the shaft must still be at the origin. However, the line of action of the resultant force of each foil on the fluid has been shown to have undergone a parallel displacement δ from the origin. This means that the asymptotes of the foil will have to adjust their position correspondingly.

Next consider the response to loading the shaft by an amount W in direction α (see Fig. A-9). Assume that the center of the shaft is displaced in steady state of (x, y). For the foil k, one finds

$$P_k \delta_k = T_k r_o \left(\frac{6\mu U}{T_k}\right)^{2/3} \left(H_i - H_e\right) \qquad (k = 1,2,3) \qquad \text{(A-20)}$$

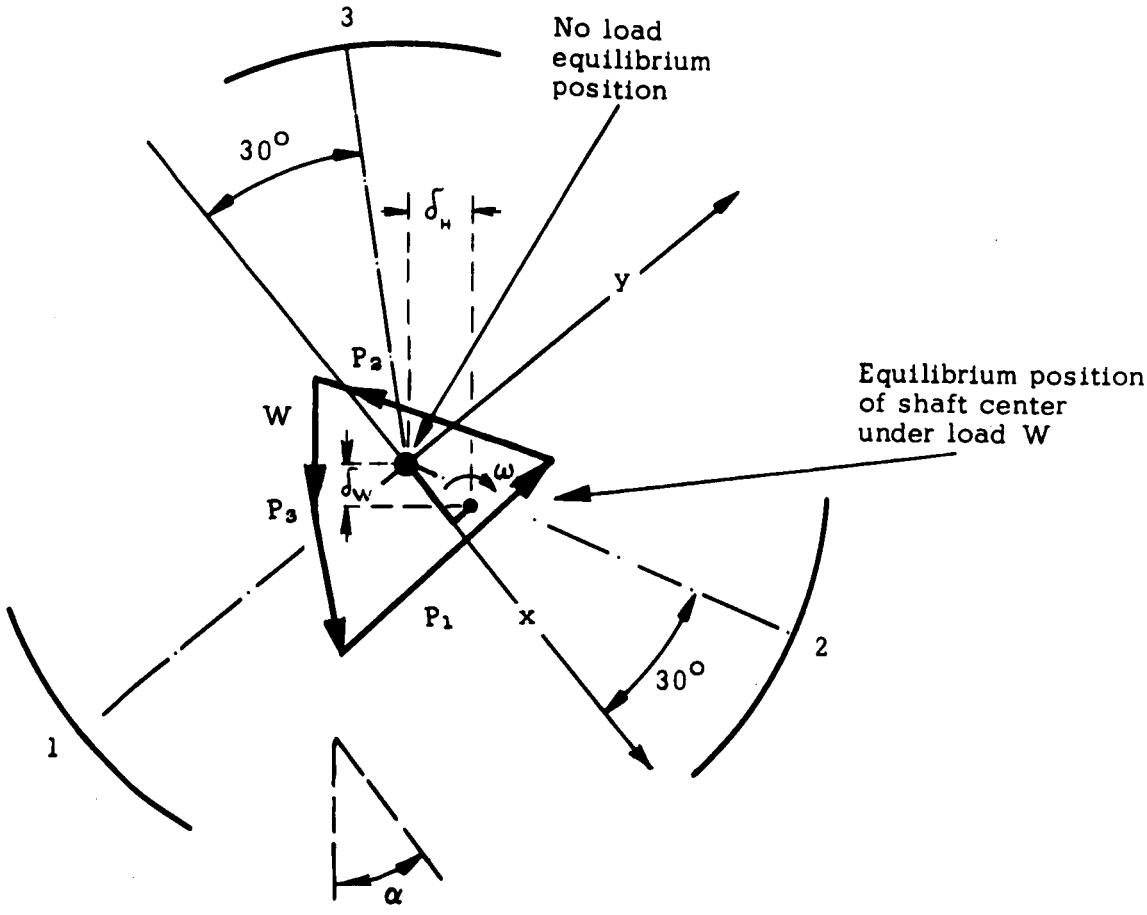

To a first approximation:

The displacement in the load direction: $\delta_w = -y\sin\alpha + x\cos\alpha = \frac{2}{9} W r_o H^* \left(\frac{6\mu U}{T}\right)^{2/3} \cdot \left(\frac{\theta}{2} + \operatorname{ctg}\frac{\theta}{2}\right)$

The displacement normal to the load :

$\delta_H = x\sin\alpha + y\cos\alpha = 0$

Fig. A-9 Three-Foil System

$$P_k = 2T_k \sin\frac{\theta}{2} \qquad (k=1,2,3) \tag{A-21}$$

$$h_k^* - h_o^* = r_o H^* \left\{ \left(\frac{6\mu U}{T_k}\right)^{2/3} - \left(\frac{6\mu U}{T_o}\right)^{2/3} \right\} \tag{A-22}$$

$$= -\frac{2}{3} r_o H^* \left(\frac{6\mu U}{T_o}\right)^{2/3} \frac{T_k - T_o}{T_o} + \cdots \qquad (k=1,2,3)$$

Using the notation $g(\theta) = \frac{\theta}{2} \sin\frac{\theta}{2} + \cos\frac{\theta}{2}$, it is found that for inextensible foil

$$\begin{aligned} q(\theta)(h_1^* - h_o^*) &= y \\ q(\theta)(h_2^* - h_o^*) &= -\frac{y}{2} - \frac{\sqrt{3}x}{2} \\ q(\theta)(h_3^* - h_o^*) &= -\frac{y}{2} + \frac{\sqrt{3}x}{2} \end{aligned} \tag{A-23}$$

Equilibrium requires

$$-P_2 \frac{\sqrt{3}}{2} + P_3 \frac{\sqrt{3}}{2} = -W\cos\alpha \tag{A-24}$$

$$P_1 - \frac{P_2}{2} - \frac{P_3}{2} = W\sin\alpha$$

This set of equations allows the evaluation of the position of the shaft (x,y), the nominal clearances h_k^*, the tension T_k, the reaction forces P_k, and their lines of action $_k$.

Using the linearized form of Eq. (A-22) it is found that the displacement in the direction of the load

$$\delta_W = -y \sin\alpha + x \cos\alpha = \frac{2}{9} \frac{W r_o H^*}{\sin\frac{\theta}{2}} \left(\frac{6\mu U}{T_o}\right)^{2/3} g(\theta) \qquad \text{(A-25)}$$

and the displacement normal to the load is

$$\delta_H = x \sin\alpha + y \cos\alpha = 0 \qquad \text{(A-26)}$$

It follows that to a first approximation the attitude angle of the three-foil system is zero.

REFERENCES

1. B. Sternlicht, "Influence of Bearings on Rotor Behavior," Proc., International Symposium on Lubrication and Wear, McCutchen Publishing Corp., Berkeley, California, 1965, p 613.

2. W. A. Gross, Gas Film Lubrication, John Wiley and Sons, Inc., New York, 1962.

3. K. S. Lion, "Nonlinear Twin T Network for Capicitive Transducers," Review of Scientific Instruments, Vol. 35, No. 3, March 1964.

4. Nicholas Minorsky, Nonlinear Oscillations, D. Van Nostrand Co., Princeton, N.J., 1962.

5. A. Eshel and H. G. Elrod, Jr., "Theory of the Infinitely Wide, Perfectly Flexible, Self-Acting Foil Bearing," Paper No. 65-LUBS-3, ASME Spring Lubrication Symposium, 1965, New York.

6. A. E. Gill, "A Mechanism for Instability of Plane Couette Flow and of Poiseuille Flow in a Pipe," J. of Fluid Mechanics, Vol. 21, Part 3, 1965.

7. H. K. Baumeister, "Further Consideration on the Nominal Clearance of the Foil Bearing," ASLE Paper 5B5, 1964.

8. O. Pinkus and B. Sternlicht, Theory of Hydrodynamic Lubrication, McGraw-Hill Book Company, Inc., New York, 1961.

9. A. Eshel, "Compressibility Effects on the Infinitely Wide, Perfectly Flexible Foil Bearing," to be published.

AMPEX